

Random Advection of a Passive Scalar

Thesis by

James P. Gleeson

In Partial Fulfillment of the Requirements

for the Degree of

Doctor of Philosophy



California Institute of Technology

Pasadena, California

1999

(Submitted May 13, 1999)

© 1999

James P. Gleeson

All Rights Reserved

Acknowledgements

I am deeply grateful to my advisor Professor Philip Saffman for his constant support and for asking the questions which led to this work. Discussions with Dr. Keri Aivazis, Dr. Donal Gallagher and Dr. David Hill helped clarify many issues.

I wish to thank my family for their encouragement and inspiration, and to record my gratitude to my roommates and friends, especially the members of the Caltech Rugby Club, Soccer Club and TACIT. You made the path easy and my steps light.

This work is partially supported by the National University of Ireland Traveling Studentship in Mathematical Physics and by the Fulbright Commission.

Abstract

A novel functional method is applied to calculate the statistics of a passive scalar in a turbulent velocity field. The method yields asymptotic series expansions for small velocity correlation time, from which approximate closure equations are derived. Analytical and numerical solutions of the equations accurately predict effective diffusivities and give new results for the scalar spectrum. Formulas expressing the Lagrangian correlation of the velocity in the terms of the Eulerian correlation are given.

Contents

Acknowledgements	iii
Abstract	iv
1 Introduction	1
2 A New Closure Method	4
2.1 Introduction	4
2.2 Novikov's Theorem	5
2.3 The stochastic oscillator example	7
2.4 Accuracy of approximations	11
2.5 Notational conventions	15
2.6 Diagram expansion	16
2.7 Applications of the diagram expansion	21
2.7.1 Using diagrams to obtain FDC approximations	22
2.7.2 The FDC series is an asymptotic series	22
3 Application to effective diffusivity	25
3.1 Introduction	25
3.2 The passive scalar equation	26
3.3 Application of the FDC method	27
3.4 Diagram rules	29
3.5 Interference of turbulent and molecular diffusion	34
3.6 Long-term effective diffusivity	35
3.7 Convergence of the FDC series	37
3.8 Symbolic computation of higher order terms	39
3.8.1 Delta-function spectrum	39

3.8.2	Padé approximation	40
3.8.3	More general spectra	41
3.9	Generalized Padé approximation for $\kappa(t)$	49
3.10	The Lagrangian correlation	50
3.11	Numerical simulation of advection by a random velocity field	53
3.12	Results	56
3.13	Approximation of the mean concentration	58
4	Application to scalar spectrum	67
4.1	Introduction	67
4.2	The scalar spectrum	68
4.3	The FDC1 equations	70
4.3.1	Unforced scalar spectrum	70
4.3.2	Forced isotropic scalar spectrum	71
4.3.3	Imposed mean gradient	72
4.4	The stationary spectrum	75
4.4.1	Analysis in physical space	76
4.4.2	Analysis of isotropic scalar equation	77
4.4.3	Realistic correlation times	80
4.4.4	Analysis of mean gradient equation	82
4.4.5	The Batchelor range	86
4.4.6	Numerics for stationary spectrum	88
4.4.7	Velocity spectra	90
4.4.8	Results	92
4.5	Decaying spectrum—comparison with DIA	95
4.5.1	Results	96
5	Conclusion	99
A	Proof of Novikov’s Theorem	100
B	Counting the FDC diagrams	102

C Proof of Lemma 1	106
D Proof of Lemma 2	107
Bibliography	108

List of Figures

2.1	Mean amplitude $\langle q(t) \rangle$ for $\tau_* = 0.45$	13
2.2	Mean amplitude $\langle q(t) \rangle$ for $\tau_* = 1.0$	14
2.3	Diagram expansion of (2.20), (2.21) and (2.37).	18
3.1	Long-term diffusivity for small molecular diffusivity.	36
3.2	Long-term diffusivity for larger values of the molecular diffusivity. . .	37
3.3	The FDC5 approximation to $\kappa(\infty)$ and its Padé approximants for spectrum E_a , time correlation R_a and $\omega_k = 1/\tau_*$	41
3.4	Padé approximants for $\kappa(\infty)$ for spectrum E_b , time correlation R_a and $\omega_k = k/\tau_*$	45
3.5	Padé approximants for $\kappa(\infty)$ for spectrum E_b , time correlation R_b and $\omega_k = k/\tau_*$	46
3.6	Padé approximants for $\kappa(\infty)$ for spectrum E_c ($\beta = 10$), time correlation R_a and $\omega_k = k/\tau_*$	46
3.7	Padé approximants for $\kappa(\infty)$ for spectrum E_c ($\beta = 10$), time correlation R_a and $\omega_k = k^2/\tau_*$	47
3.8	Padé approximants for $\kappa(\infty)$ for spectrum E_d ($\beta = 10$), time correlation R_a and $\omega_k = 1/\tau_*$	47
3.9	Padé approximants for $\kappa(\infty)$ for spectrum E_d ($\beta = 10$), time correlation R_a and $\omega_k = k/\tau_*$	48
3.10	Padé approximants for $\kappa(\infty)$ for spectrum E_a , time correlation R_c and $\omega_k = 1/\tau_*$. P_1^0 has a pole at $\tau_* = 1.96$, but P_1^1 and P_2^1 have no poles on the positive real axis.	49
3.11	Generalized Padé approximants for $\kappa(t)$ for spectrum E_a , time correlation R_a and $\omega_k = 1/\tau_*$, with $\tau_* = 1$	50

3.12	Comparison of exact (solid line) and numerical (symbols) correlation functions for spectrum E_1	55
3.13	Generalized Padé approximants (lines) and numerical values (dots) for $\kappa(t)$ for spectrum E_a , time correlation R_b and $\omega_k = 1/\tau_*$. Here τ_* is fixed, $\tau_* = \sqrt{2/3}$	56
3.14	Generalized Padé approximants (lines) and numerical values (dots) for $L(t)$ for spectrum E_b , time correlation R_b and $\omega_k = k/\tau_*$. Here τ_* is fixed, $\tau_* = \sqrt{2}$	57
3.15	Solution (3.52) for $\tau_* = 10$	62
3.16	Solution (3.52) for $\tau_* = 1$	63
3.17	Solution (3.52) for $\tau_* = 0.1$	64
3.18	Zoom of Figure 3.17.	65
4.1	Geometry of the integration variables.	74
4.2	The exponent n_+ as a function of γ	84
4.3	Logarithmic slopes of FDC (4.52) (solid,) and Batchelor's theory (4.53) (dashed.)	88
4.4	Scalar spectrum for purely inertial range velocity spectrum. The spectrum has been multiplied by $k^{1.72}$ to highlight the scaling. Inertial range is $k_1 = 0.01$, $k_2 = 0.316$, with parameter $\tau_*Pr = 0.6$	92
4.5	(a) Scalar spectrum parallel to \mathbf{g} , multiplied by $k^{1.64}$; (b) difference between longitudinal and transverse spectra, multiplied by $k^{3.12}$: Purely inertial range velocity spectrum. $k_1 = 0.01$, $k_2 = 0.316$, and parameter $\tau_*Pr = 0.8$	93
4.6	Scalar spectrum for full velocity spectrum. $\tau_*Pr = 5$. The spectrum has been multiplied by $k^{1.55}$ to highlight the scaling. $k_1 = 0.0316$, $k_2 = 0.316$	93
4.7	(a) Scalar spectrum parallel to \mathbf{g} , multiplied by $k^{1.44}$; (b) difference between longitudinal and transverse spectra, multiplied by $k^{3.14}$: Full velocity spectrum; $k_1 = 0.0316$, $k_2 = 0.316$, and parameter $\tau_*Pr = 0.04$	94

4.8	Decaying DIA (solid) and FDC1 (dashed) spectra for $\tau_* = 0.1$	97
4.9	Decaying DIA (solid) and FDC1 (dashed) spectra for $\tau_* = 0.3$	97
4.10	Decaying DIA (solid) and FDC1 (dashed) spectra for $\tau_* = 0.5$	98
B.1	T_3 , the trellis for $n = 3$	103
B.2	T_4 , the trellis for $n = 4$	103
B.3	T_3 labeling for incidence matrices.	104
B.4	T_4 labeling for incidence matrices.	104

List of Tables

2.1	Number of diagrams for iteration expansion	20
2.2	Number of diagrams for FDC expansion	20
3.1	Coefficients of the FDC series for the long-term effective diffusivity. .	42
3.2	Padé approximations to the FDC series in table 3.1.	43

Chapter 1 Introduction

Fluid in turbulent motion is characterized by an appearance of randomness—even though the governing equations and initial conditions for the motion are known, high Reynolds number flows amplify infinitesimal perturbations to the extent that the motion cannot be accurately predicted for long times. Statistical measures of the flows are therefore used, for example the mean velocity of the flow or the correlation between the velocity at two points in space or at two different times. Averaging may be over space, over time, or over an ensemble of experiments (or realizations). The goal of statistical theories of turbulence is the prediction of such statistical measures without the necessity of solving for the velocity field in each realization.

Batchelor’s theory of homogeneous turbulence [1] introduced a series of mathematical ideas that are used to this day. The fluid is assumed to obey the incompressible Navier-Stokes equations, and equations for the various statistical measures are derived by ensemble averaging. “Homogeneity” means that there is no statistically preferred point in space—in other words all statistical quantities which are measured at two or more points in space are assumed to depend only on the vector differences between those points, and are independent of the absolute positions. A further simplification is provided by the assumption of “isotropy”—there is no statistically preferred direction. Thus any vector-dependent statistics may depend only on the magnitude of the vectors and their relative orientation. The strong assumptions of homogeneity and isotropy are not valid for most experimental situations (with some important exceptions, e.g., the smallest scales of grid-generated turbulence), but they provide a mathematical foothold in what is otherwise an apparently intractable problem. Above all, the case of isotropic homogeneous turbulence is considered a first testbed for any theories which aspire to real-world applications.

The most common mathematical approach to predicting velocity statistics is based upon the consideration of successive moments of the velocity field, and leads to the

so-called “closure problem.” This problem arises when predicting moments for any quantity obeying a nonlinear equation. For ease of exposition consider the inviscid Burgers’ equation

$$\frac{\partial}{\partial t}u = \frac{\partial}{\partial x}(u^2) \quad (1.1)$$

for a one-dimensional velocity $u(x, t)$ with appropriate initial and boundary conditions. To find the mean velocity $\langle u(x, t) \rangle$, equation (1.1) may be averaged to yield

$$\frac{\partial}{\partial t}\langle u \rangle = \frac{\partial}{\partial x}\langle u^2 \rangle. \quad (1.2)$$

The mean velocity depends on the correlation (second moment) $\langle u^2 \rangle$. An equation for the correlation is found by multiplying (1.1) by u and then averaging; thus the second moment is found to depend upon the third moment. Clearly this process of multiplying and averaging may be continued to derive an arbitrarily large hierarchy of moment equations, yet in order to solve the system it must be closed at some level. The analogous closure problem for the Navier-Stokes equation is finding a closed system of equations for the moments (usually first and second order) of the velocity at arbitrary points in space and time.

A related but simpler hydrodynamic problem is provided by the turbulent advection (transport) of scalar quantity like dye concentration or temperature. For sufficiently low values of the scalar, the flow will not be affected by its presence, and the scalar field $\theta(\mathbf{x}, t)$ obeys the passive scalar equation

$$\frac{\partial}{\partial t}\theta + \mathbf{u} \cdot \nabla\theta - \kappa\nabla^2\theta = 0, \quad (1.3)$$

with the velocity \mathbf{u} being the solution of, say, the incompressible Navier-Stokes equations. If the scalar represents dye concentration, then the constant κ is the value of the molecular diffusivity; for temperature κ is the conductivity of the fluid. A long-standing problem of fluid mechanics is the calculation of the statistics of the scalar θ from (1.3), given the statistics of the velocity \mathbf{u} . The solution is of considerable

importance in many areas, including applications in atmospheric and oceanic pollution, mixing processes and the scattering of electromagnetic waves by turbulence in the atmosphere.

Although equation (1.3) is dynamically linear, the convection term $\mathbf{u} \cdot \nabla \theta$ is nonlinear in stochastic (random) quantities and so any attempt to find equations for the moments of the scalar must encounter the ubiquitous closure problem outlined above. This stochastic nonlinearity is the fundamental obstacle to closure and remains even if simplifying assumptions on the velocity field (e.g., time-independence [2]) are made. Hence this passive scalar closure problem is a useful starting point for statistical methods in turbulence, and also has interesting applications in its own right.

We simplify the problem by assuming that the velocity field is Gaussian, i.e., the velocity statistics are multivariate normal, and introduce a new closure method called the functional derivative closure (FDC). We employ this method to expand statistics of the scalar as renormalized (i.e., formally resummed) series which are shown to be asymptotic series for small velocity correlation time. We solve the lowest order FDC equations for the scalar spectrum and show how power law ranges for the scalar are related to the velocity statistics. We calculate the mean concentration and dispersion of the scalar and employ a generalized Padé resummation method to derive simple formulas relating the effective (turbulent) diffusivity and the Lagrangian correlation to the known Eulerian velocity correlations. These formulas are valid for velocity correlation times which are not necessarily small. Numerical simulations of random velocity fields confirm the accuracy and range of validity of these theoretical results.

Chapter 2 gives details and simple demonstrations of our closure method. The application to mean concentration and dispersion is considered in Chapter 3, along with the Padé resummation method and the approximate formulas for the effective diffusivity and Lagrangian correlation of the velocity. Closed equations for the second order scalar statistics, i.e., the correlation and spectrum, are formulated in Chapter 4 and are solved by analytical and numerical methods.

Chapter 2 A New Closure Method

2.1 Introduction

Suppose we know the statistics of a stochastic variable or function b and are concerned with finding the statistics of $R[b]$, some non-trivial functional of b . In general b and $R[b]$ may be vectors or tensors and may be functions of position and/or time. The problem frequently reduces to finding $\langle bR[b] \rangle$, where the angle brackets denote averaging over multiple realizations of b . We will see this later when considering advection of a passive scalar by a random velocity field: in this case the passive scalar equation yields

$$\frac{\partial}{\partial t} \langle \theta \rangle - \kappa \nabla^2 \langle \theta \rangle = -\nabla \cdot \langle \mathbf{u}\theta \rangle,$$

and to solve for $\langle \theta \rangle$ we must find $\langle \mathbf{u}\theta \rangle$. This is of the form $\langle bR[b] \rangle$ if we take b to represent the velocity vector \mathbf{u} and R the passive scalar θ . First we consider a simplified example, the stochastic oscillator, which has the following governing equation for each realization of $b(t)$:

$$\begin{aligned} \frac{d}{dt}q(t) &= ib(t)q(t) \\ q(0) &= 1 \end{aligned} \tag{2.1}$$

The stochastic function $b(t)$ has a Gaussian distribution, mean zero, and correlation function

$$\langle b(t_1)b(t_2) \rangle = \Gamma(t_1, t_2). \tag{2.2}$$

We will use the notation $\Gamma(t_1, t_2)$ throughout this chapter to refer to the known correlation function of b . Closure schemes are used to approximate $\langle b(t)q(t) \rangle$, and then (2.1) yields a solution for the mean amplitude $\langle q(t) \rangle$.

Kraichnan [3] and Orszag [4] discuss the stochastic oscillator and use it as an example to demonstrate various closure methods which are also applicable to more complex stochastic problems, such as those which arise in statistical theories of turbulence. These include the iteration (“bare perturbation series”) approximation, the quasi-normal (“cumulant-discard”) approximations and the direct interaction approximation. Kraichnan and Orszag show that the iteration and quasi-normal approximations are valid only under certain restrictions and that the direct interaction approximation is a useful generalization of the others. They further discuss diagram expansions of the perturbation series generated by (2.1) and interpret their closure schemes in terms of resummations of this series.

In this chapter we introduce a new closure method which we have coined the functional derivative closure (hereafter abbreviated to FDC). Application of this method to an unknown like $\langle bR[b] \rangle$ which is nonlinear in stochastic quantities generates a series, the terms of which involve $\langle R[b] \rangle$ and the statistics of b . In the stochastic oscillator example (and later in turbulent advection problems) we show that truncation of the FDC series yields integrodifferential equations for $\langle q(t) \rangle$. We solve these equations and compare the resulting approximations to those obtained from previous closures. To highlight the underlying structure of the equations (as well as facilitate the extension of the method to more complex problems), we examine the diagram expansion of the FDC series. The diagram expansion provides an easy way to write down the FDC approximations and we employ it to prove that when the problem contains a correlation time τ_* , the FDC series is an asymptotic series for $\langle bR[b] \rangle$ as $\tau_* \rightarrow 0$.

2.2 Novikov’s Theorem

In most of what follows we will be concerned with stochastic variables b which are Gaussian with mean zero, $\langle b \rangle = 0$. By “Gaussian” we mean that all odd moments of b vanish and all even moments may be factored into products of the correlation $\langle b(1)b(2) \rangle$. (Here we use the digits 1 and 2 to represent aggregates of arguments

on which the random function depends). For example the fourth order moment $\langle b(1)b(2)b(3)b(4) \rangle$ may be written as a sum of three terms, each being the product of a pair of correlations:

$$\langle b(1)b(2)b(3)b(4) \rangle = \langle b(1)b(2) \rangle \langle b(3)b(4) \rangle + \langle b(1)b(3) \rangle \langle b(2)b(4) \rangle + \langle b(1)b(4) \rangle \langle b(2)b(3) \rangle. \quad (2.3)$$

The sixth order moment factors into a sum of 15 triple-pairs and in general the $2n$ th moment factors into a sum of $(2n)!/n!2^n$ n -pairs. This represents the number of different ways to choose n unordered pairs from $2n$ objects.

The statement of what we call Novikov's Theorem appeared in a paper by E. A. Novikov in 1965 [5]. Although it is applied there only to the simple case of b delta-correlated (white-noise) in time, the proof as presented by Novikov applies for arbitrary correlations.

In coordinate-free form the theorem may be stated as follows.

Theorem 1 (Novikov, 1965) *If R is a functional of a Gaussian random function b and $\langle b \rangle = 0$, then*

$$\langle b(1)R[b] \rangle = \int \langle b(1)b(2) \rangle \left\langle \frac{\delta R[b]}{\delta b(2)} \right\rangle d2, \quad (2.4)$$

where the integration is over the region in which the functions are defined.

More concretely, if we take \mathbf{b} to be a vector function of position and time (e.g., the velocity field we will consider later), then Novikov's Theorem states that

$$\langle b_i(\mathbf{x}, t)R[\mathbf{b}] \rangle = \int_{-\infty}^{\infty} dt' \int d\mathbf{x}' \langle b_i(\mathbf{x}, t)b_j(\mathbf{x}', t') \rangle \left\langle \frac{\delta R[\mathbf{b}]}{\delta b_j(\mathbf{x}', t')} \right\rangle, \quad (2.5)$$

for functionals R of \mathbf{b} . Novikov's proof of his theorem is described in Appendix A.

A word on functional differentiation is in order here. The standard definition (e.g.,

[6]) obeys the rules of normal differentiation, i.e.,

$$\begin{aligned}\frac{\delta}{\delta f(x)} \{R_1[f] + R_2[f]\} &= \frac{\delta R_1[f]}{\delta f(x)} + \frac{\delta R_2[f]}{\delta f(x)} \\ \frac{\delta}{\delta f(x)} \{R_1[f]R_2[f]\} &= R_1[f] \frac{\delta R_2[f]}{\delta f(x)} + \frac{\delta R_1[f]}{\delta f(x)} R_2[f],\end{aligned}$$

and in addition

$$\frac{\delta f(y)}{\delta f(x)} = \delta(x - y).$$

2.3 The stochastic oscillator example

We turn now to the stochastic oscillator example (2.1) to demonstrate the application of Novikov's Theorem to generate a closure scheme. To begin, a formal solution of the governing equation must be found. In general the formal solution involves an integral over the time-history of the function—in this example it is simply

$$q(t) = 1 + i \int_0^t ds b(s)q(s). \quad (2.6)$$

Note that q appears on both sides of (2.6), so this is merely a *formal* solution, in other words a restatement of (2.1) and the initial condition. Nevertheless the form of (2.6) will permit us to generate a series which approximates $\langle bq \rangle$. Each term in this series will depend on the unknown $\langle q \rangle$; such series are referred to as “renormalized.”

Before detailing the FDC closure method, let us consider the most straightforward way of approximating $\langle q \rangle$ from (2.6). This involves generating a solution to (2.6) by

iteration, then taking the average. The first few iteration approximations are

$$\begin{aligned}
q^{(0)}(t) &= 1 \\
q^{(1)}(t) &= 1 + i \int_0^t ds b(s) q^{(0)}(s) \\
&= 1 + i \int_0^t ds b(s) \\
q^{(2)}(t) &= 1 + i \int_0^t ds b(s) q^{(1)}(s) \\
&= 1 + i \int_0^t ds b(s) - \int_0^t ds \int_0^s ds_1 b(s) b(s_1) \\
&\vdots \\
q^{(4)}(t) &= 1 + i \int_0^t ds b(s) - \int_0^t ds \int_0^s ds_1 b(s) b(s_1) - i \int_0^t ds \int_0^s ds_1 \int_0^{s_1} ds_2 b(s) b(s_1) b(s_2) \\
&\quad + \int_0^t ds \int_0^s ds_1 \int_0^{s_1} ds_2 \int_0^{s_2} ds_3 b(s) b(s_1) b(s_2) b(s_3),
\end{aligned}$$

with averages:

$$\langle q^{(0)}(t) \rangle = \langle q^{(1)}(t) \rangle = 1 \quad (2.7)$$

$$\langle q^{(2)}(t) \rangle = \langle q^{(3)}(t) \rangle = 1 - \int_0^t ds \int_0^s ds_1 \Gamma(s, s_1) \quad (2.8)$$

$$\vdots \quad (2.9)$$

$$\begin{aligned}
\langle q^{(4)}(t) \rangle &= 1 - \int_0^t ds \int_0^s ds_1 \Gamma(s, s_1) \\
&\quad + \int_0^t ds \int_0^s ds_1 \int_0^{s_1} ds_2 \int_0^{s_2} ds_3 [\Gamma(s, s_2) \Gamma(s_1, s_3) + \\
&\quad \quad + \Gamma(s, s_3) \Gamma(s_1, s_2) + \Gamma(s, s_1) \Gamma(s_2, s_3)]. \quad (2.10)
\end{aligned}$$

The terms in the expression for $\langle q^{(4)} \rangle$ containing $\Gamma(\cdot)\Gamma(\cdot)$ arise from the Gaussian decomposition (2.3) of $\langle b(s)b(s_1)b(s_2)b(s_3) \rangle$. We will refer to this iteration solution again later.

Now we consider how Novikov's Theorem is applied to the equation (2.1), using

the formal (integral equation) solution (2.6). By Novikov's Theorem,

$$\langle b(t)q(t) \rangle = \int_0^\infty dt_1 \langle b(t)b(t_1) \rangle \left\langle \frac{\delta q(t)}{\delta b(t_1)} \right\rangle. \quad (2.11)$$

To evaluate the functional derivative $\frac{\delta q(t)}{\delta b(t_1)}$ we differentiate (2.6):

$$\frac{\delta q(t)}{\delta b(t_1)} = iH(t, t_1)q(t_1) + i \int_0^\infty dt_2 H(t, t_2)b(t_2) \frac{\delta q(t_2)}{\delta b(t_1)}, \quad (2.12)$$

where $H(x, y)$ is the Heaviside step function

$$H(x, y) = \begin{cases} 1 & \text{if } x > y \\ 0 & \text{if } x < y \end{cases},$$

and its appearance here is a consequence of causality, i.e., $q(t)$ can be affected by changes in $b(t_1)$ only if t_1 is an earlier time than t . We have also assumed that q and b are independent at time $t = 0$. Again, (2.12) is a formal solution or integral equation, this time for $\frac{\delta q}{\delta b}$. Averaging this gives

$$\left\langle \frac{\delta q(t)}{\delta b(t_1)} \right\rangle = iH(t, t_1) \langle q(t_1) \rangle + i \int_0^\infty dt_2 H(t, t_2) \left\langle b(t_2) \frac{\delta q(t_2)}{\delta b(t_1)} \right\rangle. \quad (2.13)$$

Using (2.13) to substitute for $\left\langle \frac{\delta q}{\delta b} \right\rangle$ in (2.11) gives

$$\langle b(t)q(t) \rangle = i \int_0^\infty dt_1 \Gamma(t, t_1) H(t, t_1) \langle q(t_1) \rangle + i \int_0^\infty dt_1 \int_0^\infty dt_2 \Gamma(t, t_1) H(t, t_2) \left\langle b(t_2) \frac{\delta q(t_2)}{\delta b(t_1)} \right\rangle. \quad (2.14)$$

We recognize $\left\langle b(t_2) \frac{\delta q(t_2)}{\delta b(t_1)} \right\rangle$ as the type of term to which we can again apply Novikov's Theorem:

$$\left\langle b(t_2) \frac{\delta q(t_2)}{\delta b(t_1)} \right\rangle = \int_0^\infty dt_3 \Gamma(t_2, t_3) \left\langle \frac{\delta}{\delta b(t_3)} \frac{\delta q(t_2)}{\delta b(t_1)} \right\rangle \quad (2.15)$$

and differentiating (2.12) yields the second functional derivative:

$$\begin{aligned}
\frac{\delta^2 q(t_2)}{\delta b(t_3) \delta b(t_1)} &= iH(t_2, t_1) \frac{\delta q(t_1)}{\delta b(t_3)} + iH(t_2, t_3) \frac{\delta q(t_3)}{\delta b(t_1)} + i \int_0^\infty dt_4 H(t_2, t_4) b(t_4) \frac{\delta^2 q(t_4)}{\delta b(t_3) \delta b(t_1)} \\
&= -H(t_2, t_1) H(t_1, t_3) q(t_3) - H(t_2, t_1) \int_0^\infty dt_4 H(t_1, t_4) b(t_4) \frac{\delta q(t_4)}{\delta b(t_3)} \\
&\quad - H(t_2, t_3) H(t_3, t_1) q(t_1) - H(t_2, t_3) \int_0^\infty dt_4 H(t_3, t_4) b(t_4) \frac{\delta q(t_4)}{\delta b(t_1)} \\
&\quad + i \int_0^\infty dt_4 H(t_2, t_4) b(t_4) \frac{\delta^2 q(t_4)}{\delta b(t_3) \delta b(t_1)},
\end{aligned} \tag{2.16}$$

where we have used (2.12) again to expand $\frac{\delta q(t_1)}{\delta b(t_3)}$ and $\frac{\delta q(t_3)}{\delta b(t_1)}$. Substituting (2.15) and (2.16) into (2.14) we have

$$\begin{aligned}
\langle b(t)q(t) \rangle &= i \int_0^\infty dt_1 \Gamma(t, t_1) H(t, t_1) \langle q(t_1) \rangle \\
&\quad - i \int_0^\infty dt_1 \int_0^\infty dt_2 \int_0^\infty dt_3 \Gamma(t, t_1) \Gamma(t_2, t_3) [H(t, t_2) H(t_2, t_1) H(t_1, t_3) \langle q(t_3) \rangle \\
&\quad\quad + H(t, t_2) H(t_2, t_3) H(t_3, t_1) \langle q(t_1) \rangle] \\
&\quad\quad + \text{terms involving } \langle b \frac{\delta q}{\delta b} \rangle \text{ and } \langle b \frac{\delta^2 q}{\delta b \delta b} \rangle.
\end{aligned} \tag{2.17}$$

We may continue to apply Novikov's Theorem to each of the terms on the right-hand side of equation (2.17) which still involve $\langle b \frac{\delta q}{\delta b} \rangle$ and $\langle b \frac{\delta^2 q}{\delta b \delta b} \rangle$, and so develop a series expansion for $\langle b(t)q(t) \rangle$ involving integrals over $\langle q \rangle$. We make successive approximations FDC1, FDC2, ... by truncating this series—the n in FDC n refers to the number of times Γ appears in the last retained term of the series expansion (i.e., we neglect all terms where Γ appears more than n times). Thus the FDC1 approximation to the right-hand side of (2.17) is

$$\langle b(t)q(t) \rangle_{\text{FDC1}} = i \int_0^\infty dt_1 \Gamma(t, t_1) H(t, t_1) \langle q(t_1) \rangle, \tag{2.18}$$

and the FDC2 approximation is

$$\begin{aligned} \langle b(t)q(t) \rangle_{\text{FDC2}} &= \langle b(t)q(t) \rangle_{\text{FDC1}} \\ &\quad - i \int_0^\infty dt_1 \int_0^\infty dt_2 \int_0^\infty dt_3 \Gamma(t, t_1) \Gamma(t_2, t_3) [H(t, t_2) H(t_2, t_1) H(t_1, t_3) \langle q(t_3) \rangle \\ &\quad \quad \quad + H(t, t_2) H(t_2, t_3) H(t_3, t_1) \langle q(t_1) \rangle]. \end{aligned} \quad (2.19)$$

Then by (2.18) and the original differential equation (2.1), the FDC1 approximation for $\langle q(t) \rangle$ is the solution of the integrodifferential equation

$$\frac{d}{dt} \langle q(t) \rangle_{\text{FDC1}} = - \int_0^t dt_1 \Gamma(t, t_1) \langle q(t_1) \rangle, \quad (2.20)$$

and the FDC2 approximation is the solution of

$$\begin{aligned} \frac{d}{dt} \langle q(t) \rangle_{\text{FDC2}} &= - \int_0^t dt_1 \Gamma(t, t_1) \langle q(t_1) \rangle \\ &\quad + \int_0^t dt_2 \int_0^{t_2} dt_1 \int_0^{t_1} dt_3 \Gamma(t, t_1) \Gamma(t_2, t_3) \langle q(t_3) \rangle \\ &\quad + \int_0^t dt_2 \int_0^{t_2} dt_3 \int_0^{t_3} dt_1 \Gamma(t, t_1) \Gamma(t_2, t_3) \langle q(t_1) \rangle. \end{aligned} \quad (2.21)$$

2.4 Accuracy of approximations

We will compare the results of these approximations to the exact solution of (2.1), which is

$$\langle q(t) \rangle = \exp \left[-\frac{1}{2} \int_0^t ds \int_0^t ds_1 \Gamma(s, s_1) \right]. \quad (2.22)$$

This exact solution can be derived as follows [4]. Consider the governing equation (2.1), which in each realization of b has the solution

$$\begin{aligned} q(t) &= \exp \left(i \int_0^t b(s) ds \right) \\ &= \sum_{n=0}^{\infty} \frac{1}{n!} \left(i \int_0^t b(s) ds \right)^n. \end{aligned} \quad (2.23)$$

Taking the average of (2.23) and recalling that all odd moments of a Gaussian $b(t)$ are zero, we have

$$\langle q(t) \rangle = \sum_{n=0}^{\infty} \frac{(-1)^n}{(2n)!} \left\langle \left(\int_0^t b(s) ds \right)^{2n} \right\rangle. \quad (2.24)$$

But

$$\begin{aligned} \left\langle \left(\int_0^t b(s) ds \right)^{2n} \right\rangle &= \int_0^t ds_1 \int_0^t ds_2 \dots \int_0^t ds_{2n} \langle b(s_1) b(s_2) \dots b(s_{2n}) \rangle \\ &= \frac{(2n)!}{2^n n!} \left(\int_0^t ds \int_0^t ds_1 \langle b(s) b(s_1) \rangle \right)^n, \end{aligned} \quad (2.25)$$

and so

$$\begin{aligned} \langle q(t) \rangle &= \sum_{n=0}^{\infty} \frac{(-1)^n}{2^n} \frac{1}{n!} \left(\int_0^t ds \int_0^t ds_1 \Gamma(s, s_1) \right)^n \\ &= \exp \left[-\frac{1}{2} \int_0^t ds \int_0^t ds_1 \Gamma(s, s_1) \right] \end{aligned} \quad (2.26)$$

as claimed.

It is interesting to note that this exact solution is the solution of a differential equation of form similar to (2.20):

$$\frac{d}{dt} \langle q(t) \rangle = - \langle q(t) \rangle \int_0^t \Gamma(t, s) ds. \quad (2.27)$$

The difference between the FDC1 approximate equation (2.20) and (2.27) lies in the argument of $\langle q \rangle$ on the right-hand side. This determines whether the equation in question is a differential or integrodifferential equation.

As a concrete example let us now take $b(t)$ to be stationary (i.e., $\Gamma(t, t_1)$ depends only on the difference $t - t_1$), with covariance

$$\Gamma(t, t_1) = \langle b(0)^2 \rangle \exp[-|t - t_1|/\tau_*], \quad (2.28)$$

for a constant parameter τ_* which we call the correlation time of b . We nondimen-

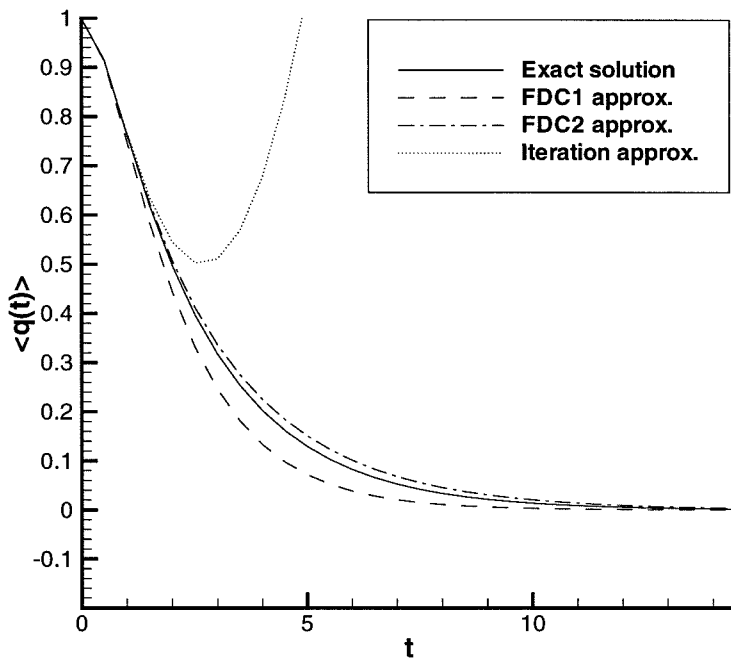


Figure 2.1: Mean amplitude $\langle q(t) \rangle$ for $\tau_* = 0.45$.

sionalize all times by reference to $T = \langle b(0)^2 \rangle^{-1/2}$. Then the exact solution (2.22) is

$$\langle q(t) \rangle = \exp \left[\tau_*^2 - t\tau_* - \tau_*^2 e^{-t/\tau_*} \right], \quad (2.29)$$

and the FDC1 and FDC2 approximations may be reduced to constant coefficient ordinary differential equations by repeated differentiation with respect to t . Solving these equations yields approximations $\langle q_1(t) \rangle$ and $\langle q_2(t) \rangle$. We also record here the first few terms of the iteration approximation (2.10):

$$\langle q_{it}(t) \rangle = 1 + \tau_*^2 - t\tau_* - \tau_*^2 e^{-t/\tau_*} + \frac{1}{2} \left(\tau_*^2 - t\tau_* - \tau_*^2 e^{-t/\tau_*} \right)^2 + \dots \quad (2.30)$$

In Figures 2.1 and 2.2 we plot the exact solution, the iteration approximation (2.30) and the two FDC approximations for correlation time $\tau_* = 0.45$ and $\tau_* = 1$ respectively. For $\tau_* = 0.45$ the approximations are quite good, and their accuracy im-

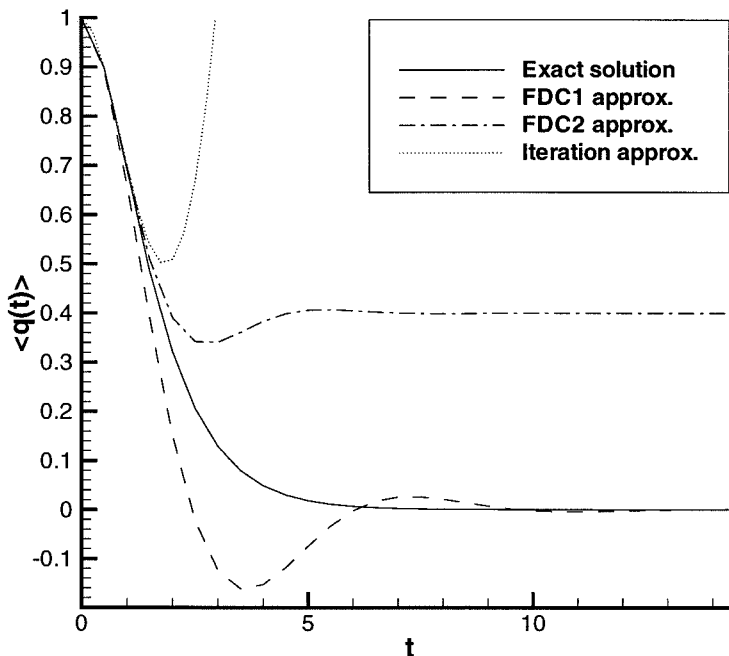


Figure 2.2: Mean amplitude $\langle q(t) \rangle$ for $\tau_* = 1.0$.

proves as τ_* decreases (indeed for τ_* much below 0.4 the curves are indistinguishable). Clearly, however, there is trouble at $\tau_* = 1$. This is not surprising since the FDC approximation series will be shown (in Section 2.7.2) to be asymptotically correct as τ_* approaches zero but is not proven to be convergent. Therefore, the approximations cannot be expected to be valid for arbitrarily large τ_* .

In fact, if we expand the iteration approximation (2.30) and the FDC approximations as series in t or in τ_* , the following becomes apparent: the iteration approximation is valid if $t \ll 1$ but blows up for larger t , whereas the FDC method gives successively improving approximations if either $t \ll 1$ or $\tau_* \ll 1$. In this latter case (small correlation time), the FDC n approximations are *uniform* in the sense that their error is small ($O(\tau_*^n)$ in fact) for all t . To prove these statements we will use the diagram expansion of the FDC series which first requires some simplified notation.

2.5 Notational conventions

The full expressions for the FDC integrodifferential equations (e.g., (2.20) and (2.21)) quickly become cumbersome to handle, and obscure the basic structure of the approximations. For clarity we introduce the following notational conventions:

- Function arguments t_m will be abbreviated to the digit m . Thus $\int d2 \Gamma(1, 2) \langle q(2) \rangle$ represents $\int dt_2 \Gamma(t_1, t_2) \langle q(t_2) \rangle$. The digit 0 represents t .
- This can be further simplified by writing the argument as a subscript to the function, so q_2 will represent $q(t_2)$.
- Functional differentiation is always with respect to b , and so we abbreviate $\frac{\delta q(t_1)}{\delta b(t_2)}$ to $q_{1,2}$, where the digits following the subscripted comma represent the derivative operations.
- The Heaviside step function $H(t_1, t_2)$ is represented by H_{12} .

We now rewrite the equations of the previous section using these conventions.

$$(2.11) \longrightarrow \langle b_0 q_0 \rangle = \int d1 \Gamma(0, 1) \langle q_{0,1} \rangle, \quad (2.31)$$

$$(2.12) \longrightarrow q_{0,1} = i H_{01} q_1 + i \int d2 H_{02} b_2 q_{2,1}, \quad (2.32)$$

$$(2.13) \longrightarrow \langle q_{0,1} \rangle = i H_{01} \langle q_1 \rangle + i \int d2 H_{02} \langle b_2 q_{2,1} \rangle, \quad (2.33)$$

$$(2.14) \longrightarrow \langle b_0 q_0 \rangle = i \int d1 \Gamma(0, 1) H_{01} \langle q_1 \rangle + i \int d1 \int d2 \Gamma(0, 1) H_{02} \langle b_2 q_{2,1} \rangle, \quad (2.34)$$

⋮

$$(2.18) \longrightarrow \langle b_0 q_0 \rangle_{\text{FDC1}} = i \int d1 \Gamma(0, 1) H_{01} \langle q_1 \rangle, \quad (2.35)$$

$$(2.19) \longrightarrow \langle b_0 q_0 \rangle_{\text{FDC2}} = \langle b_0 q_0 \rangle_{\text{FDC1}} - i \int d1 \int d2 \int d3 \Gamma(0, 1) \Gamma(2, 3) [H_{02} H_{21} H_{13} \langle q_3 \rangle + H_{02} H_{23} H_{31} \langle q_1 \rangle], \quad (2.36)$$

The FDC3 approximation is presented now without details of derivation:

$$\begin{aligned}
\frac{d}{dt} \langle q_0 \rangle = & - \int d1 \Gamma(0, 1) H_{01} \langle q_1 \rangle \\
& + \int d1 \int d2 \int d3 \Gamma(0, 1) \Gamma(2, 3) [H_{02} H_{21} H_{13} \langle q_3 \rangle + H_{02} H_{23} H_{31} \langle q_1 \rangle] \\
& - \int d1 \int d2 \int d3 \int d4 \int d5 \Gamma(0, 1) \Gamma(2, 3) \Gamma(4, 5) [H_{02} H_{21} H_{14} H_{43} H_{35} \langle q_5 \rangle \\
& \quad + H_{02} H_{21} H_{14} H_{45} H_{53} \langle q_3 \rangle + H_{02} H_{23} H_{34} H_{41} H_{15} \langle q_5 \rangle \\
& \quad + H_{02} H_{23} H_{34} H_{45} H_{51} \langle q_1 \rangle + H_{02} H_{24} H_{41} H_{13} H_{35} \langle q_5 \rangle \\
& \quad + H_{02} H_{24} H_{41} H_{15} H_{53} \langle q_3 \rangle + H_{02} H_{24} H_{43} H_{31} H_{15} \langle q_5 \rangle \\
& \quad + H_{02} H_{24} H_{43} H_{35} H_{51} \langle q_1 \rangle + H_{02} H_{24} H_{45} H_{51} H_{13} \langle q_3 \rangle \\
& \quad + H_{02} H_{24} H_{45} H_{53} H_{31} \langle q_1 \rangle] \tag{2.37}
\end{aligned}$$

Though lengthy, the derivation of the higher approximations is clearly a straightforward application of the method outlined above. In the next section a diagrammatic method for representing terms is presented which enables us to write down higher order approximations like (2.37) without tedious derivation.

2.6 Diagram expansion

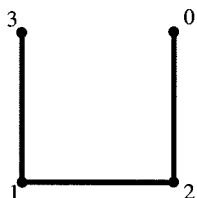
It is evident from the form of the equations (2.20), (2.21) and (2.37) that the closure method described above lends a certain structure to the resulting integrodifferential equations. This structure may be illuminated by using a diagram representation of these equations.

The FDC n integrals contain n Γ -factors in their integrands. We define the corresponding *diagrams of order n* to be polygons with $2n$ sides. Fixing one vertex and labeling it 0, we choose numbers for the remaining vertices from the set $\{1, 2, \dots, 2n-1\}$ based upon the ordering implied by the Heaviside functions in the integrand. For in-

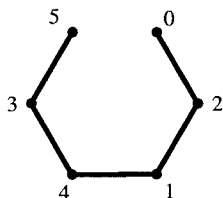
stance, the Heaviside factors in

$$\int d1 \int d2 \int d3 \Gamma(0, 1) \Gamma(2, 3) H_{02} H_{21} H_{13} \langle q_3 \rangle \quad (2.38)$$

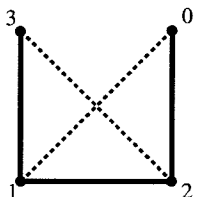
give the vertex-ordering $t_0 > t_2 > t_1 > t_3$, and so we proceed clockwise from vertex 0 to label the $n = 2$ diagram as:



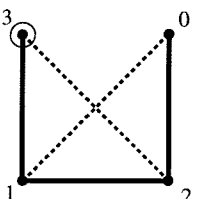
Similarly the $H_{02} H_{21} H_{14} H_{43} H_{35}$ factor in one of the $n = 3$ diagrams give the ordering $t_0 > t_2 > t_1 > t_4 > t_3 > t_5$ and the corresponding diagram is



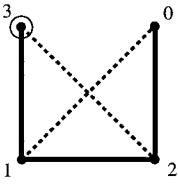
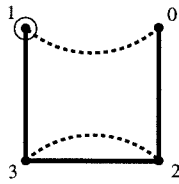
Having thus defined the diagrams, we insert n internal dotted lines joining vertex i to vertex j to represent each factor of $\Gamma(i, j)$. For example (2.38) contains $\Gamma(0, 1) \Gamma(2, 3)$, so we join vertex 0 to vertex 1 and vertex 2 to vertex 3:



Finally the vertex m corresponding to $\langle q_m \rangle$ term is enclosed in a circle (this vertex is always the last vertex numbered, i.e., the furthest clockwise from vertex 0).



$$\frac{d}{dt} \langle q_0 \rangle = \text{Diagram 1} \quad (2.39)$$


$$\frac{d}{dt} \langle q_0 \rangle = \text{Diagram 1} + \text{Diagram 2} + \text{Diagram 3} \quad (2.40)$$



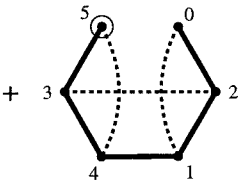
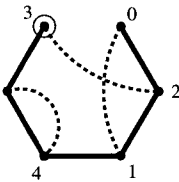
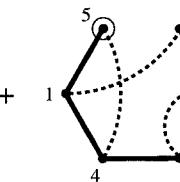
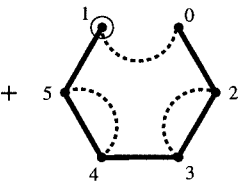
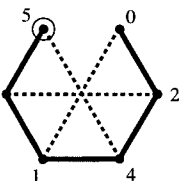
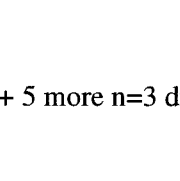
$$\begin{aligned} \frac{d}{dt} \langle q_0 \rangle = & \text{Diagram 1} + \text{Diagram 2} + \text{Diagram 3} \\ & + \text{Diagram 4} + \text{Diagram 5} + \text{Diagram 6} \\ & + \text{Diagram 7} + \text{Diagram 8} + \text{Diagram 9} + 5 \text{ more } n=3 \text{ diagrams} \end{aligned} \quad (2.41)$$







Figure 2.3: Diagram expansion of (2.20), (2.21) and (2.37).

A little thought will suffice to convince that the diagrams just described are a simple method of representing the FDC approximations outlined in the previous section. The integrals are over all vertices except 0. Figure 2.3 shows the diagram expansion representing the right-hand side of the FDC1, FDC2 and FDC3 approximate equations ((2.20), (2.21) and (2.37) respectively).

The iteration approximation (2.8)-(2.10) may also be written in the form of a diagram expansion. It is instructive to compare this expansion to the functional derivative closure expansion derived above. For example, the second iteration ap-

proximate equations, (2.10), is equivalent to

$$\begin{aligned} \frac{d}{dt} \langle q_0 \rangle &= - \int d1 \Gamma(0, 1) H_{01} \\ &+ \int d1 \int d2 \int d3 \Gamma(0, 1) \Gamma(2, 3) [H_{02} H_{21} H_{13} + H_{02} H_{23} H_{31} + H_{01} H_{12} H_{23}], \end{aligned} \quad (2.42)$$

which has the diagram expansion:

$$\begin{aligned} \frac{d}{dt} \langle q_0 \rangle &= 1 \text{ --- } 0 \\ &\quad \text{---} \text{---} \text{---} \\ &+ \begin{array}{c} 3 \quad 0 \\ \diagup \quad \diagdown \\ 1 \quad 2 \end{array} \quad + \begin{array}{c} 1 \quad 0 \\ \text{---} \text{---} \text{---} \\ 3 \quad 2 \end{array} \quad + \begin{array}{c} 3 \quad 0 \\ \text{---} \text{---} \text{---} \\ 2 \quad 1 \end{array} \end{aligned} \quad (2.43)$$

Clearly there exists a relationship between the iteration expansion (2.42) and the corresponding FDC expansion (2.21) and (2.40). Two major differences are clear from the diagram representations: the $\langle q_i \rangle$ term in the integrand (represented by a circled vertex in (2.40)) does not appear in the iteration expansion (2.42); in fact its place is taken by the value of $\langle q_i \rangle$ at time $t = 0$, which is simply 1. Also, the iteration expansion contains extra diagrams which do not appear in the FDC expansion. Indeed the iteration expansion contains $(2n)!/n!2^n$ diagrams of order n , corresponding to the number of ways $2n$ vertices may be divided into n pairs, each connected by a dotted line. Thus the numbers of diagrams in the first few orders of the iteration expansion are given in Table 2.1. The number of diagrams in the FDC expansion is a little more complicated to compute (see Appendix B). The results are given in Table 2.2. Both the iteration expansion and the FDC expansion are formally exact—in other words if every term in the infinite series is retained, then they are each equal to the exact value of $\langle b(t)q(t) \rangle$. Approximations are made when the series are terminated after some finite number of terms, as must be done for computational purposes. The

n	number of diagrams of order n in the iteration expansion
1	1
2	3
3	15
4	105
5	945
6	10395

Table 2.1: Number of diagrams for iteration expansion.

n	number of diagrams of order n in the FDC expansion
1	1
2	2
3	10
4	74
5	706
6	8162

Table 2.2: Number of diagrams for FDC expansion.

formal identity of the iteration and the FDC expansions becomes clear if we replace the $\langle q_i \rangle$ term appearing in the integrand of the FDC expansion with its Taylor series about $t = 0$. This makes clear the difference between the two series: each term in the FDC expansion equals a sum of terms of all orders from the iteration expansion which have been “resummed” to give the $\langle q_i \rangle$ term in the FDC integrand. By resumming the unknown quantity $\langle q_i \rangle$ in each term of the expansion, the FDC method reduces the number of diagrams of each order. Such an infinite series, in which the unknown quantity to be solved for appears in each term on the right-hand side of the equation, is called a *renormalized* series.

2.7 Applications of the diagram expansion

If we “flatten out” the diagrams of (2.41) so that the vertices lie in a straight line, we get:

$$\begin{aligned}
 \frac{d}{dt} \langle q_0 \rangle = & \text{Diagram 1} \\
 & + \text{Diagram 2} + \text{Diagram 3} \\
 & + \text{Diagram 4} + \dots
 \end{aligned}
 \tag{2.44}$$

A remarkable fact about all these diagrams is that they cannot be split into two disconnected parts using only a single cut through the solid line. This is in contrast to, say, the third $n = 2$ diagram of the iteration expansion (2.43), which when unfolded is:

$$\text{Diagram 5}
 \tag{2.45}$$

and which may be separated into two disconnected parts by a single cut, thus:

$$\text{Diagram 5} \xrightarrow{\text{cut}} \text{Diagram 6} + \text{Diagram 7}
 \tag{2.46}$$

To highlight this property we call all the diagrams which cannot be split by a cut through the solid line *connected*, and all other diagrams are termed *unconnected*. Thus all the FDC diagrams we have listed so far are connected, whereas the iteration expansion contains both connected and unconnected diagrams.

2.7.1 Using diagrams to obtain FDC approximations

We have introduced the diagram expansion as a consequence of the FDC approximation, and shown how to associate a connected diagram with each $\text{FDC}n$ integral. However, the chief reason for using diagrams stems from the fact that we can reverse this correspondence, and associate with each connected diagram of order n an $\text{FDC}n$ integral. This is summed up in the following lemma:

Lemma 1 *A diagram of order n is an $\text{FDC}n$ diagram if and only if it is connected.*

We defer the proof to Appendix C. This lemma provides a labor-saving shortcut to writing down the FDC equations; instead of repeatedly taking functional derivatives we simply write down all $(2n)!/n!2^n$ diagrams of order n , throw away those which are not connected and then interpret the remainder as $\text{FDC}n$ integrals according to the diagram rules of Section 2.6. This then gives us the full $\text{FDC}n$ contribution. In practice the $\text{FDC}n$ approximations are all calculated using this method, for example equation (2.37). Moreover, as we shall see in the next chapter, the diagram rules are easily interpreted as an algorithm which can be used with a symbolic manipulation program to obtain high order FDC approximations.

2.7.2 The FDC series is an asymptotic series

Another application of the diagram expansion is the elucidation of properties of the corresponding FDC series; in particular we will show that the FDC series is an asymptotic series for small correlation time τ_* .

Lemma 2 *If there exists M such that $|\langle q(t) \rangle| < M$ for all t and $\Gamma(t, t_1) = \Gamma(t - t_1)$ decays to zero sufficiently quickly (e.g., exponentially) at infinity, then all connected diagrams are bounded as $t \rightarrow \infty$.*

In other words each $\text{FDC}n$ diagram is bounded as $t \rightarrow \infty$ (since by Lemma 1 every FDC diagram is connected). Deferring the proof of the lemma to Appendix D, let's look at a simple example. Consider the stochastic oscillator again, with $\Gamma(t, t_1) =$

$\exp[-|t - t_1|/\tau_*]$ and examine the FDC2 approximation given by (2.21):

$$\begin{aligned} \frac{d}{dt} \langle q(t) \rangle &= - \int_0^t dt_1 e^{-\frac{|t-t_1|}{\tau_*}} \langle q(t_1) \rangle \\ &+ \int_0^t dt_2 \int_0^{t_2} dt_1 \int_0^{t_1} dt_3 e^{-\frac{|t-t_1|}{\tau_*}} e^{-\frac{|t_2-t_3|}{\tau_*}} \langle q(t_3) \rangle \\ &+ \int_0^t dt_2 \int_0^{t_2} dt_3 \int_0^{t_3} dt_1 e^{-\frac{|t-t_1|}{\tau_*}} e^{-\frac{|t_2-t_3|}{\tau_*}} \langle q(t_1) \rangle, \end{aligned} \quad (2.47)$$

then

$$\begin{aligned} \left| \frac{d}{dt} \langle q(t) \rangle \right| &\leq M \left\{ \int_0^t dt_1 e^{-\frac{|t-t_1|}{\tau_*}} \right. \\ &+ \int_0^t dt_2 \int_0^{t_2} dt_1 \int_0^{t_1} dt_3 e^{-\frac{|t-t_1|}{\tau_*}} e^{-\frac{|t_2-t_3|}{\tau_*}} \\ &\left. + \int_0^t dt_2 \int_0^{t_2} dt_3 \int_0^{t_3} dt_1 e^{-\frac{|t-t_1|}{\tau_*}} e^{-\frac{|t_2-t_3|}{\tau_*}} \right\}. \end{aligned} \quad (2.48)$$

The limit as t goes to infinity of each integral exists and yields

$$\lim_{t \rightarrow \infty} \left| \frac{d}{dt} \langle q(t) \rangle \right| \leq M \left\{ \tau_* + \frac{1}{2} \tau_*^3 + \frac{1}{2} \tau_*^3 \right\}. \quad (2.49)$$

Note this nice behavior of the FDC diagrams is not true for the diagrams representing the iteration series. To see this, consider the second order iteration approximation to the previous example (2.10):

$$\begin{aligned} \frac{d}{dt} \langle q(t) \rangle &= - \int_0^t dt_1 e^{-\frac{|t-t_1|}{\tau_*}} \\ &+ \int_0^t ds_1 \int_0^{s_1} ds_2 \int_0^{s_2} ds_3 \left[e^{-\frac{|t-s_2|}{\tau_*}} e^{-\frac{|s_1-s_3|}{\tau_*}} \right. \\ &\quad \left. + e^{-\frac{|t-s_3|}{\tau_*}} e^{-\frac{|s_1-s_2|}{\tau_*}} + e^{-\frac{|t-s_1|}{\tau_*}} e^{-\frac{|s_2-s_3|}{\tau_*}} \right], \end{aligned} \quad (2.50)$$

and note that the final integral blows up as $t \rightarrow \infty$, i.e., some iteration diagrams are unbounded.

The bound M on the absolute value of $\langle q(t) \rangle$, which is assumed in Lemma 2, is not known to exist *a priori*. If the approximation is reasonably valid we expect $\langle q(t) \rangle$ to

be close to its physical value, which is bounded, and then we can invoke Lemma 2 to ensure the FDC diagrams are connected. This is indeed the case in all the examples we consider.

Given Lemma 2, it is straightforward now to prove the following:

Theorem 2 *If there exists M such that $|\langle q(t) \rangle| < M$ for all t and Γ decays to zero sufficiently quickly (e.g., exponentially) at infinity, then the FDC series for $\frac{d}{dt} \langle q(t) \rangle$ is an asymptotic series as $\tau_* \rightarrow 0$, with each FDC n contribution being $O(\tau_*^{2n-1})$.*

The proof follows from the observation that each FDC n term contains $2n - 1$ time integrations (equivalently: each FDC n diagram has $2n - 1$ sides). If we change each time variable t_i by setting $\tilde{t}_i = t_i/\tau_*$, then we pull a factor of τ_*^{2n-1} outside the integral, and the integral itself is bounded for all t (by Lemma 2 and the fact that $\langle q(t) \rangle$ is bounded). To clarify with an example, take the first FDC2 diagram for the stochastic oscillator and write $\Gamma(t, t_1) = R\left(\frac{t-t_1}{\tau_*}\right)$:

$$\int_0^t dt_2 \int_0^{t_2} dt_1 \int_0^{t_1} dt_3 R\left(\frac{t-t_1}{\tau_*}\right) R\left(\frac{t_2-t_3}{\tau_*}\right) \langle q(t_3) \rangle. \quad (2.51)$$

Now let $\tilde{t} = t/\tau_*$, $\tilde{t}_1 = t_1/\tau_*$, etc., and so the contribution of the first FDC2 diagram to $\frac{1}{\tau_*} \frac{d}{dt} \langle q(\tilde{t}\tau_*) \rangle$ is

$$\tau_*^3 \int_0^{\tilde{t}} d\tilde{t}_2 \int_0^{\tilde{t}_2} d\tilde{t}_1 \int_0^{\tilde{t}_1} d\tilde{t}_3 R(\tilde{t} - \tilde{t}_1) R(\tilde{t}_2 - \tilde{t}_3) \langle q(\tilde{t}_3\tau_*) \rangle. \quad (2.52)$$

Since we assumed $\langle q(t) \rangle$ is bounded for all t and we know from Lemma 2 that the FDC2 integral is bounded, we conclude that (2.51) is indeed $O(\tau_*^3)$ as $\tau_* \rightarrow 0$.

Thus the FDC method generates an asymptotic series in τ_* for $\frac{d}{dt} \langle q(t) \rangle$ and so for $\langle q(t) \rangle$. We will use this fact repeatedly in later chapters, so it worth noting that the basis for these facts is the time-structure of the diagrams. For more complex problems the FDC series is still governed by the same type of behavior in time as described here, and so the interpretation of the FDC approximation as an asymptotic series remains valid.

Chapter 3 Application to effective diffusivity

3.1 Introduction

In the previous chapter we presented the functional derivative closure method and demonstrated its application to a simple example. It is now time to examine a more complicated problem which is of real physical interest. When a pollutant tracer or small amount of heat is transported (or *advected*) by a turbulent fluid, it doesn't affect the flow by its presence. Such a quantity is therefore called a *passive scalar*. Since the advecting fluid is in turbulent motion, it can only be described by its statistical characteristics, notably the mean value of the fluid velocity and the energy spectrum of the flow. It is to be expected that the passive scalar will also require such a statistical representation. An outstanding problem in fluid mechanics is to describe the statistics of the scalar, given the velocity statistics.

In this chapter we will attack this problem using our closure method. We calculate the mean scalar concentration, the dispersion of tracers in time and the so-called effective diffusivity. The resulting equations look complicated, but the underlying structure is highlighted when we recast the FDC method in terms of the diagram expansion. We confirm that the molecular diffusivity interferes destructively with the turbulent diffusivity [7] and use Padé approximation techniques to show how the FDC can be useful even when the correlation time is not small. A generalized Padé approximant is defined and used to relate the Lagrangian velocity correlation to the known Eulerian correlations. We perform numerical simulations of Gaussian velocity fields and find the FDC-Padé approximations to be accurate for correlation times on the order of the eddy circulation time.

The effective diffusivity has been examined by various workers using different

closure schemes, e.g., Roberts' [8] application of Kraichnan's [9] direct interaction approximation and the self-consistent theory of Pythian and Curtis [10]. The fact that a series expansion in terms of the correlation time can give successively improving approximations has been recognized (see Silantév [11]), but the actual calculation of terms beyond second order and the application of Padé methods is, we believe, entirely new. Our diagram expansion method is similar to that employed by Dean et al. [2] in their consideration of advection by a time-independent velocity field. The connection between Lagrangian and Eulerian correlation functions is motivated by Saffman's [12] application of Corrsin's conjecture to obtain a quasi-normal type closure. This and related methods are reviewed in the context of one-dimensional fields by Davis [13].

3.2 The passive scalar equation

Let $\theta(\mathbf{x}, t)$ denote the solution of the passive scalar equation

$$\begin{aligned} \frac{\partial}{\partial t}\theta + \mathbf{u} \cdot \nabla\theta - \kappa\nabla^2\theta &= 0 \\ \theta(\mathbf{x}, 0) &= \delta(\mathbf{x} - \mathbf{x}_0). \end{aligned} \tag{3.1}$$

The constant κ is the molecular diffusivity of the pollutant (or the conductivity if θ represents temperature). Note that without the advection term (3.1) is simply a diffusion (or "heat") equation. Here $\mathbf{u}(\mathbf{x}, t)$ is the velocity of the advecting turbulent fluid and so is a random function of position and time. In reality the velocity would of course be calculated by solving the Navier-Stokes equations, but for simplicity here we will suppose it to be a Gaussian random function with known correlation $\langle u_i(\mathbf{x}, t)u_j(\mathbf{x}', t') \rangle$ and we assume that the velocity statistics are homogeneous and isotropic. By choosing a reference frame traveling with the mean velocity, we may set $\langle \mathbf{u} \rangle = 0$.

Then $\theta d\mathbf{x}$ is the probability, for one realization of the turbulence, that a marked particle which was at \mathbf{x}_0 at time $t = 0$ will be in the volume element $d\mathbf{x}$ at time t . The average probability density $\langle \theta(\mathbf{x}, t) \rangle$ is found by averaging over the velocity statistics.

The *dispersion* or *mean-square displacement* of the marked particles at a time t is a measurement of their distance from the source at the origin and can be calculated as

$$D(t) = \frac{1}{3} \int x_\alpha x_\alpha \langle \theta(\mathbf{x}, t) \rangle d\mathbf{x} = \frac{1}{3} \int (x^2 + y^2 + z^2) \langle \theta(\mathbf{x}, t) \rangle dx dy dz, \quad (3.2)$$

where $\mathbf{x} = (x, y, z)$ and the integration is over all of space. The quantity

$$\frac{1}{2} \frac{dD(t)}{dt}$$

is often called the *effective diffusivity* or *eddy diffusivity*. These names arise from the use of this quantity in diffusion equation approximations for turbulent advection [14].

It is clear from (3.2) that to find the dispersion and the effective diffusivity it will be necessary to first find the mean probability density or mean concentration $\langle \theta(\mathbf{x}, t) \rangle$. Writing $\Theta(\mathbf{x}, t) = \langle \theta(\mathbf{x}, t) \rangle$ for convenience and averaging equation (3.1) yields

$$\frac{\partial}{\partial t} \Theta - \kappa \nabla^2 \Theta = - \langle \mathbf{u} \cdot \nabla \theta \rangle. \quad (3.3)$$

The term on the right-hand side of this equation is quadratic in stochastic quantities and is symptomatic of the closure problem which arises in all moment-based approaches to turbulence. In the next section we will apply the FDC method to approximate the $\langle \mathbf{u} \cdot \nabla \theta \rangle$ term. The resulting equations are complicated, but their structure is made evident by considering the equivalent diagram expansion. We construct diagram rules which enable us to employ symbolic manipulation computer programs to calculate high order terms in the FDC series.

3.3 Application of the FDC method

The FDC method is most easily applied to the passive scalar equation (3.1) rewritten in wavenumber space (i.e., Fourier transformed with respect to the spatial variable).

We define

$$\widehat{\Theta}(\mathbf{k}, t) = \frac{1}{(2\pi)^3} \int \Theta(\mathbf{x}, t) e^{-i\mathbf{k}\cdot\mathbf{x}} d\mathbf{x}, \quad (3.4)$$

and Fourier transform (3.1) to obtain an evolution equation for $\widehat{\Theta}(\mathbf{k}, t)$. The FDC method is applied to obtain successive approximations to the averaged advection term on the right-hand side of (3.1). The first approximation (FDC1) is

$$\begin{aligned} \frac{\partial}{\partial t} \widehat{\Theta}(\mathbf{k}, t) + \kappa k^2 \widehat{\Theta}(\mathbf{k}, t) = \\ - \int_0^t dt_1 \int d\mathbf{p} [(\mathbf{k} - \mathbf{p}) \cdot \mathbf{Q}(\mathbf{p}, t - t_1) \cdot \mathbf{k}] e^{-\kappa|\mathbf{k}-\mathbf{p}|^2(t-t_1)} \widehat{\Theta}(\mathbf{k}, t_1). \end{aligned} \quad (3.5)$$

We have adopted the notation $k^2 \equiv \mathbf{k} \cdot \mathbf{k}$ and $\mathbf{a} \cdot \mathbf{Q} \cdot \mathbf{b} \equiv a_i Q_{ij} b_j$. Here Q_{ij} is the Fourier transform of the Eulerian velocity space-time correlation, i.e.,

$$Q_{ij}(\mathbf{k}, \tau) = \frac{1}{(2\pi)^3} \int \langle u_i(\mathbf{x}, t) u_j(\mathbf{x} + \mathbf{r}, t + \tau) \rangle e^{-i\mathbf{k}\cdot\mathbf{r}} d\mathbf{r},$$

and for incompressible velocity with isotropic and stationary statistics (which we consider hereafter) it may be written

$$Q_{ij}(\mathbf{k}, \tau) = Q(k, \tau) \left(\delta_{ij} - \frac{k_i k_j}{k^2} \right),$$

with $Q(k, \tau) = E(k)R(\tau, k)/4\pi k^2$ for the energy spectrum $E(k)$ and time correlation function $R(t, k)$.

The second approximation FDC2 is found through straightforward though lengthy application of the functional derivative closure method. The resulting FDC2 equation

for $\widehat{\Theta}(\mathbf{k}, t)$ is

$$\begin{aligned}
\frac{\partial}{\partial t} \widehat{\Theta}(\mathbf{k}, t) + \kappa k^2 \widehat{\Theta}(\mathbf{k}, t) = & \\
& - \int_0^t dt_1 \int d\mathbf{p} [(\mathbf{k} - \mathbf{p}) \cdot \mathbf{Q}(\mathbf{p}, t - t_1) \cdot \mathbf{k}] e^{-\kappa|\mathbf{k}-\mathbf{p}|^2(t-t_1)} \widehat{\Theta}(\mathbf{k}, t_1) \\
& + \int_0^t dt_2 \int_0^{t_2} dt_1 \int_0^{t_1} dt_3 \iint d\mathbf{p} d\mathbf{q} \left\{ [(\mathbf{k} - \mathbf{p}) \cdot \mathbf{Q}(\mathbf{p}, t - t_1) \cdot (\mathbf{k} - \mathbf{q})] \right. \\
& \quad \times [(\mathbf{k} - \mathbf{p} - \mathbf{q}) \cdot \mathbf{Q}(\mathbf{q}, t_2 - t_3) \cdot \mathbf{k}] \\
& \quad \left. \times e^{-\kappa[|\mathbf{k}-\mathbf{p}|^2(t-t_2)+|\mathbf{k}-\mathbf{p}-\mathbf{q}|^2(t_2-t_1)+|\mathbf{k}-\mathbf{q}|^2(t_1-t_3)]} \right\} \widehat{\Theta}(\mathbf{k}, t_3) \\
& + \int_0^t dt_2 \int_0^{t_2} dt_3 \int_0^{t_3} dt_1 \iint d\mathbf{p} d\mathbf{q} \left\{ [(\mathbf{k} - \mathbf{p}) \cdot \mathbf{Q}(\mathbf{p}, t - t_1) \cdot \mathbf{k}] \right. \\
& \quad \times [(\mathbf{k} - \mathbf{p} - \mathbf{q}) \cdot \mathbf{Q}(\mathbf{q}, t_2 - t_3) \cdot (\mathbf{k} - \mathbf{p})] \\
& \quad \left. \times e^{-\kappa[|\mathbf{k}-\mathbf{p}|^2(t-t_2)+|\mathbf{k}-\mathbf{p}-\mathbf{q}|^2(t_2-t_3)+|\mathbf{k}-\mathbf{p}|^2(t_3-t_1)]} \right\} \widehat{\Theta}(\mathbf{k}, t_1).
\end{aligned} \tag{3.6}$$

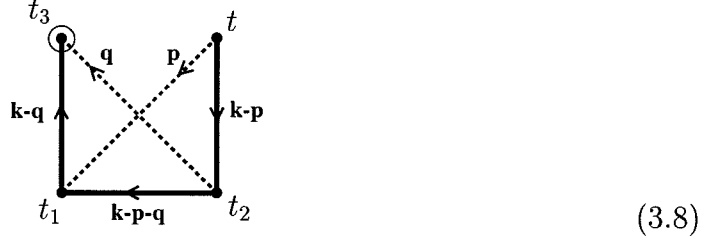
3.4 Diagram rules

Clearly the FDC approximation equations quickly become very complicated to write down. Therefore, it is important to realize that the equations may be reproduced from the diagram expansion corresponding to the FDC series by following a few simple diagram rules. Consider the FDC2 approximation for example. As we saw in Chapter 1, the two FDC2 terms may be represented by diagrams with four vertices each and two internal dotted lines signifying the correlation function:

$$\tag{3.7}$$

For the case under consideration here the basic structure of the FDC2 diagrams remains the same, but we associate additional meanings with the vertices and lines.

Consider the diagram



(3.8)

which represents the first FDC2 term

$$\int_0^\infty dt_2 \int_0^\infty dt_1 \int_0^\infty dt_3 H_{tt_2} H_{t_2 t_1} H_{t_1 t_3} \iint d\mathbf{p} d\mathbf{q} [(\mathbf{k} - \mathbf{p}) \cdot \mathbf{Q}(\mathbf{p}, t - t_1) \cdot (\mathbf{k} - \mathbf{q})] \\ \times [(\mathbf{k} - \mathbf{p} - \mathbf{q}) \cdot \mathbf{Q}(\mathbf{q}, t_2 - t_3) \cdot \mathbf{k}] e^{-\kappa[|\mathbf{k}-\mathbf{p}|^2(t-t_2)+|\mathbf{k}-\mathbf{p}-\mathbf{q}|^2(t_2-t_1)+|\mathbf{k}-\mathbf{q}|^2(t_1-t_3)]} \widehat{\Theta}(\mathbf{k}, t_3). \quad (3.9)$$

Note that we have added only vertex labels, line labels and arrows to the first term of (3.7) to get (3.8), and observe that (3.9) may be produced from (3.8) by applying the following rules:

1. Vertex labels are the time integration variables, except for the first vertex (which is always labeled t).
2. The time integral limits are determined by associating a factor of $H_{t_i t_j}$ with the solid line joining vertices labeled t_i and t_j .
3. The wavevector integration variables are the wavevectors labeling the internal dotted lines; these integrals are over all wavevector space.
4. The vector sum of wavevectors at each vertex is zero, except for the first vertex (labeled t) which has sum $+\mathbf{k}$, and the final (circled) vertex which has sum $-\mathbf{k}$.

To compose the integrand, we multiply the factors resulting from each of the following rules:

5. For each internal dotted line, consider the start and end vertices. For example, in (3.8) for the internal dotted line labeled \mathbf{p} , the start vertex is labeled t and

the end vertex is labeled t_1 . Both the start and the end vertex have solid lines emanating from them; suppose the wavevector labels on these lines are \mathbf{a} and \mathbf{b} respectively. Then the factor we seek is $-\mathbf{a} \cdot \mathbf{Q}(\mathbf{p}, t - t_1) \cdot \mathbf{b}$ where \mathbf{p} is the dotted line label and t and t_1 are the start and end vertex labels. (If the end vertex is the circled vertex, then let $\mathbf{b} = \mathbf{k}$). In the (3.8) example, $\mathbf{a} = \mathbf{k} - \mathbf{p}$ and $\mathbf{b} = \mathbf{k} - \mathbf{q}$, so that the factor is $-(\mathbf{k} - \mathbf{p}) \cdot \mathbf{Q}(\mathbf{p}, t - t_1) \cdot (\mathbf{k} - \mathbf{q})$. By applying this rule again to the second dotted line, we find another factor of $-(\mathbf{k} - \mathbf{p} - \mathbf{q}) \cdot \mathbf{Q}(\mathbf{q}, t_2 - t_3) \cdot \mathbf{k}$.

6. For each solid line joining t_i to t_j say, and labeled by \mathbf{a} , multiply by a factor of $\exp(-\kappa|\mathbf{a}|^2(t_i - t_j))$. In the (3.8) example this gives us three factors of $\exp(-\kappa|\mathbf{k} - \mathbf{p}|^2(t - t_2))$, $\exp(-\kappa|\mathbf{k} - \mathbf{p} - \mathbf{q}|^2(t_2 - t_1))$ and $\exp(-\kappa|\mathbf{k} - \mathbf{q}|^2(t_1 - t_3))$.
7. Finally, the circled vertex carries a factor of $\widehat{\Theta}(\mathbf{k}, t_i)$, where t_i is the label of the circled vertex.

These rules enable us to write the FDC2 equation for $\widehat{\Theta}(\mathbf{k}, t)$, (3.6), in the diagram form

$$\begin{aligned}
 \frac{\partial}{\partial t} \widehat{\Theta}(\mathbf{k}, t) + \kappa k^2 \widehat{\Theta}(\mathbf{k}, t) = & \text{Diagram 1} \\
 & + \text{Diagram 2} + \text{Diagram 3}
 \end{aligned}
 \tag{3.10}$$

The diagram rules apply at each order in the FDC series, thus allowing us to take the higher order diagrams described in Chapter 1 and derive from them the FDC terms in the evolution equation for $\widehat{\Theta}(\mathbf{k}, t)$. Furthermore, the rules form a simple algorithm for finding the FDC terms and so may be implemented using a symbolic manipulation program like *Mathematica*. The calculation of the FDC5 approximation

for the effective diffusivity in this way will be described below.

We recall that the quantities of interest to us are the mean concentration $\Theta(\mathbf{x}, t)$, the dispersion $D(t)$ and the effective diffusivity $\dot{D}/2$ (recall (3.2)). Here we show how the FDC approximations for $\hat{\Theta}(\mathbf{k}, t)$ yield these statistics. First, the mean concentration is simply the inverse Fourier (spatial) transform of $\hat{\Theta}(\mathbf{k}, t)$ and so may be found by

$$\Theta(\mathbf{x}, t) = \int \hat{\Theta}(\mathbf{k}, t) e^{i\mathbf{k}\cdot\mathbf{x}} d\mathbf{k}. \quad (3.11)$$

Effecting this transformation on the FDC1 equation for $\hat{\Theta}(\mathbf{k}, t)$, (3.5), yields the integrodifferential equation

$$\begin{aligned} \frac{\partial}{\partial t} \Theta(\mathbf{x}, t) - \kappa \nabla^2 \Theta(\mathbf{x}, t) = \\ \frac{\partial^2}{\partial x_i \partial x_j} \int_0^t dt_1 \int d\mathbf{y} \langle u_i(\mathbf{x}, t) u_j(\mathbf{y}, t_1) \rangle G(\mathbf{x} - \mathbf{y}, t - t_1) \Theta(\mathbf{y}, t_1). \end{aligned} \quad (3.12)$$

Here $G(\mathbf{z}, \tau)$ is the Green's function for the heat equation,

$$G(\mathbf{z}, \tau) = (4\pi\kappa\tau)^{-\frac{3}{2}} \exp(-z^2/4\kappa\tau). \quad (3.13)$$

In Section 3.13 we consider some solutions of (3.12), but now we move on to the dispersion. Recalling the definition (3.2) and the relation between $\Theta(\mathbf{x}, t)$ and $\hat{\Theta}(\mathbf{k}, t)$ given by (3.4), we find

$$D(t) = -(2\pi)^3 \frac{1}{3} \frac{\partial^2}{\partial k_\alpha \partial k_\alpha} \hat{\Theta}(\mathbf{k}, t) \Big|_{\mathbf{k}=0}. \quad (3.14)$$

This relation allows us to find expressions for the dispersion (or more readily the effective diffusivity $\dot{D}/2$) from the FDC evolution equations for $\hat{\Theta}(\mathbf{k}, t)$, for example (3.5) and (3.6)¹. Taking the evolution equation for $\hat{\Theta}(\mathbf{k}, t)$, applying the operator $-(2\pi)^3 \frac{1}{3} \frac{\partial^2}{\partial k_\alpha \partial k_\alpha}$, then setting \mathbf{k} to zero (and noting $\hat{\Theta}(0, t) = 1$ since Θ is a probability

¹It is a remarkable fact that the iteration expansion considered in Chapter 1 gives the same series for $D(t)$ (but not for the mean concentration) as does the FDC. The spatial averaging (3.14) sets to zero the disconnected diagrams which would otherwise be unbounded in time.

density) yields the FDC2 equation for $D(t)$:

$$\begin{aligned}
\frac{d}{dt}D(t) &= 2\kappa + \frac{4}{3} \int_0^t dt_1 \int d\mathbf{p} Q(p, t_1) e^{-\kappa p^2 t_1} \\
&\quad - \frac{2}{3} \int_0^t dt_2 \int_0^{t_2} dt_1 \int_0^{t_1} dt_3 \iint d\mathbf{p} d\mathbf{q} \left\{ pq\mu(\mu^2 - 1)Q(p, t - t_1)Q(q, t_2 - t_3) \right. \\
&\quad \quad \quad \times e^{-\kappa[p^2(t-t_2)+(p^2+q^2+2pq\mu)(t_2-t_1)+q^2(t_1-t_3)]} \\
&\quad \quad \quad \left. + 2p^2(1 - \mu^2)Q(p, t - t_3)Q(q, t_2 - t_1)e^{-\kappa[p^2(t-t_2)+(p^2+q^2+2pq\mu)(t_2-t_1)+p^2(t_1-t_3)]} \right\}.
\end{aligned} \tag{3.15}$$

We denote by μ the cosine of the angle between \mathbf{p} and \mathbf{q} , i.e., $\mu = \mathbf{p} \cdot \mathbf{q}/pq$. Note that this equation has no Θ terms—the right-hand side gives a simple series representation of the effective diffusivity.

When we consider higher order FDC terms (or diagrams), we see that (3.15) gives the first few terms of an infinite series. For convenience we will adopt the following notation:

$$D(t) = 2\kappa t + D_1(t) + D_2(t) + \dots \tag{3.16}$$

where $D_n(t)$ represents the new term appearing in the FDC n approximation. Thus

$$\frac{d}{dt}D_1(t) = \frac{4}{3} \int_0^t dt_1 \int d\mathbf{p} Q(p, t_1) e^{-\kappa p^2 t_1}, \tag{3.17}$$

and

$$\begin{aligned}
\frac{d}{dt}D_2(t) &= -\frac{2}{3} \int_0^t dt_2 \int_0^{t_2} dt_1 \int_0^{t_1} dt_3 \iint d\mathbf{p} d\mathbf{q} \left\{ pq\mu(\mu^2 - 1)Q(p, t - t_1)Q(q, t_2 - t_3) \right. \\
&\quad \quad \quad \times e^{-\kappa[p^2(t-t_2)+(p^2+q^2+2pq\mu)(t_2-t_1)+q^2(t_1-t_3)]} \\
&\quad \quad \quad \left. + 2p^2(1 - \mu^2)Q(p, t - t_3)Q(q, t_2 - t_1)e^{-\kappa[p^2(t-t_2)+(p^2+q^2+2pq\mu)(t_2-t_1)+p^2(t_1-t_3)]} \right\}.
\end{aligned} \tag{3.18}$$

Note that (3.16), (3.17) and (3.18) permit the calculation of the effective diffusivity given only the energy spectrum of the turbulence (recall $Q(k, t) = E(k, t)/4\pi k^2$) and the value of the molecular diffusivity κ . It is usual to postulate a separable form for $Q(k, t)$ —in the following two sections we will take

$$Q(k, t) = \frac{1}{4\pi k^2} E(k) e^{-|t|/\tau_*(k)}, \quad (3.19)$$

and we call $\tau_*(k)$ the *correlation time* of the velocity. In general the correlation time may depend on the wavenumber k .

We now proceed to examine some consequences of the above expansions for the effective diffusivity.

3.5 Interference of turbulent and molecular diffusion

In the absence of molecular diffusivity ($\kappa = 0$) the effect denoted by $D^{\kappa=0}(t)$ is referred to as pure turbulent diffusion. In general $\kappa > 0$ and the molecular diffusivity interferes non-trivially with the turbulent diffusivity. Saffman [7] has considered this question and by considering solutions of the passive scalar equation on short time and length scales he demonstrates that

$$D(t) = D^{\kappa=0}(t) - \frac{1}{9} \kappa t^3 \overline{\omega^2} + O(t^4), \quad (3.20)$$

for small times t . Here $\overline{\omega^2}$ is the root-mean-square vorticity. We consider the FDC expansions for $D_1(t)$ and $D_2(t)$ and examine the influence of nonzero κ . Expanding the integrand in (3.17) as a series in t we obtain

$$\begin{aligned} D_1(t) = & D_1^{\kappa=0}(t) - \frac{2}{9} \kappa t^3 \int d\mathbf{p} p^2 Q(p) + \\ & + \frac{1}{18} t^4 \left[\kappa^2 \int d\mathbf{p} p^4 Q(p) + 2\kappa \int d\mathbf{p} \frac{p^2}{\tau_*(p)} Q(p) \right] + O(t^5). \end{aligned} \quad (3.21)$$

Similarly expanding the integrand in (3.18) we find

$$D_2(t) = D_2^{\kappa=0}(t) + t^5 \int_0^\infty dp 4\pi p^2 \int_0^\infty dq 2\pi q^2 Q(p)Q(q) \left[\frac{2}{45}\kappa p^4 + \frac{8}{675}\kappa p^2 q^2 \right] + O(t^6). \quad (3.22)$$

Since (see, for example [1])

$$\int d\mathbf{k} k^2 Q(k) = \frac{1}{2}\overline{\boldsymbol{\omega}^2}$$

and

$$\int d\mathbf{k} k^4 Q(k) = \frac{1}{2}\overline{[\nabla \times \boldsymbol{\omega}]^2},$$

we may rewrite (3.21) and (3.22) in physical space as

$$D_1(t) = D_1^{\kappa=0}(t) - \frac{1}{9}\kappa t^3 \overline{\boldsymbol{\omega}^2} + \frac{1}{18}t^4 \left[\kappa^2 \frac{1}{2}\overline{[\nabla \times \boldsymbol{\omega}]^2} + 2\kappa \int d\mathbf{p} \frac{p^2}{\tau_*(p)} Q(p) \right] + O(t^5); \quad (3.23)$$

$$D_2(t) = D_2^{\kappa=0}(t) + O(t^5). \quad (3.24)$$

Evidently to $O(t^3)$ Saffman's conclusion of destructive interference of the molecular diffusivity with the turbulent diffusivity is confirmed. However, the positive sign of the t^4 term in (3.23) raises the possibility that the interference may not remain destructive at larger values of t . In other words we wish to investigate whether $D(t) < D^{\kappa=0}(t)$ at large values of t .

3.6 Long-term effective diffusivity

To address this question of long-term interference, we consider in this section a simplified case wherein the energy spectrum of the flow is given by

$$E(k, 0) = \frac{3}{2}u^2\delta(k - k_0). \quad (3.25)$$

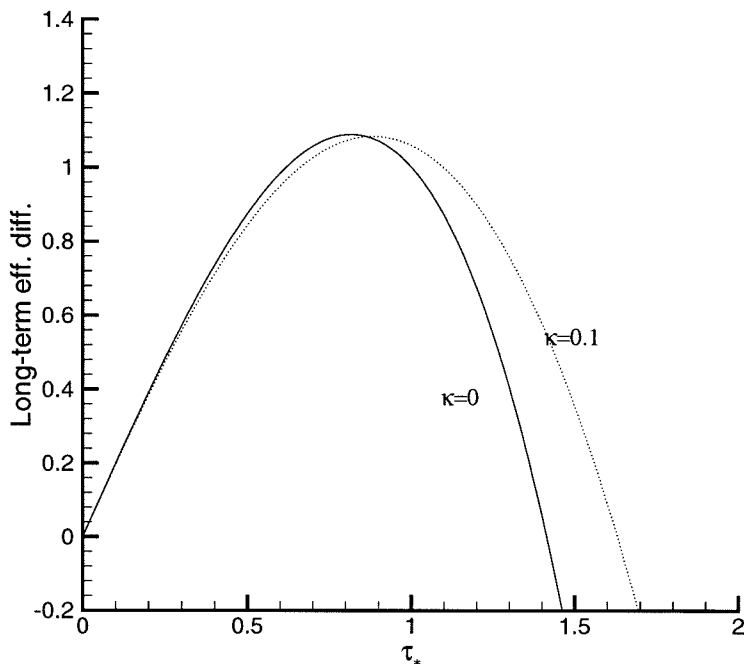


Figure 3.1: Long-term diffusivity for small molecular diffusivity.

The time correlation function is as in (3.19), so

$$Q(k, t) = \frac{3u^2}{8\pi k_0^2} \delta(k - k_0) e^{-|t|/\tau_*},$$

and the correlation time τ_* does not depend on the scale. The FDC2 equation for $D(t)$, (3.15) then simplifies considerably, and taking the limit as $t \rightarrow \infty$ gives (twice) the long-term effective diffusivity

$$\begin{aligned} \dot{D}(\infty) \equiv \lim_{t \rightarrow \infty} \frac{d}{dt} D(t) &= 2\kappa + \frac{2u^2}{\tau_*^{-1} + \kappa k_0^2} \\ &- \frac{1}{8\kappa^4 k_0^8 (\tau_*^{-1} + \kappa k_0^2)} \left\{ 2\kappa k_0^2 (3\tau_*^{-2} + 12\kappa k_0^2 \tau_*^{-1} + 7\kappa^2 k_0^4) - \right. \\ &\left. - 3\tau_*^{-1} (\tau_*^{-1} + 3\kappa k_0^2) (\tau_*^{-1} + 2\kappa k_0^2) \log(1 + 2\kappa k_0^2 \tau_*^{-1}) \right\}. \end{aligned} \quad (3.26)$$

In Figures 3.1 and 3.2 the values of $k_0 \dot{D}(\infty)/u$ are plotted against the nondimensional correlation time $\tilde{\tau}_* \equiv u k_0 \tau_*$ for various values of the nondimensional molecular

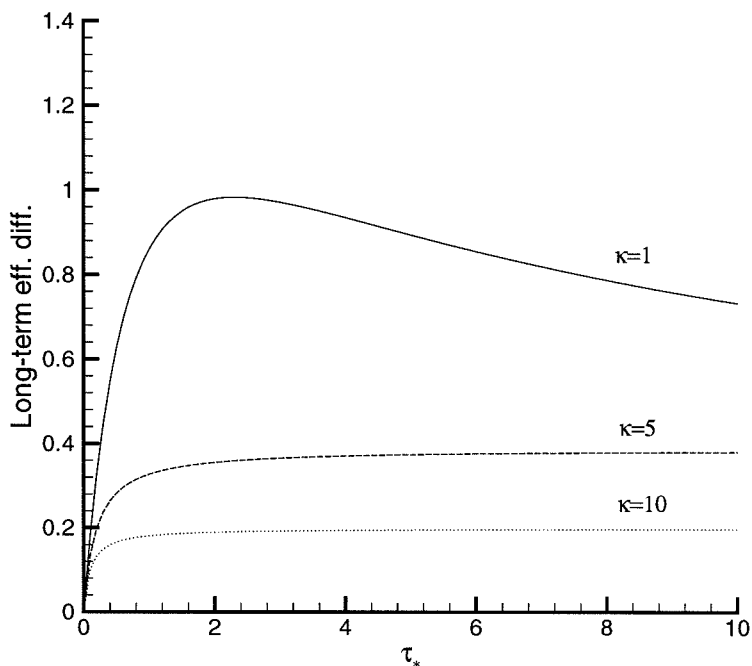


Figure 3.2: Long-term diffusivity for larger values of the molecular diffusivity.

diffusivity $\tilde{\kappa} \equiv k_0 \kappa / u$. Henceforth we will use these nondimensional quantities (unless indicated otherwise) and drop the tildes. From Figure 3.1 we see that for low values of τ_* the nonzero molecular diffusivity lowers the effective diffusivity, indicating that the effect found by Saffman persists in the long term, at least for the spectrum (3.25).

3.7 Convergence of the FDC series

The functional derivative closure method has been shown in Chapter 2 to provide a perturbation series in τ_* for a simpler one-dimensional problem. The negative diffusivities shown in Figure 3.1 for τ_* above 1.4 indicate that the FDC approximation is failing to give physically reasonable results when τ_* is not sufficiently small, at least when κ is also small. In Figure 3.2, however, κ is larger and the values of the effective diffusivity are more physically plausible. The convergence properties of the FDC

series can be elucidated by taking the $\kappa \rightarrow 0$ limit of (3.26):

$$\lim_{\kappa \rightarrow 0} \dot{D}(\infty) = 2u^2\tau_* - u^4k_0^2\tau_*^3 \quad (\text{dimensional}), \quad (3.27)$$

or when nondimensionalized:

$$\lim_{\kappa \rightarrow 0} \frac{k_0}{u} \dot{D}(\infty) = 2\tau_* - \tau_*^3. \quad (3.28)$$

We expect that further terms in the series are higher powers of τ_* , thus leading to the necessary condition for convergence of $\tau_* \ll 1$. This applies to the $\kappa \rightarrow 0$ limit which we have taken above, but by rewriting (3.26) in terms of κ and $\lambda \equiv 1/(\kappa\tau_*)$:

$$\begin{aligned} \frac{k_0}{u} \dot{D}(\infty) = & 2\kappa + \frac{1}{\kappa} \frac{2}{(1+\lambda)} - \\ & - \frac{1}{8\kappa^3} \frac{1}{(1+\lambda)^2} \left\{ 2(3\lambda^2 + 12\lambda + 7) - 3\lambda(\lambda + 3)(\lambda + 2) \log \left(1 + \frac{2}{\lambda} \right) \right\}, \end{aligned} \quad (3.29)$$

we see that for finite λ the series may be considered an expansion in powers of $\frac{1}{\kappa}$ for large κ . This explains the improvement in behavior of Figure 3.2 over Figure 3.1: because the nondimensional molecular diffusivity κ is larger, the retention of just two terms of the FDC series gives a better approximation to the true value of the effective diffusivity—in particular we no longer get the negative values for $\dot{D}(\infty)$; instead it approaches an asymptotic positive value as $\tau_* \rightarrow \infty$.

This improvement in convergence of the FDC series is not surprising when we consider that the nondimensional molecular diffusivity is the inverse of the Péclet number Pe , which in turn is equal to the product of the Prandtl and Reynolds numbers:

$$\kappa^{-1} = Pe = PrRe \equiv \frac{\nu}{\kappa} \frac{u}{\nu k_0} \quad (\text{dimensional}).$$

Thus the large- κ region of improved convergence corresponds to small Péclet number, i.e., small Prandtl and/or Reynolds numbers. This small parameter is available to generate a perturbation series when τ_* is not sufficiently small.

3.8 Symbolic computation of higher order terms

3.8.1 Delta-function spectrum

As mentioned in Section 3.4 the diagram rules facilitate symbolic computation of the $\widehat{\Theta}(\mathbf{k}, t)$ approximations and so too of the long-term diffusivity. Let us review the setup which yielded equation (3.28) above: we had $Q(k, t)$ given by

$$\begin{aligned} Q(k, t) &= \frac{3u^2}{8\pi k_0^2} \delta(k - k_0) e^{-|t|/\tau_*}, \\ &= \frac{1}{4\pi k^2} E_a(k) R_a(t, k), \end{aligned}$$

with $E_a = 3/2u^2\delta(k - k_0)$ and $R_a = \exp(-|t|/\tau_*)$, and then we took $\kappa \rightarrow 0$ and examined the $t \rightarrow \infty$ or long-term limit. As we are taking $\kappa = 0$ from here on, we will adopt the convenient symbol $\kappa(t)$ for the nondimensional effective diffusivity, i.e.,

$$\kappa(t) \equiv \lim_{\kappa \rightarrow 0} \frac{k_0}{2u} \dot{D}(t).$$

With a view to obtaining further terms in the series (3.28), we implement the diagram rules with the above setup in *Mathematica*. The delta-function spectrum reduces all wavevector integrals to angular integrals, while the time integrals may be done separately and straightforwardly to yield the appropriate power of τ_* . Finally the angular integrals are also performed on *Mathematica*. All integration is done analytically so the results for each diagram are exact. The following is the expression for the nondimensional long-term diffusivity, correct to order τ_*^9 :

$$\kappa(\infty) = \tau_* - \frac{1}{2}\tau_*^3 + \frac{11}{24}\tau_*^5 - \frac{4061}{7200}\tau_*^7 + \frac{8775029}{10080000}\tau_*^9 + \dots \quad (3.30)$$

Note the alternating signs of the coefficients, and the fact that all coefficients are $O(1)$. This series does not converge quickly (if at all), nor should we expect it to—the FDC method is justified (see Chapter 1) as a perturbation method for small correlation time, so we must accept (3.30) as a possibly divergent asymptotic series.

3.8.2 Padé approximation

We are thus motivated to examine methods for summing perturbation series. One well-known method is Padé approximation [15]. Briefly, given a power series $f(z) = \sum_{n=0}^{\infty} a_n z^n$, the Padé approximant $P_M^N(z)$ is a rational function, i.e., a ratio of two polynomials, with numerator of degree N and denominator of degree M , whose Taylor series agrees with $f(z)$ for the first $N + M + 1$ terms. To examine the Padé approximants to (3.30) we rewrite

$$\kappa(\infty) = \tau_* \left[1 - \frac{1}{2}\tau_*^2 + \frac{11}{24}\tau_*^4 - \frac{4061}{7200}\tau_*^6 + \frac{8775029}{10080000}\tau_*^8 + \dots \right], \quad (3.31)$$

let $z = \tau_*^2$, and consider the Padé approximants for the term in square brackets in (3.31):

$$\begin{aligned} P_1^0(z) &= \frac{1}{1 + \frac{1}{2}z} \\ P_1^1(z) &= \frac{1 + \frac{5}{12}z}{1 + \frac{11}{12}z} \\ P_2^1(z) &= \frac{1 + \frac{1661}{1500}z}{1 + \frac{2411}{1500}z + \frac{259}{750}z^2} \\ P_2^2(z) &= \frac{1 + \frac{8514637}{4351200}z + \frac{18482041}{52214400}z^2}{1 + \frac{10690237}{4351200}z + \frac{58691863}{52214400}z^2}. \end{aligned} \quad (3.32)$$

From Figure 3.3 we can see that the Padé approximants appear to be converging and doing so much more rapidly than the basic series (3.30).

The convergence theory of Padé approximants is chiefly based upon Stieltjes series, i.e., a series of the form

$$\sum_{n=0}^{\infty} a_n (-z)^n,$$

where the coefficients a_n are the moments of a real nonnegative function $\rho(s)$:

$$a_n = \int_0^{\infty} s^n \rho(s) ds, \quad \rho(s) \geq 0 \quad (0 \leq s < \infty).$$

For these series it can be shown (see [15], [16]) that when z is fixed, $P_M^N(z)$ decreases

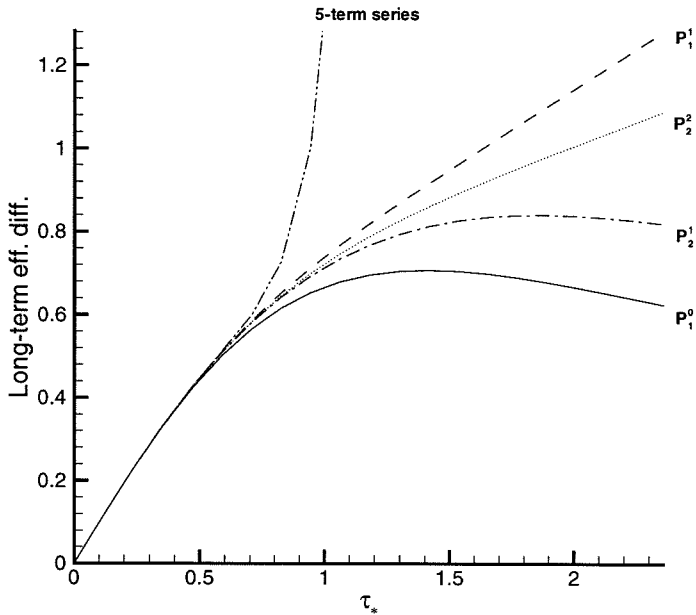


Figure 3.3: The FDC5 approximation to $\kappa(\infty)$ and its Padé approximants for spectrum E_a , time correlation R_a and $\omega_k = 1/\tau_*$.

monotonically as N increases, $P_{N+1}^N(z)$ increases monotonically as N increases, and that $P_N^N(z) \rightarrow P_{N+1}^N(z)$ as $N \rightarrow \infty$. Although we cannot prove that our series (3.30) is a Stieltjes series, the available Padé approximants do indeed have these properties. Thus we conjecture that $\tau_* P_2^1(\tau_*^2)$ provides a lower bound for the nondimensional effective diffusivity and that $\tau_* P_2^2(\tau_*^2)$ provides an upper bound, i.e.,

$$\tau_* P_2^1(\tau_*^2) \leq \kappa(\infty) \leq \tau_* P_2^2(\tau_*^2). \quad (3.33)$$

Since $P_2^1(\tau_*^2)$ and $P_2^2(\tau_*^2)$ differ by only about 1% even at $\tau_* = 1$, we conclude that (3.33) gives an accurate approximation for the long term effective diffusivity for correlation times as large as $(uk_0)^{-1}$.

3.8.3 More general spectra

Even when the energy spectrum does not have the simple delta-function form considered above, the FDC integrals can always be reduced to multiple integrals over

Energy spectrum	Time correlation	ω_k	Coeff. of τ_*	Coeff. of τ_*^3	Coeff. of τ_*^5	Coeff. of τ_*^7	Figure
E_a	R_a	$1/\tau_*$	1.000	-0.500	0.459	-0.564	3.3
E_a	R_b	$1/\tau_*$	0.886	-0.184	0.050		
E_a	R_c	$1/\tau_*$	0.200	0.052	-0.016	0.0047	
E_b	R_a	$1/\tau_*$	1.000	-1.250	3.906	-19.13	
E_b	R_a	k/τ_*	0.753	-0.352	0.323	-0.413	3.4
E_b	R_a	k^2/τ_*	0.667	-0.222	0.140	-0.116	
E_b	R_b	$1/\tau_*$	0.886	-0.459	0.429		
E_b	R_b	k/τ_*	0.667	-0.128	0.034		3.5
E_b	R_b	k^2/τ_*	0.591	-0.087	0.019		
E_b	R_c	k/τ_*	0.113	0.034	-0.007	0.0013	
$E_c, \beta = 1$	R_a	$1/\tau_*$	1.000	-1.027	2.221	-6.925	
$E_c, \beta = 10$	R_a	$1/\tau_*$	1.000	-7.35	318.1	-23711	
$E_c, \beta = 1$	R_a	k/τ_*	0.741	-0.363	0.333	-0.416	
$E_c, \beta = 10$	R_a	k/τ_*	0.492	-0.211	0.189	-0.254	3.6
$E_c, \beta = 1$	R_a	k^2/τ_*	0.569	-0.162	0.085	-0.060	3.7
$E_c, \beta = 10$	R_a	k^2/τ_*	0.313	-0.049	0.015	-0.006	
$E_d, \beta = 1$	R_a	$1/\tau_*$	1.000	-1.167	2.810	-9.585	
$E_d, \beta = 10$	R_a	$1/\tau_*$	1.000	-22.17	1424	-133109	3.8
$E_d, \beta = 1$	R_a	k/τ_*	0.693	-0.340	0.312	-0.389	3.9
$E_d, \beta = 10$	R_a	k/τ_*	0.240	-0.098	0.089	-0.120	
$E_d, \beta = 1$	R_a	k^2/τ_*	0.500	-0.125	0.056	-0.036	
$E_d, \beta = 10$	R_a	k^2/τ_*	0.091	-0.004	0.0004		

Table 3.1: Coefficients of the FDC series for the long-term effective diffusivity.

wavenumbers and time by doing all the angular integrals exactly. Moreover, for simple forms of the time correlation R , the time integrals may also be done exactly. We have calculated the first few terms in the FDC series for the long-term effective diffusivity for variety of spectral shapes and time correlation functions. Specifically, we list in Tables 3.1 and 3.2 results of the form (3.31) for the following energy spectra

Energy spectrum	Time correlation	ω_k	$P_1^0(\tau_*^2)$ at $\tau_* = 1$	$P_1^1(\tau_*^2)$ at $\tau_* = 1$	$P_2^1(\tau_*^2)$ at $\tau_* = 1$	Figure
E_a	R_a	$1/\tau_*$	0.667	0.739	0.714	3.3
E_a	R_b	$1/\tau_*$	0.734	0.742		
E_a	R_c	$1/\tau_*$	0.270	0.240	0.240	
E_b	R_a	$1/\tau_*$	0.444	0.697	0.541	3.4
E_b	R_a	k/τ_*	0.513	0.569	0.549	
E_b	R_a	k^2/τ_*	0.500	0.530	0.522	
E_b	R_b	$1/\tau_*$	0.584	0.649		3.5
E_b	R_b	k/τ_*	0.559	0.565		
E_b	R_b	k^2/τ_*	0.515	0.520		
E_b	R_c	k/τ_*	0.160	0.140	0.140	
$E_c, \beta = 1$	R_a	$1/\tau_*$	0.493	0.675	0.578	
$E_c, \beta = 10$	R_a	$1/\tau_*$	0.120	0.834	0.208	
$E_c, \beta = 1$	R_a	k/τ_*	0.497	0.551	0.532	
$E_c, \beta = 10$	R_a	k/τ_*	0.345	0.381	0.367	3.6
$E_c, \beta = 1$	R_a	k^2/τ_*	0.443	0.463	0.458	3.7
$E_c, \beta = 10$	R_a	k^2/τ_*	0.271	0.275	0.274	
$E_d, \beta = 1$	R_a	$1/\tau_*$	0.462	0.658	0.549	
$E_d, \beta = 10$	R_a	$1/\tau_*$	0.043	0.660	0.080	3.8
$E_d, \beta = 1$	R_a	k/τ_*	0.465	0.516	0.498	3.9
$E_d, \beta = 10$	R_a	k/τ_*	0.170	0.189	0.182	
$E_d, \beta = 1$	R_a	k^2/τ_*	0.400	0.415	0.411	
$E_d, \beta = 10$	R_a	k^2/τ_*	0.087	0.087	0.087	

Table 3.2: Padé approximations to the FDC series in Table 3.1.

and time correlation functions:

$$\begin{aligned}
E_a(k) &= \frac{3}{2}u^2\delta(k - k_0) \\
E_b(k) &= \frac{4u^2k^4}{\sqrt{\pi}k_0^5} \exp(-k^2/k_0^2) \\
E_c(k) &= \begin{cases} \frac{1}{1-(1+\beta)^{-\frac{2}{3}}}u^2k_0^{\frac{2}{3}}k^{-\frac{5}{3}} & \text{for } k_0 < k < (1 + \beta)k_0, \\ 0 & \text{otherwise} \end{cases} \\
E_d(k) &= \begin{cases} \frac{3u^2}{2k_0\beta} & \text{for } k_0 < k < (1 + \beta)k_0, \\ 0 & \text{otherwise} \end{cases} \\
R_a(t, k) &= \exp(-\omega_k|t|) \\
R_b(t, k) &= \exp(-\omega_k^2t^2)
\end{aligned} \tag{3.34}$$

where the “inverse correlation time” ω_k equals one of $1/\tau_*$, k/τ_* or k^2/τ_* . Spectrum E_b is often used to approximate the final stages of decaying turbulence; spectrum E_c models an “inertial range,” and the constant spectrum E_d is used to investigate the behavior of the approximation when the spectrum does not decrease with increasing k . Each spectrum is normalized so that

$$\int_0^\infty E(k)dk = \frac{3}{2}u^2.$$

The time correlation function R_a makes the time integrals very simple; however, it is not differentiable at $t = 0$ and so we include R_b as a more realistic model. Note that both the above time correlation functions are positive for all t ; we also consider the effect of negative loops in R when we use

$$R_c(t, k) = e^{-|t|/\tau_*} \cos(2t/\tau_*).$$

Padé approximants like (3.32) for certain cases from Table 3.1 are plotted in

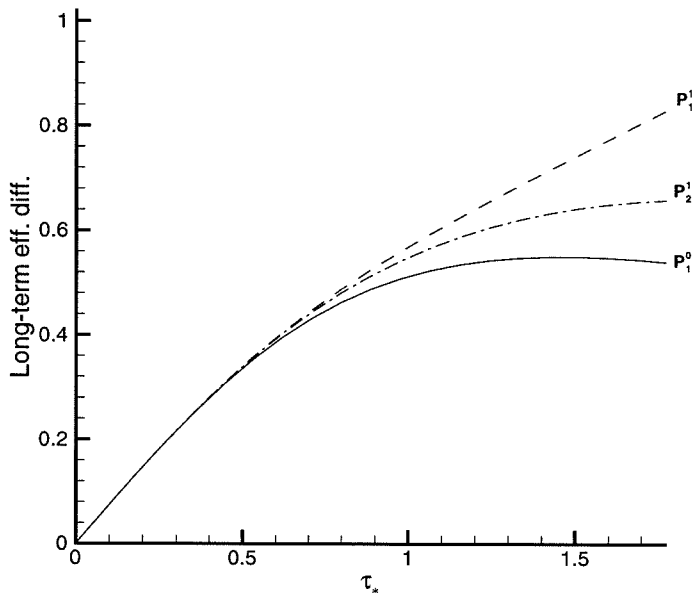


Figure 3.4: Padé approximants for $\kappa(\infty)$ for spectrum E_b , time correlation R_a and $\omega_k = k/\tau_*$.

Figures 3.3 to 3.10. For each case we calculate the integral length

$$L = \frac{3\pi \int_0^\infty k^{-1} E(k) dk}{4 \int_0^\infty E(k) dk}$$

and plot the available approximants for values of τ_* running from zero to L/u .

In general there is not much difference between the approximations resulting from correlations R_a and R_b (see Figures 3.4 and 3.5), indicating that the shape of the correlation function near $t = 0$ is not critical to the value of $\kappa(\infty)$. Note also that the convergence of the approximations is improved when passing from $\omega_k = 1/\tau_*$ to $\omega_k = k/\tau_*$ to $\omega_k = k^2/\tau_*$ (Figures 3.6 to 3.9). Indeed the pathological case shown in Figure 3.8 which results from the constant spectrum E_d and $\omega_k = 1/\tau_*$ is dramatically improved when we take $\omega_k = k/\tau_*$ instead— see Figure 3.9. This bodes well for application to realistic velocity fields, as we expect the correlation time to have some dependence on the scale k , for example $\omega_k = k/\tau_*$ rather than the scale-independent $\omega_k = 1/\tau_*$.

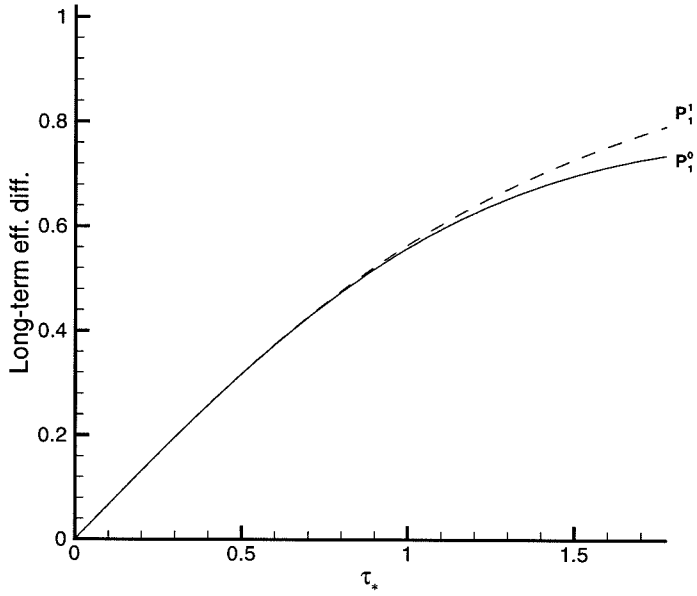


Figure 3.5: Padé approximants for $\kappa(\infty)$ for spectrum E_b , time correlation R_b and $\omega_k = k/\tau_*$.

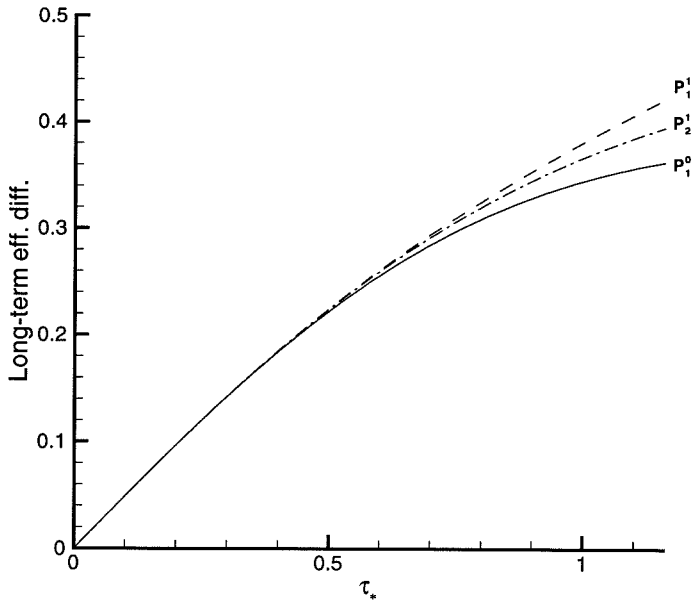


Figure 3.6: Padé approximants for $\kappa(\infty)$ for spectrum E_c ($\beta = 10$), time correlation R_a and $\omega_k = k/\tau_*$.

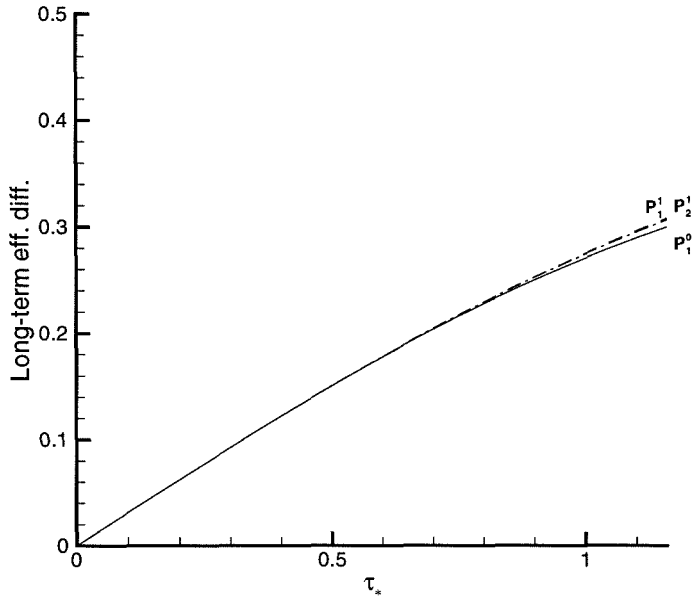


Figure 3.7: Padé approximants for $\kappa(\infty)$ for spectrum E_c ($\beta = 10$), time correlation R_a and $\omega_k = k^2/\tau_*$.

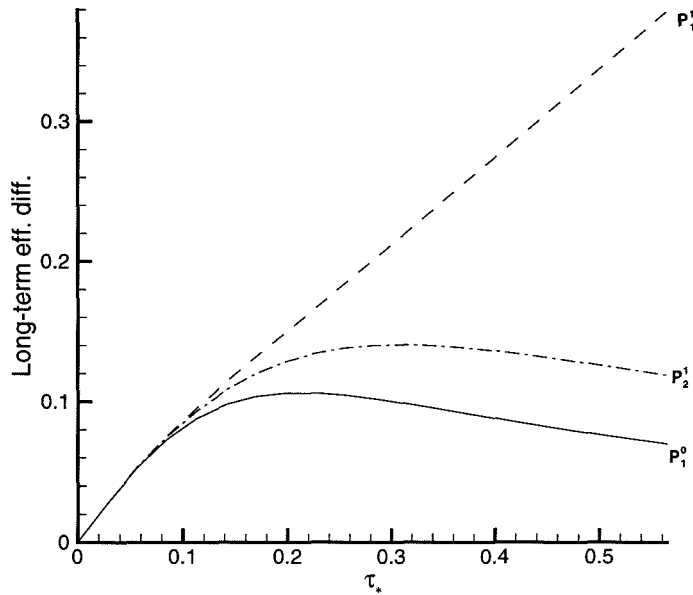


Figure 3.8: Padé approximants for $\kappa(\infty)$ for spectrum E_d ($\beta = 10$), time correlation R_a and $\omega_k = 1/\tau_*$.

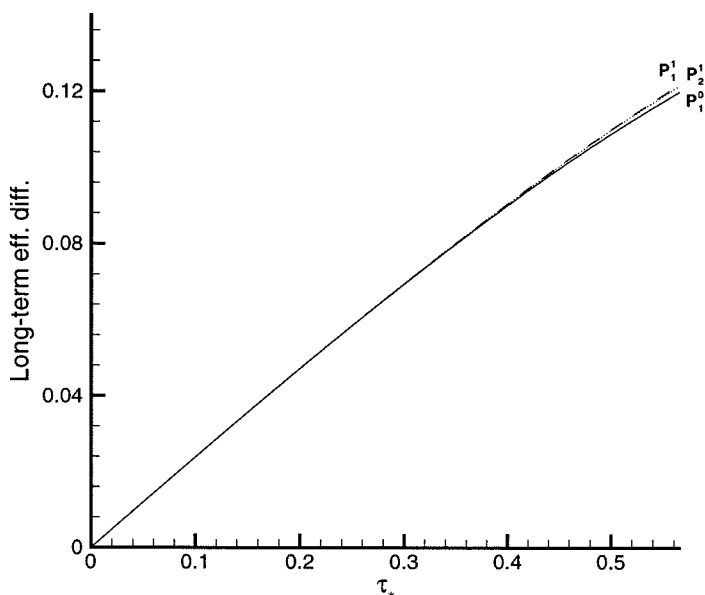


Figure 3.9: Padé approximants for $\kappa(\infty)$ for spectrum E_d ($\beta = 10$), time correlation R_a and $\omega_k = k/\tau_*$.

In all cases with time correlation R_a and R_b we find behavior of the Padé approximants which we term *Stieltjes-like*, i.e., the power series coefficients alternate in sign, P_N^N decreases monotonically and P_{N+1}^N increases monotonically as N increases, with no poles of the approximants being on the positive real axis. This leads us to conjecture that Padé approximants provide successively improving upper and lower bounds on the long-term effective diffusivity (as they are known to do for Stieltjes series), when the time correlation function is always positive. However, for time correlation R_c the sign pattern of the power series coefficients violates the Stieltjes rule, and indeed we find a pole of the P_1^0 approximant for energy spectrum E_a at $\tau_* = 1.96$. Nevertheless the higher order Padé approximants still converge rapidly, so we can still find close approximations for the value of the long-term effective diffusivity although without the neat bounding behavior of the Stieltjes-like series. The accuracy of these approximations is demonstrated by comparison with numerical calculations of the effective diffusivity in Section 3.11.

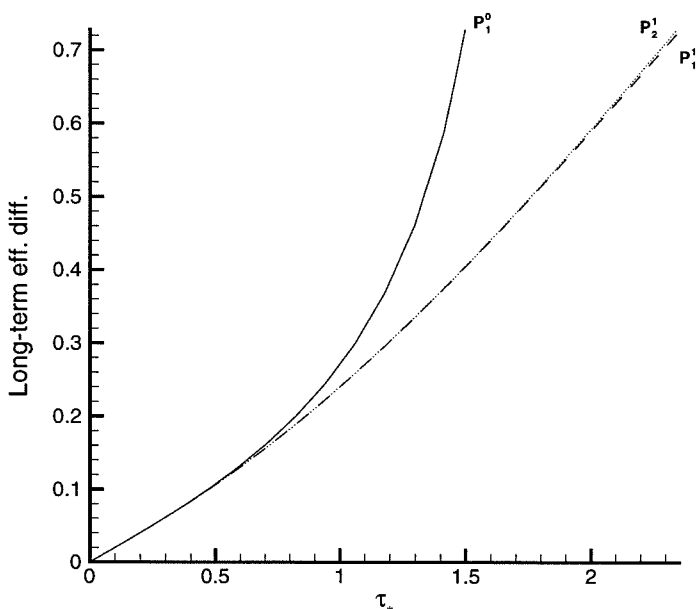


Figure 3.10: Padé approximants for $\kappa(\infty)$ for spectrum E_a , time correlation R_c and $\omega_k = 1/\tau_*$. P_1^0 has a pole at $\tau_* = 1.96$, but P_1^1 and P_2^1 have no poles on the positive real axis.

3.9 Generalized Padé approximation for $\kappa(t)$

We wish to generalize the ideas of the preceding section to the calculation of $\kappa(t)$, the effective diffusivity at finite time. Clearly each diagram contribution can be calculated as before and now generates a function of t . We alter the time variable to $\tilde{t} = t/\tau_*$ and change each integration variable to $\tilde{t}_i = t_i/\tau_*$ to pull a factor of τ_*^{2n-1} outside each FDC n integral (cf. Theorem 2 of Chapter 2). The generalization of (3.31) then has the form

$$\kappa(t) = \tau_* \kappa_1(t/\tau_*) - \tau_*^3 \kappa_2(t/\tau_*) + \tau_*^5 \kappa_3(t/\tau_*) + \dots \quad (3.35)$$

with $\kappa_n(\infty)$ being the FDC n contribution to the long-term effective diffusivity as calculated previously. For example, for the energy spectrum $E_a(k)$ we know from (3.31) that $\kappa_1(\infty) = 1$, $\kappa_2(\infty) = \frac{1}{2}$ and $\kappa_3(\infty) = \frac{11}{24}$. Now we generate the *generalized Padé approximants* to (3.35) by treating each $\kappa_i(t/\tau_*)$ as if it were a constant coefficient in

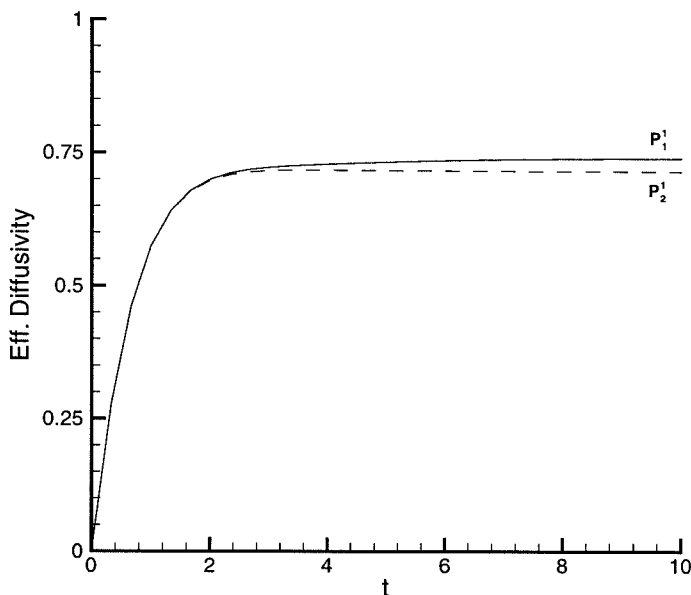


Figure 3.11: Generalized Padé approximants for $\kappa(t)$ for spectrum E_a , time correlation R_a and $\omega_k = 1/\tau_*$, with $\tau_* = 1$.

a τ_* power series. Thus we set

$$P_1^0(\tau_*^2; t) = \frac{\kappa_1(t/\tau_*)}{1 + \frac{\kappa_2(t/\tau_*)}{\kappa_1(t/\tau_*)} \tau_*^2},$$

$$P_1^1(\tau_*^2; t) = \frac{\kappa_1(t/\tau_*) + \frac{\kappa_1(t/\tau_*)\kappa_3(t/\tau_*) - \kappa_2^2(t/\tau_*)}{\kappa_2(t/\tau_*)} \tau_*^2}{1 + \frac{\kappa_3(t/\tau_*)}{\kappa_2(t/\tau_*)} \tau_*^2}.$$

In Figure 3.11 we fix $\tau_* = 1$ and plot the approximations $\tau_* P_1^0(\tau_*^2; t)$ and $\tau_* P_1^1(\tau_*^2; t)$ to $\kappa(t)$ as functions of the time t . The generalized Padé approximants are found to give good approximations for all t and for τ_* up to order one, i.e., for dimensional correlation times on the order of the eddy circulation time, $(uk_0)^{-1}$.

3.10 The Lagrangian correlation

Having introduced the generalized Padé approximation to $\kappa(t)$ for τ_* of order one, we go a step further and consider how this method can approximate the Lagrangian

correlation for isotropic turbulence

$$L(t) = \frac{1}{3} \langle u_i(\mathbf{x}_0, 0) u_i(\mathbf{r}(t), t) \rangle, \quad (3.36)$$

where $\mathbf{r}(t)$ is the position vector of the fluid particle which was at \mathbf{x}_0 at time 0, i.e.,

$$\begin{aligned} \frac{d}{dt} \mathbf{r}(t) &= \mathbf{u}(\mathbf{r}(t), t) \\ \mathbf{r}(0) &= \mathbf{x}_0. \end{aligned} \quad (3.37)$$

The Lagrangian correlation is a very useful quantity in studies of turbulent diffusion and particle dispersion, but for experimental flows the Eulerian correlation (which is measured at two points fixed in space, instead of following a fluid particle as for (3.36)) is much easier to measure. It is therefore of considerable interest to investigate whether a connection can be made between the Lagrangian correlation and the known Eulerian correlation.

It follows from the definition of the Lagrangian correlation that

$$L(t) = \frac{d}{dt} \kappa(t) = \frac{1}{2} \frac{d^2}{dt^2} D(t). \quad (3.38)$$

As we have already detailed an accurate approximation scheme for $\kappa(t)$, it is straightforward to apply it to $L(t)$. We take the series of FDC n integrals (3.35) for $\kappa(t)$:

$$\kappa(t) = \tau_* \kappa_1(t/\tau_*) - \tau_*^3 \kappa_2(t/\tau_*) + \dots \quad (3.39)$$

and differentiate with respect to t to get a series for $L(t)$:

$$L(t) = \frac{d}{dt} \kappa(t) = \kappa'_1(t/\tau_*) - \tau_*^2 \kappa'_2(t/\tau_*) + \dots \quad (3.40)$$

As each of the $\kappa_i(t)$ functions is produced from repeated time integrals, the derivative $\kappa'_i(t)$ reduces to an integral of one dimension less than $\kappa_i(t)$. For example, the FDC2

term $\kappa_2(t)$ is defined by

$$\kappa_2(t) = \frac{1}{3} \int_0^\infty dk_1 \int_0^\infty dk_2 \int_0^t dt_1 \int_0^{t_1} dt_2 \int_0^{t_2} dt_3 E(k_1)E(k_2) \frac{8k_1^2}{3} R(t-t_3, k_1) R(t_1-t_2, k_2),$$

which can be put in a more convenient form by employing the change of variables

$s_1 = t - t_1, s_2 = t_1 - t_2, s_3 = t_2 - t_3$ to obtain:

$$\kappa_2(t) = \frac{1}{3} \int_0^\infty dk_1 \int_0^\infty dk_2 \int_0^t ds_1 \int_0^{t-s_1} ds_2 \int_0^{t-s_1-s_2} ds_3 E(k_1)E(k_2) \frac{8k_1^2}{3} R(s_1+s_2+s_3, k_1) R(s_2, k_2)$$

and then the differentiation is easy to perform:

$$\begin{aligned} \kappa_2'(t) &= \frac{1}{3} \int_0^\infty dk_1 \int_0^\infty dk_2 \int_0^t ds_1 \int_0^{t-s_1} ds_2 E(k_1)E(k_2) \frac{8k_1^2}{3} R(t, k_1) R(s_2, k_2) \\ &= \frac{1}{3} \int_0^\infty dk_1 \int_0^\infty dk_2 \int_0^t dt_1 \int_0^{t_1} dt_2 E(k_1)E(k_2) \frac{8k_1^2}{3} R(t, k_1) R(t_1 - t_2, k_2). \end{aligned}$$

From (3.40) we generate the generalized Padé approximants for $L(t)$ as we did above for $\kappa(t)$. In the cases we have calculated these converge remarkably quickly, so that $P_1^0(\tau_*^2; t)$ and $P_1^1(\tau_*^2; t)$ give very good approximations even at $\tau_* = 1$. It is therefore worth explicitly recording the approximations these give for $L(t)$ in terms of the Eulerian correlation functions:

$$L(t) = L_1(t/\tau_*) - \tau_*^2 L_2(t/\tau_*) + \dots$$

with

$$\begin{aligned} L_1(t) &= \frac{1}{3} \int_0^\infty dk_1 E(k_1) R(t, k_1) \\ L_2(t) &= \frac{1}{3} \int_0^\infty dk_1 \int_0^\infty dk_2 \int_0^t dt_1 \int_0^{t_1} dt_2 E(k_1)E(k_2) \frac{8k_1^2}{3} R(t, k_1) R(t_1 - t_2, k_2), \end{aligned}$$

and the Padé approximants to $L(t)$ are then

$$P_1^0(\tau_*^2; t) = \frac{L_1(t/\tau_*)}{1 + \frac{L_2(t/\tau_*)}{L_1(t/\tau_*)}\tau_*^2}$$

$$P_1^1(\tau_*^2; t) = \frac{L_1(t/\tau_*) + \frac{L_1(t/\tau_*)L_3(t/\tau_*) - L_2^2(t/\tau_*)}{L_2(t/\tau_*)}\tau_*^2}{1 + \frac{L_3(t/\tau_*)}{L_2(t/\tau_*)}\tau_*^2}$$

In the next section we generate a random velocity field with a given Eulerian spectrum and advect particles according to (3.37). These numerical simulations show that the FDC-Padé approximations to the Lagrangian correlation are indeed accurate for τ_* of order 1, i.e., for dimensional correlation times on the order of the eddy circulation time, $(uk_0)^{-1}$.

3.11 Numerical simulation of advection by a random velocity field

We create a random velocity field with prescribed statistics and follow fluid particles as they advect, recording the statistical quantities for comparison with the theory of the previous sections. We consider Gaussian velocity fields and choose the velocity spectrum to be of the form

$$Q(k, t) = \frac{1}{4\pi k^2} E_m(k) R_l(t, k), \text{ with } m, l = 1 \text{ or } 2.$$

and

$$E_1(k) = E_a(k) = \frac{3}{2} u^2 \delta(k - k_0)$$

$$E_2(k) = E_b(k) = \frac{4u^2 k^4}{\sqrt{\pi} k_0^5} \exp(-k^2/k_0^2)$$

$$R_1(t, k) = \exp(-\omega_0^2 t^2)$$

$$R_2(t, k) = \exp(-\frac{1}{2} k^2 t^2). \tag{3.41}$$

The velocity field is generated using a method based on that used by Kraichnan [17]. In each realization, we set

$$\mathbf{u}(\mathbf{x}, t) = A \sum_{n=1}^N \{ \mathbf{z}_n \cos [\mathbf{k}_n \cdot \mathbf{x} + \omega_n t] + \mathbf{y}_n \sin [\mathbf{k}_n \cdot \mathbf{x} + \omega_n t] \}. \quad (3.42)$$

To ensure incompressibility, we have

$$\mathbf{z}_n = \mathbf{k}_n \times \boldsymbol{\xi}_n \text{ and } \mathbf{y}_n = \mathbf{k}_n \times \boldsymbol{\eta}_n,$$

with $\boldsymbol{\xi}_n$ and $\boldsymbol{\eta}_n$ chosen from independent Gaussian distributions. The frequencies ω_n are chosen from a Gaussian distribution with standard deviation ω_0 to produce R_1 ; for R_2 we set $\omega_n = |\mathbf{k}_n|$. The vectors \mathbf{k}_n are chosen from a distribution shaped so as to produce the desired energy spectrum $E_m(k)$: for $E_1(k)$ the \mathbf{k}_n are isotropically distributed on a sphere of radius k_0 , whereas for $E_2(k)$ each component of \mathbf{k}_n is selected from independent Gaussian distributions of standard deviation k_0 . The amplitude A is chosen so that

$$\begin{aligned} \langle u_i(\mathbf{x}, t) u_i(\mathbf{x}, t) \rangle &= 2 \int_0^\infty E(k) dk \\ &= 3u^2, \end{aligned} \quad (3.43)$$

so for E_1 , $A = \sqrt{\frac{3}{2N}} \frac{u}{k_0}$ and for E_2 , $A = \frac{1}{\sqrt{N}} \frac{u}{k_0}$. The number of modes N is taken to be 100. In Figure 3.12 we plot the average over 2000 realizations of $u_i(\mathbf{x}, t) u_i(\mathbf{x} + \mathbf{r}, t)$ as a function of $r = |\mathbf{r}|$ for the spectrum $E_1(k)$ —this is compared to the exact correlation function which is

$$\begin{aligned} \langle u_i(\mathbf{x}, t) u_i(\mathbf{x} + \mathbf{r}, t) \rangle &= 2 \int_0^\infty E_1(k) \frac{\sin(kr)}{kr} dk \\ &= 3u^2 \frac{\sin(k_0 r)}{k_0 r}. \end{aligned} \quad (3.44)$$

Having obtained a satisfactory velocity field, we proceed to follow fluid particles

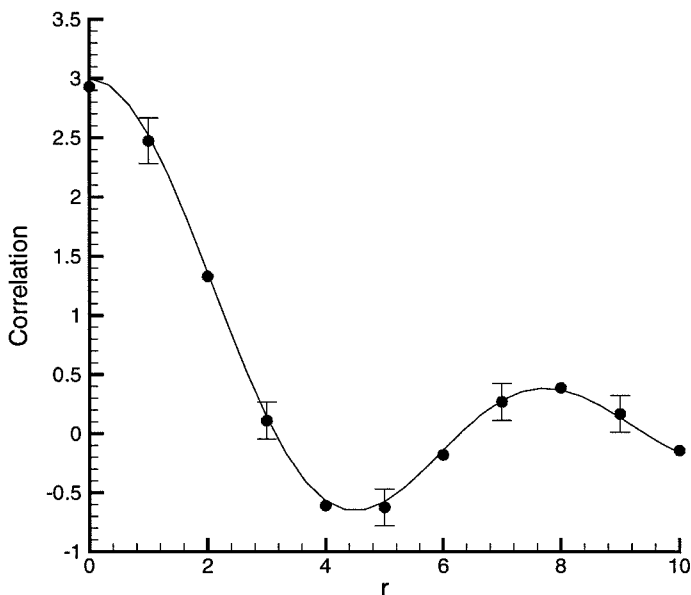


Figure 3.12: Comparison of exact (solid line) and numerical (symbols) correlation functions for spectrum E_1 .

as they are advected by:

$$\begin{aligned} \frac{d}{dt}\mathbf{r}(t) &= \mathbf{u}(\mathbf{r}(t), t) \\ \mathbf{r}(0) &= \mathbf{0}. \end{aligned} \tag{3.45}$$

In each realization, (3.45) is solved by using a fourth-order predictor-corrector scheme due to Hamming [18], with starting values formed by iteration of Newton's interpolation formula [19]. A time step of 0.2 was found to be satisfactory, and each fluid particle was advected for up to 75 steps (i.e., 15 eddy circulation times). The numerical approximations for the effective diffusivity $\kappa(t)$ and the Lagrangian

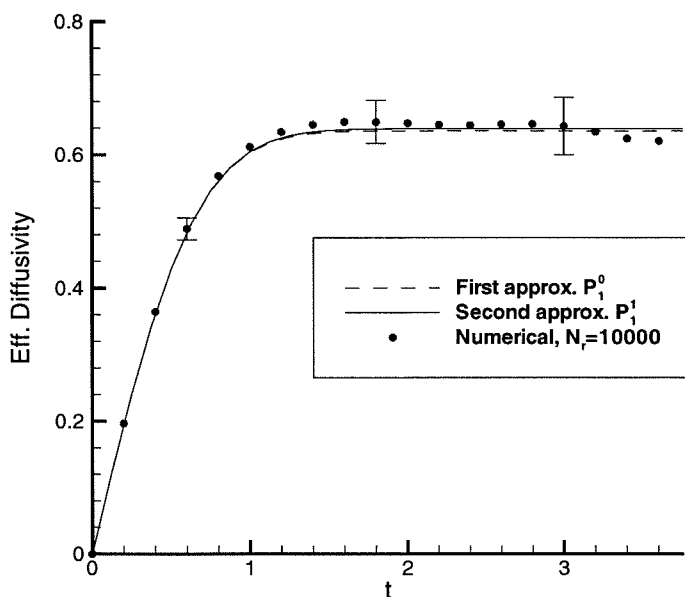


Figure 3.13: Generalized Padé approximants (lines) and numerical values (dots) for $\kappa(t)$ for spectrum E_a , time correlation R_b and $\omega_k = 1/\tau_*$. Here τ_* is fixed, $\tau_* = \sqrt{2/3}$.

correlation $L(t)$ are then calculated from

$$\begin{aligned}\kappa(t) &= \frac{1}{3N_r} \sum_{i=1}^{N_r} \mathbf{r}^{(i)}(t) \cdot \mathbf{u}^{(i)}(\mathbf{r}^{(i)}(t), t), \\ L(t) &= \frac{1}{3N_r} \sum_{i=1}^{N_r} \mathbf{u}^{(i)}(\mathbf{0}, 0) \cdot \mathbf{u}^{(i)}(\mathbf{r}^{(i)}(t), t).\end{aligned}\quad (3.46)$$

3.12 Results

In Figures 3.13 and 3.14 the statistical quantities (3.46) are compared to the corresponding FDC-Padé approximations which are calculated as outlined in Sections 3.9 and 3.10. The number of realizations, N_r , is recorded in the legend. The 95% confidence intervals are marked as error bars. Figure 3.13 uses energy spectrum E_1 and time correlation R_1 with $\omega_0 = 1/\tau_* = \sqrt{2/3}$. In Figure 3.14 we use the spectrum E_2 and time correlation R_2 which are equivalent to the spectrum E_b and correlation R_b of Section 3.8.3 if τ_* is taken to be $\sqrt{2}$. Thus the space-time correlation function

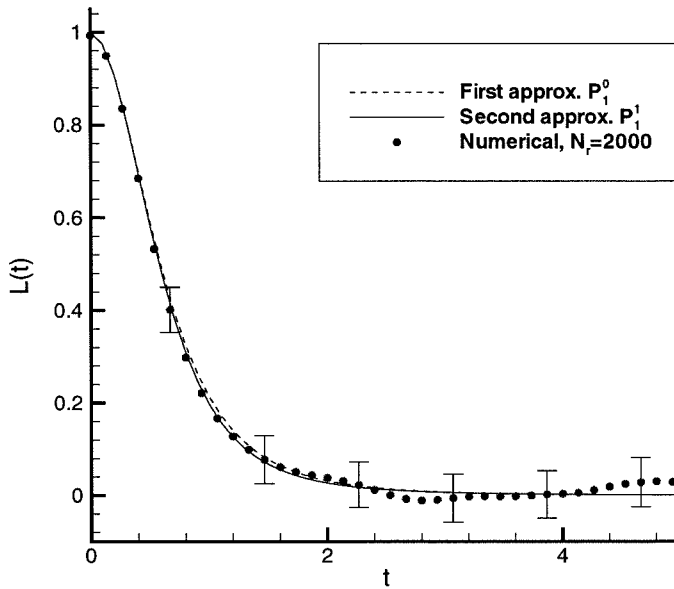


Figure 3.14: Generalized Padé approximants (lines) and numerical values (dots) for $L(t)$ for spectrum E_b , time correlation R_b and $\omega_k = k/\tau_*$. Here τ_* is fixed, $\tau_* = \sqrt{2}$.

is

$$Q(k, t) = \frac{u^2 k^2}{\pi^{\frac{3}{2}} k_0^5} \exp(-k^2/k_0^2) \exp(-\frac{1}{2} u^2 k^2 t^2) \quad (\text{dimensional}), \quad (3.47)$$

which is was also used by Saffman [12].

It is clear that the FDC-Padé approximations are extremely good, even for values of the correlation time τ_* of order one. In each case the second approximation P_1^1 gives a small but definite improvement over the first approximation P_1^0 . Even the lowest order Padé approximants give reasonable results which means the lowest order FDC diagrams are all that need to be calculated in order to closely approximate the effective diffusivity and Lagrangian correlation using the methods of Sections 3.9 and 3.10.

3.13 Approximation of the mean concentration

We consider here the FDC1 equation for the mean concentration $\Theta(\mathbf{x}, t)$ which was derived as equation (3.12):

$$\frac{\partial}{\partial t}\Theta(\mathbf{x}, t) - \kappa\nabla^2\Theta(\mathbf{x}, t) = \frac{\partial^2}{\partial x_i\partial x_j} \int_0^t dt_1 \int d\mathbf{y} \langle u_i(\mathbf{x}, t)u_j(\mathbf{y}, t_1) \rangle G(\mathbf{x} - \mathbf{y}, t - t_1)\Theta(\mathbf{y}, t_1).$$

In many cases of interest, the molecular diffusivity is negligible compared to the turbulent diffusivity, so we can set κ to zero. Then $G(\mathbf{x} - \mathbf{y}, t - t_1)$ becomes a delta function and we have

$$\frac{\partial}{\partial t}\Theta(\mathbf{x}, t) = \frac{\partial^2}{\partial x_i\partial x_j} \int_0^t \langle u_i(\mathbf{x}, t)u_j(\mathbf{x}, t_1) \rangle \Theta(\mathbf{x}, t_1) dt_1 \quad (3.48)$$

For isotropic stationary turbulence, $\langle u_i(\mathbf{x}, t)u_j(\mathbf{x}, t_1) \rangle = u^2\delta_{ij}R(t - t_1)$, where u is the r.m.s. velocity and $R(t)$ is the Eulerian two-time correlation function. Equation (3.48) becomes

$$\frac{\partial\Theta}{\partial t}(\mathbf{x}, t) = u^2\nabla^2 \int_0^t R(t - t_1)\Theta(\mathbf{x}, t_1) dt_1. \quad (3.49)$$

This equation is a common approximation and arises in many different closure schemes. In particular Saffman [20] derives it using a Wiener-Hermite expansion. He solves for the evolution of $\Theta(\mathbf{x}, t)$ from a delta function initial condition, i.e., $\Theta(\mathbf{x}, 0) = \delta(\mathbf{x})$. He notes that the solution contains a term like $\delta'(|x| - ut)$ and so propagates like a wave of speed u , with negative values of Θ . Since Θ represents a physically positive quantity like concentration, the occurrence of negative values in the solution of the approximate equation is a serious problem. Saffman comments that

The method may work better when the material is initially more diffuse or is closer to a concentration of a type that exists some time after the initial conditions...

We decided to investigate whether equation (3.49) does indeed give physically reasonable solutions if the initial scalar “blob” is of finite extent. We find that Saffman’s conjecture is basically correct: for sufficiently smooth initial conditions with characteristic length a , it is possible to find physically reasonable results (e.g., Θ positive) for all time. Furthermore, we highlight the importance of the velocity correlation time T_E . Our major result is that the dimensionless parameter $\tau_* \equiv uT_E/a$ must be small in order to guarantee that Θ will be positive for all time. In light of this fact it is not surprising that Saffman found unphysical behavior. The delta function initial condition he used corresponds to the limit $a \rightarrow 0$ or $\tau_* \rightarrow \infty$.

The simplest generalization of Saffman’s work is to take an initial condition with some finite characteristic length a . With a view to solving the equation using Laplace transforms, we choose

$$\Theta(\mathbf{x}, 0) = \frac{3}{4\pi a^3} H\left(1 - \frac{r^2}{a^2}\right), \quad (3.50)$$

with $H(z)$ the one-dimensional Heaviside step function ($H(z) = 1$ for $z > 0$, $H(z) = 0$ for $z < 0$) and $r = |\mathbf{x}|$. We also follow Saffman in taking $R(t) = \exp(-|t|/T_E)$. We note in passing that this form of R permits us to cast the integrodifferential equation (3.49) in the form of a damped-wave or telegraph equation:

$$\frac{\partial^2 \Theta}{\partial t^2} + \frac{1}{T_E} \frac{\partial \Theta}{\partial t} - \nabla^2 \Theta = 0. \quad (3.51)$$

We have nondimensionalized lengths with a reference length L and times with a reference time L/u . Hereafter a is the nondimensional length characteristic of the initial condition, and T_E is the nondimensional correlation time.

We solve (3.51), (3.50) by Laplace transforms, and find after some work that

$$\begin{aligned}
\Theta(\mathbf{x}, t) &= \frac{3}{8\pi a^3} \frac{1}{r} \left\{ H\left(\frac{t}{r+a} - 1\right) \left[ae^{-\frac{r+a}{2T_E}} + a(r+a) \int_{r+a}^t e^{-\frac{y}{2T_E}} \frac{I_1\left(\frac{\sqrt{y^2-(r+a)^2}}{2T_E}\right)}{2T_E \sqrt{y^2-(r+a)^2}} dy \right. \right. \\
&\quad \left. \left. + \int_{r+a}^t e^{-\frac{y}{2T_E}} I_0\left(\frac{\sqrt{y^2-(r+a)^2}}{2T_E}\right) dy \right] \right. \\
&\quad \left. + H\left(\frac{t}{r-a} - 1\right) \left[ae^{-\frac{r-a}{2T_E}} + a(r-a) \int_{r-a}^t e^{-\frac{y}{2T_E}} \frac{I_1\left(\frac{\sqrt{y^2-(r-a)^2}}{2T_E}\right)}{2T_E \sqrt{y^2-(r-a)^2}} dy \right. \right. \\
&\quad \left. \left. - \int_{r-a}^t e^{-\frac{y}{2T_E}} I_0\left(\frac{\sqrt{y^2-(r-a)^2}}{2T_E}\right) dy \right] \right\}, \quad \text{if } r > a; \\
&= \frac{3}{8\pi a^3} \frac{1}{r} \left\{ H\left(\frac{t}{r+a} - 1\right) \left[ae^{-\frac{r+a}{2T_E}} + a(r+a) \int_{r+a}^t e^{-\frac{y}{2T_E}} \frac{I_1\left(\frac{\sqrt{y^2-(r+a)^2}}{2T_E}\right)}{2T_E \sqrt{y^2-(r+a)^2}} dy \right. \right. \\
&\quad \left. \left. + \int_{r+a}^t e^{-\frac{y}{2T_E}} I_0\left(\frac{\sqrt{y^2-(r+a)^2}}{2T_E}\right) dy \right] \right. \\
&\quad \left. - H\left(\frac{t}{a-r} - 1\right) \left[ae^{-\frac{a-r}{2T_E}} + a(a-r) \int_{r-a}^t e^{-\frac{y}{2T_E}} \frac{I_1\left(\frac{\sqrt{y^2-(a-r)^2}}{2T_E}\right)}{2T_E \sqrt{y^2-(a-r)^2}} dy \right. \right. \\
&\quad \left. \left. + \int_{a-r}^t e^{-\frac{y}{2T_E}} I_0\left(\frac{\sqrt{y^2-(a-r)^2}}{2T_E}\right) dy \right] + 2r \right\}, \quad \text{if } r < a \quad (3.52)
\end{aligned}$$

In the limit as $a \rightarrow 0$ the expression for $r > a$ should reduce to the solution of the delta-function initial condition considered by Saffman. His solution is given by equation (31) of [20] and in our dimensionless variables is

$$\begin{aligned}
\Theta(\mathbf{x}, t) &= \frac{\exp(-t/2T_E)}{4\pi r} \left\{ \delta'\left(\frac{t}{r} - 1\right) + \delta\left(\frac{t}{r} - 1\right) \left(\frac{T_E + r}{8T_E^2}\right) \right. \\
&\quad \left. + H\left(\frac{t}{r} - 1\right) \left[I_1\left(\frac{\sqrt{t^2 - r^2}}{2T_E}\right) + \frac{t}{\sqrt{t^2 - r^2}} I_2\left(\frac{\sqrt{t^2 - r^2}}{2T_E}\right) \right] \frac{r}{4T_E^2} \right\}. \quad (3.53)
\end{aligned}$$

Our analysis indicates that in fact the term in square brackets above should be divided by an additional factor of $\sqrt{t^2 - r^2}$. Without this factor the solution as given by (3.53) does not satisfy the equation (3.51) for $t > r$.

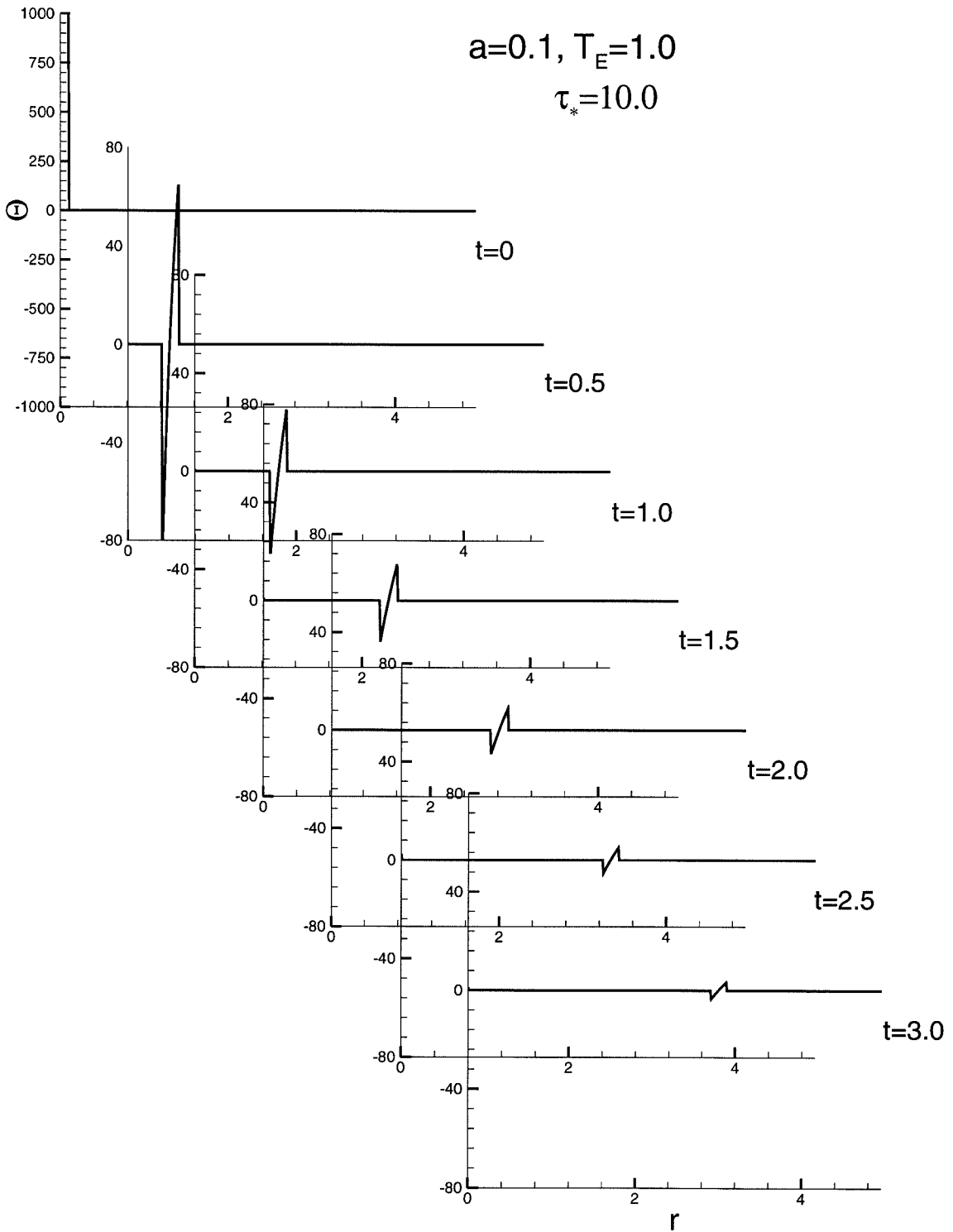
Next we plot Θ as given by (3.52) for various values of a and T_E . Recall that these dimensionless variables are defined by $a = \hat{a}/\hat{L}$ and $T_E = \hat{u}\hat{T}_E/\hat{L}$ (here we use hats to denote dimensional quantities). The reference length \hat{L} is not present in the original problem, so eliminating it leaves $\tau_* \equiv T_E/a = \hat{u}\hat{T}_E/\hat{a}$ as the only control parameter of the problem. In other words solutions for different values of a and T_E but with fixed τ_* will have identical forms, though on different length and time scales.

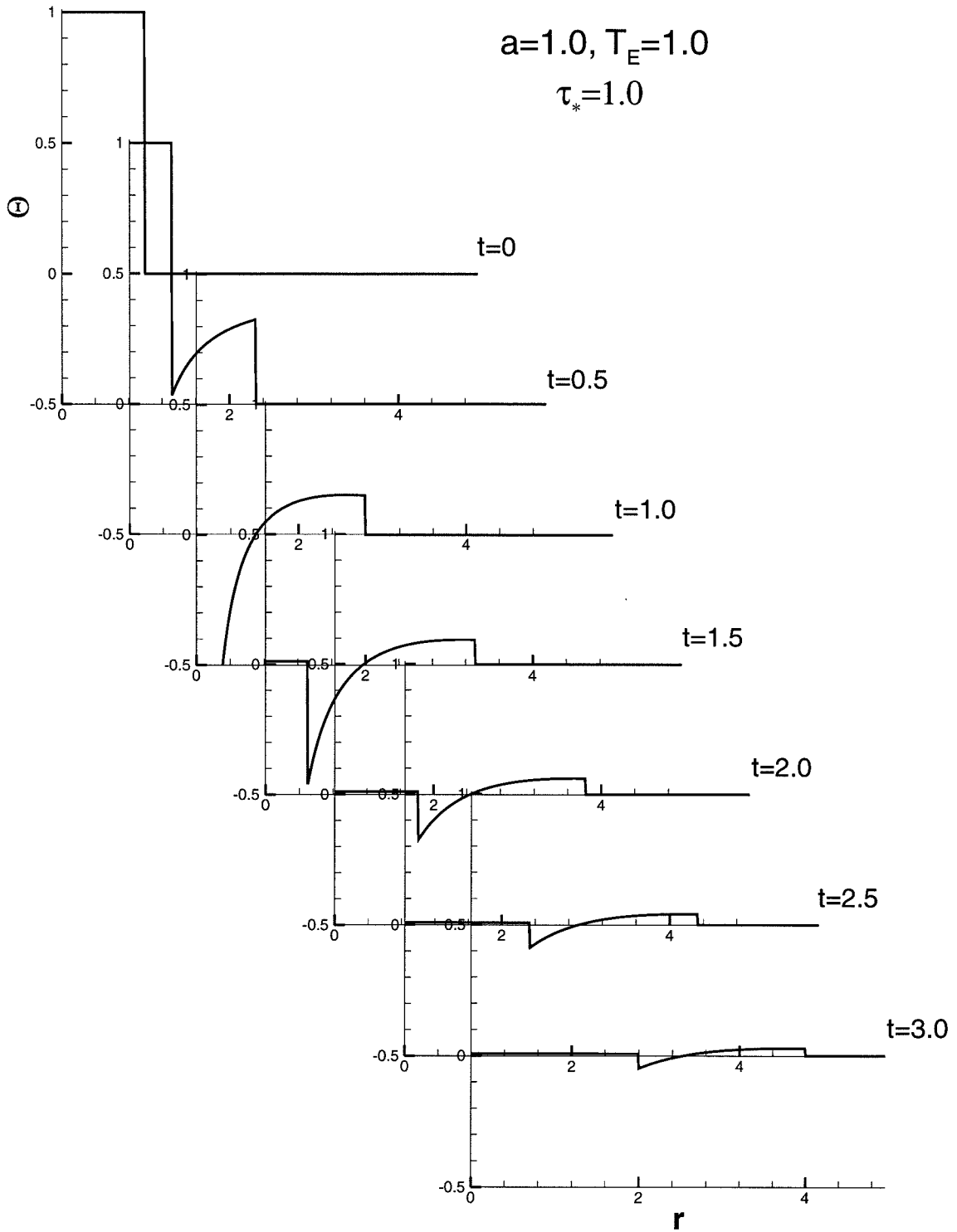
In Figure 3.15 we plot Θ as a function of r for seven different times. The parameter τ_* is 10 in this case. We see the propagating δ' -like spike, with large negative values of Θ . This corresponds to the case examined by Saffman. We set $\tau_* = 1$ in Figure 3.16. Wave-like propagation and negative Θ values are still clearly evident. However, Figure 3.17 for $\tau_* = 0.1$ displays behavior which appears to be physically reasonable—no apparent negative values and a diffusive-type smoothing of the initial profile.

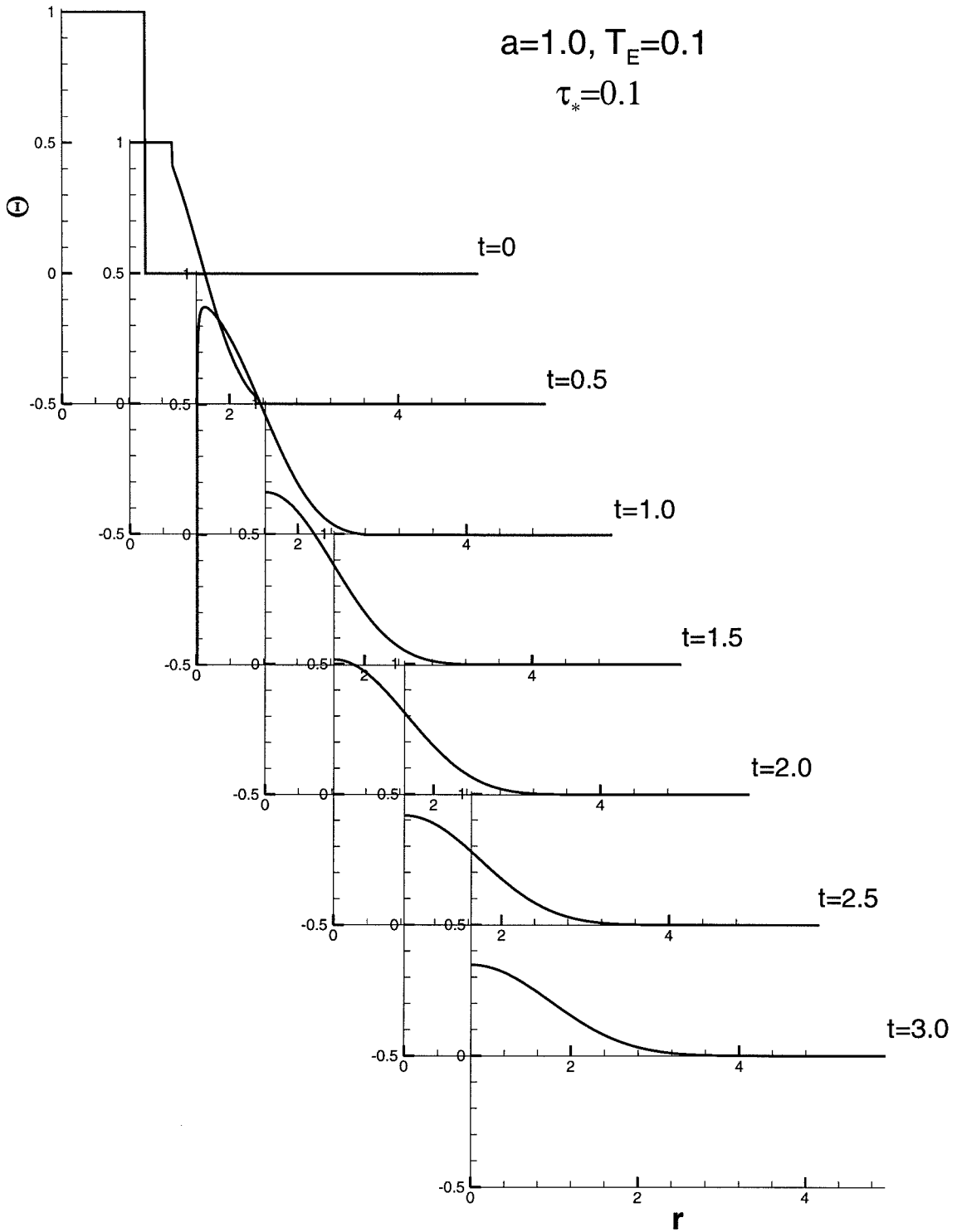
Unfortunately, even for this case Θ is not positive for all times. Careful analysis of the solution (3.52) shows that for times t with $|t - a|$ on the order of $\exp(-1/2\tau_*)$ and r of this same exponentially small order, $\Theta(\mathbf{x}, t)$ has large negative values. In Figure 3.18 we blow up the region of Figure 3.17 near $r = 0$ and $t = a$ to show this unphysical behavior of Θ .

Are we then to conclude that we cannot avoid negative solution values, even for $\tau_* \ll 1$? This is certainly true for the particular initial condition (3.50). However, we notice that the singularity in Figure 3.18 looks like the singularity which appears as $r \rightarrow 0$ and $t \rightarrow a$ in the solution of the “balloon problem” for the spherical wave equation [21]. This singularity is a consequence of using a discontinuous initial condition. Thus we are motivated to examine solutions of (3.49), or equivalently of (3.51), with initial conditions that are sufficiently smooth.

Relevant theorems are found in [22], [23]. For an initial condition that is four times differentiable, the solution of the telegraph equation (3.51) is equal to the solution of

Figure 3.15: Solution (3.52) for $\tau_* = 10$.

Figure 3.16: Solution (3.52) for $\tau_* = 1$.

Figure 3.17: Solution (3.52) for $\tau_* = 0.1$.

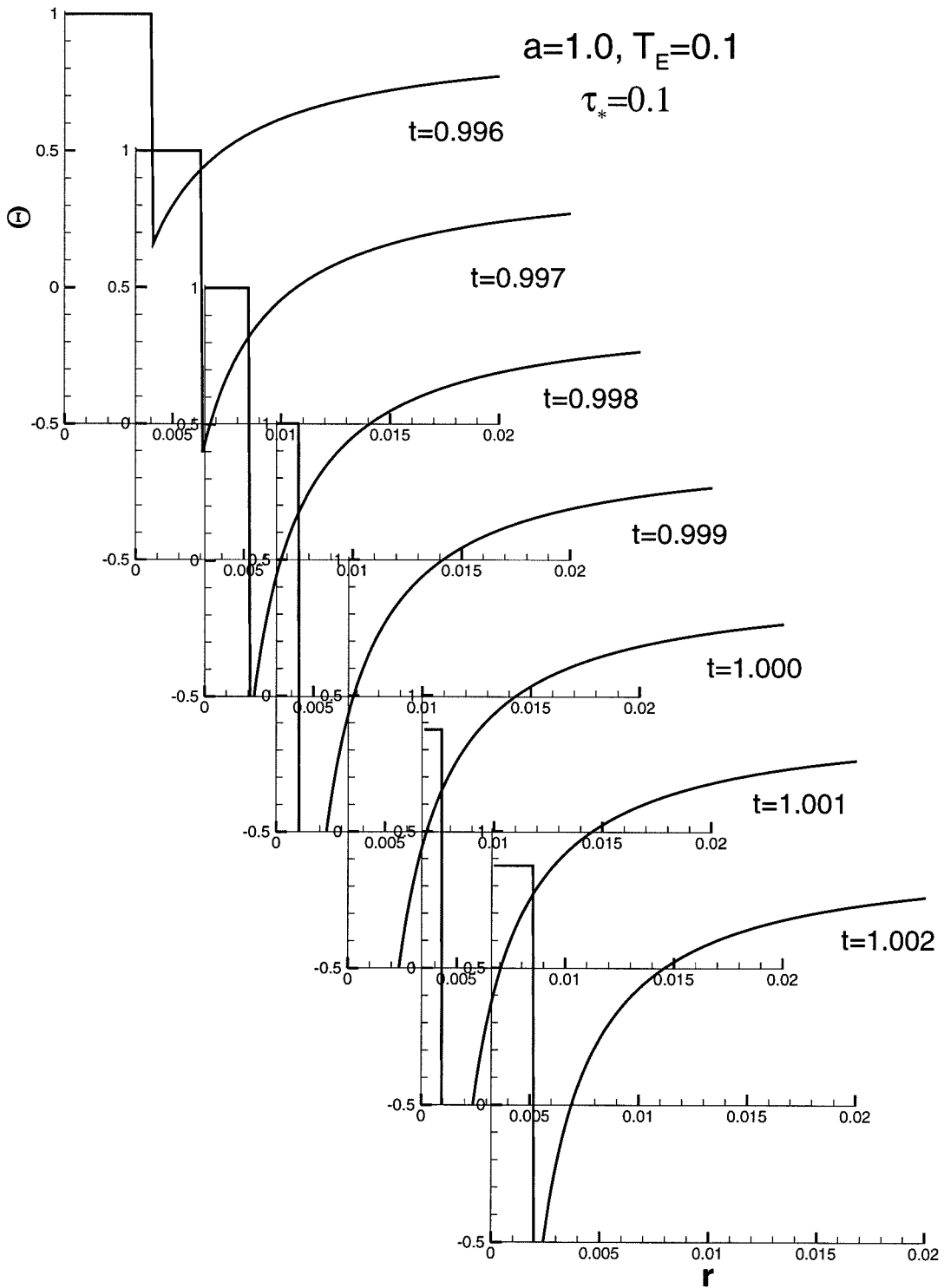


Figure 3.18: Zoom of Figure 3.17.

the corresponding heat equation

$$\frac{1}{T_E} \frac{\partial \Theta}{\partial t} - \nabla^2 \Theta = 0,$$

plus terms of order τ_*^2 . This holds for all r and all t . We conclude that when $\tau_* \ll 1$ a sufficiently smooth initial condition for the telegraph equation will evolve to solutions which are non-negative everywhere (at least up to order τ_*^2). Thus in this case the closure approximation (3.49) gives physically reasonable results, which hopefully will be close to the true Θ values. The analysis we have performed above for the step initial condition demonstrates that a condition on differentiability of the initial condition is indeed necessary in the theorems.

All this is very well, but we recall that the case of interest to us, (3.1), also has a delta function initial condition and so corresponds to infinite τ_* . As shown by Saffman, unphysical results are found in this case. It is not clear why the FDC1 approximation for $\Theta(\mathbf{x}, t)$ can have unphysical negative regions, and yet give the FDC1 expression for the effective diffusivity (3.17) which seems physically reasonable.

Chapter 4 Application to scalar spectrum

4.1 Introduction

In this chapter we apply the functional derivative closure method to derive equations for the scalar correlation and its Fourier transform, the scalar spectrum. As before the FDC1 approximation gives an integrodifferential equation which is the first term in a series expansion. We solve this equation using analytical and numerical techniques, and derive new results for power law forms of the scalar spectrum.

Obukhov [24] and Corrsin [25] independently proposed the existence of an inertial-convective range in the spectrum of a passive scalar which is advected by a turbulent fluid. Their ideas followed the universal equilibrium hypothesis of Kolmogorov [26] which leads to the famous $k^{-\frac{5}{3}}$ law for the velocity inertial range. Obukhov and Corrsin showed that for sufficiently large Prandtl number $Pr = \nu/\kappa$ there exists a range of wavenumbers where the scalar spectrum also has a $k^{-\frac{5}{3}}$ range. Batchelor [27] extended this analysis and used a model for the small-scale velocity to predict a k^{-1} scalar range when $Pr \gg 1$. The $k^{-\frac{5}{3}}$ law has been confirmed by experiment and direct numerical simulation, but the k^{-1} range is very difficult to check (because of the $Pr \gg 1$ requirement) and is still a source of some debate.

Predictions for the inertial-convective and Batchelor scaling ranges are a first test for any closure model of turbulence. Kraichnan's [9] direct interaction approximation (DIA) predicts a $k^{-\frac{3}{2}}$ inertial range for the velocity and so does not give a $k^{-\frac{5}{3}}$ scalar inertial-convective range. A $k^{-\frac{5}{3}}$ range is, however, predicted by an improved (and more complicated) version of the DIA, the so-called Lagrangian history direct interaction approximation (LHDIA [28]). The LHDIA also predicts a k^{-1} Batchelor range, as does another model due to Kraichnan which is based upon a rapidly varying

(delta-correlated) velocity field [29], [30]. Our functional derivative closure is closely related to this latter model—it may be considered as an extension of Kraichnan’s zero-correlation-time model to finite, but small, correlation times. We show that for stationary isotropic turbulence the FDC1 equation does indeed yield a k^{-1} Batchelor range, but of a slightly different form than that originally proposed by Batchelor. Moreover, the inertial-convective scaling in the FDC closure depends upon both the inertial range form of the velocity spectrum and on the scaling of the velocity correlation time—a $k^{-\frac{5}{3}}$ inertial-convective scalar range results if the correlation time scales as $k^{-\frac{2}{3}}$ in the velocity inertial range.

Recently there has been considerable interest in the case of a turbulent passive scalar with an imposed mean gradient [31], [32], [33]. Experimental and numerical work shows that the interaction between the scalar gradient and the turbulent velocity field acts as a “forcing,” or source term, for the scalar fluctuations. This case has not yet received much attention from closure modelers. Notable exceptions are the EDQNM numerical calculations of Herr et al. [34] and the renormalization group analysis of Elperin et al. [35] which predicts a k^{-3} inertial-convective power law. We find that the FDC1 closure predicts a dominant $k^{-\frac{5}{3}}$ inertial-convective scaling (just as in the isotropic case), but the difference between longitudinal and transverse spectra scales as k^p with $p \simeq -3.2$. This scaling law, unlike the $k^{-\frac{5}{3}}$ case, is not independent of the large scales of the flow.

In the final section we present the results of numerical computations of the FDC1 and DIA approximations for a freely decaying scalar and conclude that the FDC1 predictions for the scalar spectrum are likely to be valid only for small velocity correlation times.

4.2 The scalar spectrum

The scalar correlation for homogeneous turbulence is defined by

$$S(\mathbf{r}, t) = \langle \theta(\mathbf{x}, t) \theta(\mathbf{x} + \mathbf{r}, t) \rangle. \quad (4.1)$$

Note that the time arguments of the scalar are the same, so that $S(\mathbf{r}, t)$ represents a simultaneous measurement of the scalar at two points separated by the vector \mathbf{r} . By allowing S to depend on t we consider both decaying and stationary scalar correlations—if the scalar statistics are stationary, then $S(\mathbf{r}, t)$ will be independent of t .

The Fourier transform of S gives the scalar spectrum \mathcal{S} by

$$\mathcal{S}(\mathbf{k}, t) = 4\pi k^2 \frac{1}{(2\pi)^3} \int S(\mathbf{r}, t) e^{-i\mathbf{k}\cdot\mathbf{r}} d\mathbf{r}. \quad (4.2)$$

We will see below that the FDC approximations are most easily derived in wavenumber space, giving equations for the spectrum $\mathcal{S}(\mathbf{k}, t)$. These equations may be Fourier transformed using (4.2) to give corresponding physical space equations for the scalar correlation.

The advection of an unforced passive scalar is described by the equation

$$\frac{\partial}{\partial t} \theta(\mathbf{x}, t) + \mathbf{u} \cdot \nabla \theta(\mathbf{x}, t) - \kappa \nabla^2 \theta(\mathbf{x}, t) = 0. \quad (4.3)$$

To find an equation for $S(\mathbf{r}, t)$, we multiply (4.3) by $\theta(\mathbf{x} + \mathbf{r}, t)$ and add the corresponding equation for $\theta(\mathbf{x} + \mathbf{r}, t)$ multiplied by $\theta(\mathbf{x}, t)$. Using a superscripted plus to denote quantities evaluated at $\mathbf{x} + \mathbf{r}$, we have then

$$\frac{\partial}{\partial t} \langle \theta \theta^+ \rangle - \frac{\partial}{\partial r_\alpha} \langle u_\alpha \theta \theta^+ \rangle + \frac{\partial}{\partial r_\alpha} \langle u_\alpha^+ \theta \theta^+ \rangle - 2\kappa \frac{\partial^2}{\partial r_\alpha \partial r_\alpha} \langle \theta \theta^+ \rangle = 0 \quad (4.4)$$

for homogeneous turbulence in an incompressible fluid. It is straightforward to show from (4.4) that the total scalar variance $\langle \theta(\mathbf{x}, t) \theta(\mathbf{x}, t) \rangle = S(0, t)$ must be a decreasing function of t when κ is positive. In order to achieve a stationary state, with $S(\mathbf{r}, t)$ independent of time, we conclude that (4.4) and thus (4.3) must include some form of “forcing term” on the right-hand side. When considering stationary statistics below we examine two ways of introducing such a forcing. The first possibility is simply to add an artificial isotropic forcing term to (4.3) and to hope that by suitable choice of forcing statistics the effects of the forcing may mimic the effects which occur for

real isotropic stationary scalar turbulence. The second idea is to consider the effect of a mean scalar gradient imposed in one direction, so that $\langle \theta \rangle = \mathbf{x} \cdot \mathbf{g}$ instead of zero as before. Here \mathbf{g} is a constant vector with the dimensions of a gradient of θ . The equation for the fluctuations of the scalar θ about this mean is found from (4.3) by setting $\theta = \langle \theta \rangle + \tilde{\theta}$, and is

$$\frac{\partial}{\partial t} \tilde{\theta}(\mathbf{x}, t) + \mathbf{u} \cdot \nabla \tilde{\theta}(\mathbf{x}, t) - \kappa \nabla^2 \tilde{\theta}(\mathbf{x}, t) = -\mathbf{u} \cdot \mathbf{g}. \quad (4.5)$$

As we shall see below, the $-\mathbf{u} \cdot \mathbf{g}$ term on the right-hand side of this equation provides an effective forcing term for $\tilde{\theta}$. We note that in this case the existence of \mathbf{g} implies a preferred direction, so that the statistics of $\tilde{\theta}$ are no longer isotropic, but instead axisymmetric about the direction given by \mathbf{g} .

4.3 The FDC1 equations

4.3.1 Unforced scalar spectrum

We consider the FDC approximating equations for the scalar correlation $S(\mathbf{r}, t)$ and its Fourier transform $\mathcal{S}(\mathbf{k}, t)$ given by (4.2). The equations are most easily derived in wavenumber space. Briefly, we consider the Fourier transform of (4.3):

$$\frac{\partial}{\partial t} \theta(\mathbf{k}, t) + i \int d\mathbf{j} \mathbf{j} \cdot \mathbf{u}(\mathbf{k} - \mathbf{j}, t) \theta(\mathbf{j}, t) + \kappa k^2 \theta(\mathbf{k}, t) = 0, \quad (4.6)$$

where $\theta(\mathbf{k}, t)$ is the Fourier transform of $\theta(\mathbf{x}, t)$ and has the correlation function

$$\langle \theta(\mathbf{k}, t) \theta(\mathbf{k}', t) \rangle = \delta(\mathbf{k} + \mathbf{k}') \frac{\mathcal{S}(\mathbf{k}, t)}{4\pi k^2}.$$

We multiply (4.6) by $\theta(\mathbf{k}', t)$ and add the corresponding equation for $\theta(\mathbf{k}', t)$ multiplied by $\theta(\mathbf{k}, t)$. Averaging gives an equation for $\mathcal{S}(\mathbf{k}, t)$ which contains the terms $\langle u_\alpha \theta \theta' \rangle$ and $\langle u'_\alpha \theta \theta' \rangle$. These are expressed as integrals over $\mathcal{S}(\mathbf{k}, t)$ by applying Novikov's Theorem and retaining just the first, i.e., FDC1 term of the series. The result for the

unforced scalar is

$$\begin{aligned} \frac{\partial}{\partial t} \mathcal{S}(\mathbf{k}, t) + 2\kappa k^2 \mathcal{S}(\mathbf{k}, t) = \\ \int d\mathbf{j} \int_0^t d\sigma \frac{k^4 j^2}{2\pi} \frac{E(|\mathbf{k} - \mathbf{j}|, t - \sigma)}{|\mathbf{k} - \mathbf{j}|^4} (1 - \mu^2) e^{-\kappa(k^2 + j^2)(t - \sigma)} \left[\frac{\mathcal{S}(\mathbf{j}, \sigma)}{j^2} - \frac{\mathcal{S}(\mathbf{k}, \sigma)}{k^2} \right], \end{aligned} \quad (4.7)$$

where $\mu = \mathbf{k} \cdot \mathbf{j}/kj$ and $E(k, t)$ is the stationary velocity (energy) spectrum. This is an integrodifferential equation for the spectrum $\mathcal{S}(\mathbf{k}, t)$. It can be written in physical space by inverse Fourier transforming (or alternatively applying the FDC method to (4.4)) and yields

$$\begin{aligned} \frac{\partial}{\partial t} S(\mathbf{r}, t) - 2\kappa \nabla^2 S(\mathbf{r}, t) = \\ - \int_0^t d\sigma [2F_{\alpha\beta}(\mathbf{r}, t - \sigma) - 2F_{\alpha\beta}(0, t - \sigma)] \frac{\partial^2}{\partial r_\alpha \partial r_\beta} S(\mathbf{r}, \sigma), \end{aligned} \quad (4.8)$$

where $F_{\alpha\beta}(\mathbf{r}, t) = \langle u_\alpha(\mathbf{x}, t') u_\beta(\mathbf{x} + \mathbf{r}, t' + t) \rangle$.

4.3.2 Forced isotropic scalar spectrum

As discussed in the introduction, we are interested in finding possible stationary scalar spectra, i.e., $\mathcal{S}(\mathbf{k}, t)$ independent of t . To balance the effects of the diffusion terms in (4.7) we add a stochastic forcing term to (4.3):

$$\frac{\partial}{\partial t} \theta(\mathbf{x}, t) + \mathbf{u} \cdot \nabla \theta(\mathbf{x}, t) - \kappa \nabla^2 \theta(\mathbf{x}, t) = Phi(\mathbf{x}, t). \quad (4.9)$$

The forcing is taken to have isotropic, Gaussian statistics and correlation function

$$\overline{\Phi(\mathbf{x}, t) \Phi(\mathbf{x}', t')} = \delta(t - t') C(|\mathbf{x} - \mathbf{x}'|), \quad (4.10)$$

with the overbar denoting averaging over the realizations of the forcing Φ . Terms like $\overline{\theta \Phi}$ are then calculated using Novikov's Theorem; because of the delta-function time correlation in (4.10) the FDC1 approximation to $\overline{\theta \Phi}$ is exact—the delta-function in

(4.10) is equivalent to having a zero correlation time for the forcing.

We redefine the scalar statistics to include averaging over both velocity and forcing, so

$$S(\mathbf{r}, t) = \overline{\langle \theta(\mathbf{x}, t) \theta(\mathbf{x} + \mathbf{r}, t) \rangle}$$

for instance. Then the equation for the forced isotropic scalar spectrum is (4.7) with the forcing term added to the right-hand side:

$$\begin{aligned} \frac{\partial}{\partial t} \mathcal{S}(\mathbf{k}, t) + 2\kappa k^2 \mathcal{S}(\mathbf{k}, t) \\ = \int d\mathbf{j} \int_0^t d\sigma \frac{k^4 j^2}{2\pi} \frac{E(|\mathbf{k} - \mathbf{j}|, t - \sigma)}{|\mathbf{k} - \mathbf{j}|^4} (1 - \mu^2) e^{-\kappa(k^2 + j^2)(t - \sigma)} \left[\frac{\mathcal{S}(\mathbf{j}, \sigma)}{j^2} - \frac{\mathcal{S}(\mathbf{k}, \sigma)}{k^2} \right] + \mathcal{C}(k), \end{aligned} \quad (4.11)$$

where $\mathcal{C}(k)$ is the forcing spectrum

$$\mathcal{C}(k) = 4\pi k^2 \frac{1}{(2\pi)^3} \int C(r) e^{-i\mathbf{k} \cdot \mathbf{r}} d\mathbf{r}. \quad (4.12)$$

The inverse Fourier transform of (4.11) gives the physical space equation

$$\begin{aligned} \frac{\partial S(\mathbf{r}, t)}{\partial t} + 2 \int_0^t \{F_{\alpha\beta}(r, t - s) - F_{\alpha\beta}(0, t - s)\} \frac{\partial^2 S(\mathbf{r}, s)}{\partial r_\alpha \partial r_\beta} ds - \\ - 2\kappa \frac{\partial^2 S(\mathbf{r}, t)}{\partial r_\alpha \partial r_\alpha} = C(r). \end{aligned} \quad (4.13)$$

4.3.3 Imposed mean gradient

If a mean scalar gradient is imposed in one direction, the passive scalar obeys equation (4.5) instead of equation (4.3). The $-\mathbf{u} \cdot \mathbf{g}$ term on the right-hand side of (4.5) acts as a forcing term, so artificial forcing is no longer necessary. The FDC1 equation is

derived as above, and yields

$$\begin{aligned} \frac{\partial}{\partial t} \mathcal{S}(\mathbf{k}, t) + 2\kappa k^2 \mathcal{S}(\mathbf{k}, t) = & \\ & \int d\mathbf{j} \int_0^t d\sigma \frac{k^4 j^2}{2\pi} \frac{E(|\mathbf{k} - \mathbf{j}|, t - \sigma)}{|\mathbf{k} - \mathbf{j}|^4} (1 - \mu^2) e^{-\kappa(k^2 + j^2)(t - \sigma)} \left[\frac{\mathcal{S}(\mathbf{j}, \sigma)}{j^2} - \frac{\mathcal{S}(\mathbf{k}, \sigma)}{k^2} \right] + \\ & + \left[g^2 - \frac{(\mathbf{k} \cdot \mathbf{g})^2}{k^2} \right] \int_0^t d\sigma E(\mathbf{k}, \sigma). \end{aligned} \quad (4.14)$$

The direction of \mathbf{g} fixes a direction in space; let ψ be the angle between this direction and \mathbf{k} , i.e.,

$$\mathbf{k} \cdot \mathbf{g} = kg \cos \psi.$$

We consider a Fourier series for the axisymmetric scalar spectrum,

$$\mathcal{S}(\mathbf{k}, t) = \mathcal{S}_0(k, t) + \mathcal{S}_1(k, t) \cos \psi + \mathcal{S}_2(k, t) \cos 2\psi + \dots$$

and want to find equations for the $\mathcal{S}_i(k, t)$.

For calculation in the convolution integral, let

$$\mathbf{k} \cdot \mathbf{j} = kj \cos \varphi$$

$$\mathbf{j} \cdot \mathbf{g} = jg \cos \zeta$$

and let ϕ be the azimuthal angle of \mathbf{g} with respect to the \mathbf{k} - \mathbf{j} plane (see Figure 4.1).

Then from simple trigonometry,

$$\cos \zeta = \cos \psi \cos \varphi + \sin \psi \sin \varphi \cos \phi,$$

and

$$\int_0^{2\pi} \cos 2\zeta d\phi = 2\pi \left\{ \frac{1}{2} (\cos^2 \varphi - 1) + \cos 2\psi \left(\frac{3}{2} \cos^2 \varphi - \frac{1}{2} \right) \right\}. \quad (4.15)$$

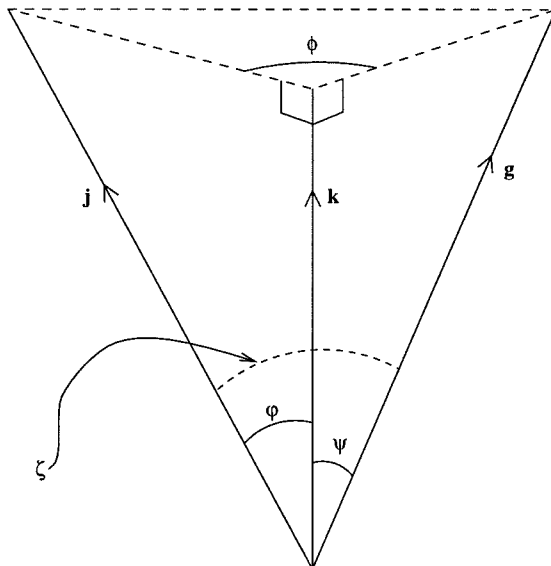


Figure 4.1: Geometry of the integration variables.

The forcing term of (4.14) is

$$\begin{aligned}
 & [g^2 - g^2 \cos^2 \psi] \int_0^t d\sigma E(k, \sigma) \\
 = & \frac{1}{2} g^2 \int_0^t d\sigma E(k, \sigma) - \frac{1}{2} g^2 \cos 2\psi \int_0^t d\sigma E(k, \sigma),
 \end{aligned}$$

and so only the constant term and the $\cos 2\psi$ term of the scalar spectrum Fourier series have non-zero forcing and appear in the stationary spectrum. We therefore write the scalar spectrum as

$$\mathcal{S}(\mathbf{k}, t) = \mathcal{S}_0(k, t) + \mathcal{S}_2(k, t) \cos 2\psi \tag{4.16}$$

and use (4.15) to find the following pair of equations for \mathcal{S}_0 and \mathcal{S}_2 :

$$\begin{aligned} \frac{\partial}{\partial t} \mathcal{S}_0(\mathbf{k}, t) + 2\kappa k^2 \mathcal{S}_0(\mathbf{k}, t) = & \\ & \int d\mathbf{j} \int_0^t d\sigma \frac{k^4 j^2}{2\pi} \frac{E(|\mathbf{k} - \mathbf{j}|, t - \sigma)}{|\mathbf{k} - \mathbf{j}|^4} (1 - \mu^2) e^{-\kappa(k^2 + j^2)(t - \sigma)} \left[\frac{\mathcal{S}_0(\mathbf{j}, \sigma)}{j^2} - \frac{\mathcal{S}_0(\mathbf{k}, \sigma)}{k^2} \right] \\ & + \int d\mathbf{j} \int_0^t d\sigma \frac{k^4 j^2}{2\pi} \frac{E(|\mathbf{k} - \mathbf{j}|, t - \sigma)}{|\mathbf{k} - \mathbf{j}|^4} (1 - \mu^2) e^{-\kappa(k^2 + j^2)(t - \sigma)} \frac{1}{2} (\mu^2 - 1) \frac{\mathcal{S}_2(\mathbf{j}, \sigma)}{j^2} \\ & - \frac{1}{2} g^2 \int_0^t d\sigma E(\mathbf{k}, \sigma), \end{aligned} \quad (4.17)$$

$$\begin{aligned} \frac{\partial}{\partial t} \mathcal{S}_2(\mathbf{k}, t) + 2\kappa k^2 \mathcal{S}_2(\mathbf{k}, t) = & \\ & \int d\mathbf{j} \int_0^t d\sigma \frac{k^4 j^2}{2\pi} \frac{E(|\mathbf{k} - \mathbf{j}|, t - \sigma)}{|\mathbf{k} - \mathbf{j}|^4} (1 - \mu^2) e^{-\kappa(k^2 + j^2)(t - \sigma)} \left[\frac{\mathcal{S}_2(\mathbf{j}, \sigma)}{j^2} - \frac{\mathcal{S}_2(\mathbf{k}, \sigma)}{k^2} \right] \\ & + \frac{1}{2} g^2 \int_0^t d\sigma E(\mathbf{k}, \sigma). \end{aligned} \quad (4.18)$$

Given the velocity spectrum, (4.18) is an integral equation for $\mathcal{S}_2(k)$. Solving for $\mathcal{S}_2(k)$ and substituting into (4.17) then allows the calculation of $\mathcal{S}_0(k)$ by solving another integral equation. The full scalar spectrum is given by (4.16).

The corresponding physical space equation for the correlation $S(\mathbf{r}, t)$ is

$$\begin{aligned} \frac{\partial S(\mathbf{r}, t)}{\partial t} + 2 \int_0^t \{F_{\alpha\beta}(r, t - s) - F_{\alpha\beta}(0, t - s)\} \frac{\partial^2 S(\mathbf{r}, s)}{\partial r_\alpha \partial r_\beta} ds \\ - 2\kappa \frac{\partial^2 S(\mathbf{r}, t)}{\partial r_\alpha \partial r_\alpha} = 2 \left[\int_0^t F_{\alpha\beta}(r, s) ds \right] g_\alpha g_\beta. \end{aligned} \quad (4.19)$$

In the next section we analyze stationary spectra using the physical space equations for $S(\mathbf{r}, t)$, and will then (in Section 4.4.6) numerically solve the spectral equations.

4.4 The stationary spectrum

When the diffusivity κ is balanced by a production term like the artificial forcing or the mean scalar gradient, the scalar spectrum may evolve to a stationary state, i.e., $\mathcal{S}(k, t) = \mathcal{S}(k)$ independent of t . To examine the form of such a stationary spectrum in wavenumber space, we let $t \rightarrow \infty$ in (4.11), (4.17), (4.18) and assume $\mathcal{S}(\mathbf{k}, t) = \mathcal{S}(\mathbf{k})$.

We will proceed to analyze these stationary equations in physical space and check our analysis with numerical solutions in wavenumber space.

4.4.1 Analysis in physical space

From (4.13), the stationary equation for the forced isotropic scalar in physical space is

$$2 \left[\int_0^\infty \{F_{\alpha\beta}(r, \tau) - F_{\alpha\beta}(0, \tau)\} d\tau \right] \frac{\partial^2 S}{\partial r_\alpha \partial r_\beta} - 2\kappa \frac{\partial^2 S}{\partial r_\alpha \partial r_\alpha} = C(r), \quad (4.20)$$

and that for the mean gradient scalar is (from (4.19))

$$2 \left[\int_0^\infty \{F_{\alpha\beta}(r, \tau) - F_{\alpha\beta}(0, \tau)\} d\tau \right] \frac{\partial^2 S}{\partial r_\alpha \partial r_\beta} - 2\kappa \frac{\partial^2 S}{\partial r_\alpha \partial r_\alpha} = 2 \left[\int_0^\infty F_{\alpha\beta}(r, \tau) d\tau \right] g_\alpha g_\beta. \quad (4.21)$$

We want to find the solutions $S = S(\mathbf{r})$ of these equations in the inertial range. Clearly a first step must be a hypothesis for the form of the time-integrated velocity correlation. For an incompressible isotropic velocity field this may be written

$$\int_0^\infty F_{\alpha\beta}(r, t) dt = u^2 \left(\frac{F - G}{r^2} r_\alpha r_\beta + G \delta_{\alpha\beta} \right),$$

with

$$F(r) = \int_0^\infty f(r, t) dt \quad \text{and} \quad G = F + \frac{1}{2} r F'(r), \quad (4.22)$$

and $f(r, 0)$ is the usual longitudinal velocity correlation function (see [1]). The function $F(r)$ is related to the time-integrated energy spectrum by

$$u^2 F(r) = 2 \int_0^\infty \int_0^\infty E(k) R(t, k) \left(\frac{\sin(kr)}{(kr)^3} - \frac{\cos(kr)}{(kr)^2} \right) dt dk. \quad (4.23)$$

Kolmogorov [26] showed that when the Reynolds number of a turbulent flow is sufficiently high there exists a range of wavenumbers called the ‘‘inertial’’ range where

the energy spectrum $E(k)$ scales as a power law, $E(k) \propto k^p$, and from dimensional considerations he found $p = -5/3$. We make the assumption that the time-integrated energy spectrum will obey a similar power law in the inertial range, i.e.,

$$\int_0^\infty E(k)R(t, k)dt \propto k^{-(1+\gamma)},$$

for some $\gamma > -1$. There is then a corresponding power law range in the correlation function—for $r \gg \eta$ and $r \ll L$,

$$\begin{aligned} F(0) - F(r) &\propto \frac{2}{u^2} \int_0^\infty k^{-(1+\gamma)} \left(\frac{1}{3} - \frac{\sin(kr)}{(kr)^3} + \frac{\cos(kr)}{(kr)^2} \right) dk + O\left(\frac{r}{L}\right) + O\left(\frac{\eta}{r}\right) \\ &= \frac{2}{u^2} [\Gamma(-3-\gamma) + \Gamma(-2-\gamma)] \sin\left((1+\gamma)\frac{\pi}{2}\right) r^\gamma + O\left(\frac{r}{L}\right) + O\left(\frac{\eta}{r}\right), \end{aligned} \quad (4.24)$$

with γ in the range ($0 < \gamma < 2$). The approximate beginning and end of the inertial range are labeled by the Kolmogorov scale η and the integral scale L respectively.

4.4.2 Analysis of isotropic scalar equation

The isotropic scalar equation (4.20) may now be written

$$u^2 \left\{ \frac{F-G}{r^2} r_\alpha r_\beta + (G-G(0)) \delta_{\alpha\beta} \right\} \frac{\partial^2 S}{\partial r_\alpha \partial r_\beta} - 2\kappa \nabla^2 S = C(r) \quad (4.25)$$

or equivalently

$$\left(F - F(0) - \frac{\kappa}{u^2} \right) S_{rr} + \frac{2}{r} \left(G - G(0) - \frac{\kappa}{u^2} \right) S_r = \frac{C(r)}{2u^2}. \quad (4.26)$$

This is expressible in the integrable form

$$\frac{d}{dr} \left\{ r^2 \left(F - F(0) - \frac{\kappa}{u^2} \right) S_r \right\} = \frac{r^2 C(r)}{2u^2},$$

whence

$$S = -\frac{1}{2u^2} \int_r^\infty \frac{\int_0^\rho s^2 C(s) ds}{\rho^2 (F(\rho) - F(0) - \frac{\kappa}{u^2})} d\rho \quad (4.27)$$

under the conditions that S_r remain bounded at the origin, and that the correlation vanishes at infinity. Equation (4.27) gives an integral representation for the scalar correlation function, in terms of the statistics of the velocity and forcing. The structure function of the scalar is then easily found from the relation

$$\overline{\langle (\theta - \theta^+)^2 \rangle} = 2S(0) - 2S(r)$$

which yields

$$\overline{\langle (\theta - \theta^+)^2 \rangle} = \frac{1}{u^2} \int_0^r \frac{\int_0^\rho s^2 C(s) ds}{\frac{\kappa}{u^2} \rho^2 - \rho^2 [F(\rho) - F(0)]} d\rho \quad (4.28)$$

We will make one further assumption: that the forcing correlation $C(r)$ is approximately constant over the range of r under consideration. This will certainly be the case if the forcing spectrum is strongly peaked at wavenumber k_f and $k_f < 1/L$, i.e., low wavenumber forcing.

Inertial-convective range

We consider r in the the inertial range:

$$\eta \ll r \ll L, \quad (4.29)$$

so by (4.24) the velocity correlation scales as

$$F(0) - F(r) = Dr^\gamma, \quad (4.30)$$

correct to $O(r/L, \eta/r)$. The scalar structure function is then

$$\overline{\langle (\theta - \theta^+)^2 \rangle} = \frac{C_0}{3u^2} \int_0^r \frac{\rho}{\frac{\kappa}{u^2} - D\rho^\gamma} d\rho,$$

so for r satisfying both (4.29) and

$$r^\gamma \gg \frac{\kappa}{u^2 D}, \quad (4.31)$$

the scalar structure function is

$$\overline{\langle (\theta - \theta^+)^2 \rangle} = -\frac{C_0}{3u^2 D} \frac{1}{(2 - \gamma)} r^{2-\gamma},$$

correct to $O(r/L, \eta/r)$. The connection between the structure function and the spectrum is given by

$$2S(0) - 2S(r) = \int_0^\infty \mathcal{S}(k) \left(1 - \frac{\sin(kr)}{kr}\right) dk,$$

and noting

$$\begin{aligned} & \int_0^\infty k^{\gamma-3} \left(1 - \frac{\sin(kr)}{kr}\right) dk + O\left(\frac{r}{L}\right) + O\left(\frac{\eta}{r}\right) \\ &= \Gamma(\gamma - 3) \sin\left((3 - \gamma)\frac{\pi}{2}\right) r^{2-\gamma} + O\left(\frac{r}{L}\right) + O\left(\frac{\eta}{r}\right), \end{aligned} \quad (4.32)$$

we infer that the stationary scalar spectrum in the inertial-convective range is

$$\mathcal{S}(k) = -\frac{C_0}{6u^2 D} \frac{1}{(2 - \gamma)} \frac{1}{\Gamma(\gamma - 3) \sin\left((\gamma - 3)\frac{\pi}{2}\right)} k^{\gamma-3}. \quad (4.33)$$

To summarize, by assuming a $k^{-(1+\gamma)}$ inertial range scaling of the time-integrated energy spectrum, we find the resulting scalar spectrum scaling is $k^{\gamma-3}$. The value of γ depends on the power law of $E(k)$ (which by Kolmogorov's theory is $k^{-\frac{5}{3}}$), but also

on the scale-dependence of $R(t, k)$, since we have defined

$$k^{-(1+\gamma)} = E(k) \int_0^\infty R(t, k) dt \quad \text{in the inertial range.}$$

Taking $R(t, k) = \exp(-|t|/\tau_*(k))$ for the purpose of illustration, we find

$$k^{-(1+\gamma)} = E(k)\tau_*(k), \quad (4.34)$$

and must now postulate a power law form for $\tau_*(k)$ in the inertial range. The question of the best power law fit for $\tau_*(k)$ has been examined by various workers in the field (see Section 4.4.3), but no conclusive result has yet emerged. One proposal is the “convective” (or “sweeping”) scaling:

$$\tau_*(k) \propto u^{-1}k^{-1}, \quad (4.35)$$

which leads to $\gamma = 5/3$, and gives a scalar spectrum scaling as $k^{-4/3}$ in the inertial-convective range. There is also some evidence that the “inertial” time scaling may be important, this is given by

$$\tau_*(k) \propto \epsilon^{-1/3}k^{-2/3}. \quad (4.36)$$

Note that this inertial time scaling gives $\gamma = 4/3$ from (4.34) and leads to a $k^{-5/3}$ scalar spectrum in (4.33). Most probably the real time scaling is some mixture of (4.35) and (4.36), with the scalar spectrum power law exponent lying between $-5/3$ and $-4/3$.

4.4.3 Realistic correlation times

We briefly digress to review the rather scanty literature related to the velocity time correlation. Sanada and Shanmugasundaram [36] consider the convective time (4.35) and the inertial time (4.36) and conclude that their DNS data is satisfactorily reduced

onto a curve of the form

$$R(t, k) = \exp(-\omega_k^2 t^2),$$

(compare to the model correlation time function R_b in (3.34)), with

$$\omega_k = uk/\tau_*.$$

The value of τ_* is found to be between 1.64 and 1.89 for microscale Reynolds numbers between 100 and 200, with τ_* decreasing with increasing Re .

McComb et al. [37] concentrate on the predictions of various closure theories for $R(t, k)$ and believe that the inertial time scale gives a better reduction of their results than does the convective scaling.

In our numerical work (Section 4.4.6) we use the experimental work of Comte-Bellot and Corrsin [39], who found that a correlation time

$$\tau_*(k) \equiv \tau_* \left\{ \frac{1}{\tau_C} + \frac{1}{\tau_R} + \frac{1}{\tau_S} + \frac{1}{\tau_D} \right\}^{-1}$$

collapsed their data onto a single curve. Here the τ_* on the right-hand side is just a fitted constant of order one; τ_C is a “convection time”

$$\tau_C \equiv \left[k^2 \int_0^k E(p) dp \right]^{-\frac{1}{2}},$$

τ_R is a “rotation time,” τ_S a “straining time”

$$\tau_R = \tau_S \equiv \left[\int_0^k p^2 E(p) dp \right]^{-\frac{1}{2}}$$

and τ_D a “diffusion time”

$$\tau_D \equiv \left[k^4 \int_k^\infty p^{-2} E(p) dp \right]^{-\frac{1}{2}}.$$

4.4.4 Analysis of mean gradient equation

Equations (4.21) and (4.22) yield the following equation for the scalar correlation in the case of a mean gradient:

$$u^2 \left\{ \frac{F-G}{r^2} r_\alpha r_\beta + (G-G(0)) \delta_{\alpha\beta} \right\} \frac{\partial S}{\partial r_\alpha \partial r_\beta} - \kappa \nabla^2 S = u^2 \left\{ \frac{F-G}{r^2} r_\alpha r_\beta + G \delta_{\alpha\beta} \right\} g_\alpha g_\beta, \quad (4.37)$$

or equivalently

$$-\frac{1}{2} r F' S_{rr} + \left(F + \frac{1}{2} r F' - F(0) \right) \nabla^2 S - \frac{\kappa}{u^2} \nabla^2 S = -\frac{1}{2} r F' g^2 \cos^2 \beta + \left(F + \frac{1}{2} r F' \right) g^2, \quad (4.38)$$

where β denotes the angle between \mathbf{r} and \mathbf{g} . The presence of the gradient \mathbf{g} breaks the isotropy of the scalar statistics—the scalar correlation now depends not only on the magnitude of \mathbf{r} , but also on its direction. In a coordinate system axisymmetric about \mathbf{g} ,

$$\nabla^2 S = \frac{1}{r^2} \frac{\partial}{\partial r} (r^2 S_r) + \frac{1}{r^2 \sin \beta} \frac{\partial}{\partial \beta} (\sin(\beta) S_\beta),$$

and we will seek a solution of (4.38) by expanding S in terms of Legendre functions:

$$S = \sum_{n=0}^{\infty} S_n(r) P_n(\cos \beta). \quad (4.39)$$

Noting that

$$\nabla^2 S = \sum_{n=0}^{\infty} \left[S_n'' + \frac{2}{r} S_n' - \frac{n(n+1)}{r^2} S_n \right] P_n(\cos \beta)$$

and

$$\cos^2 \beta = \frac{1}{3} + \frac{2}{3} P_2(\cos \beta),$$

we obtain

$$S_0'' \left[F - F(0) - \frac{\kappa}{u^2} \right] + S_0' \frac{2}{r} \left[F + \frac{1}{2} r F' - F(0) - \frac{\kappa}{u^2} \right] = \left[F + \frac{1}{3} r F' \right] g^2 \quad (4.40)$$

and

$$S_2'' \left[F - F(0) - \frac{\kappa}{u^2} \right] + S_2' \frac{2}{r} \left[F + \frac{1}{2} r F' - F(0) - \frac{\kappa}{u^2} \right] - S_2 \frac{6}{r^2} \left[F + \frac{1}{2} r F' - F(0) - \frac{\kappa}{u^2} \right] = -\frac{1}{3} g^2 r F' \quad (4.41)$$

with $S_n \equiv 0$ for $n \neq 0, 2$.

It is straightforward to solve (4.40) in a manner similar to that used to solve (4.26). The resulting structure function is

$$2S_0(0) - 2S_0(r) = 2g^2 \int_0^r \frac{\int_0^\rho s^2 [F + \frac{1}{3} s F'] ds}{\frac{\kappa}{u^2} \rho^2 - \rho^2 [F(\rho) - F(0)]} d\rho,$$

and with the inertial range form for F given by (4.30), we obtain

$$2S_0(0) - 2S_0(r) = -\frac{2g^2 F(0)}{3D} \frac{1}{(2-\gamma)} r^{2-\gamma} - \frac{g^2}{3} r^2 \quad \text{for } \eta \ll r \ll L, \quad (4.42)$$

correct to $O(r/L, \eta/r)$.

The equation (4.41) for $S_2(r)$ involves more work, though the existence of a particular solution

$$S_{2p} = \frac{1}{3} g^2 r^2 \quad (4.43)$$

which is independent of both $F(r)$ and κ is noteworthy. To find homogeneous solutions we make a further assumption $\kappa \rightarrow 0$ (which is reasonable in the inertial-convective range), and then (4.41) is simply

$$S_2'' + S_2' \frac{1}{r} (2 + \gamma) - S_2 \frac{3}{r^2} (2 + \gamma) = -\frac{1}{3} g^2 \gamma,$$

which has homogeneous solutions r^{n+} and r^{n-} with

$$n_{\pm} = \frac{-(1 + \gamma) \pm \sqrt{\gamma^2 + 14\gamma + 25}}{2}. \quad (4.44)$$

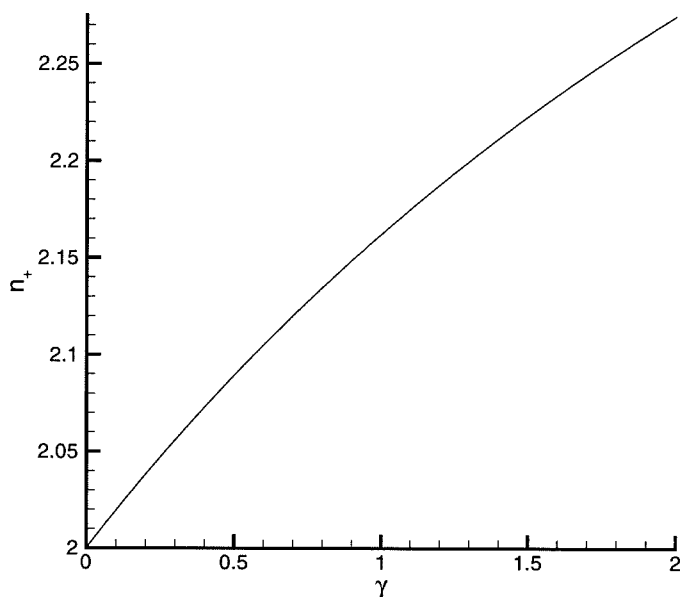


Figure 4.2: The exponent n_+ as a function of γ .

For $S_2(r)$ bounded as $r \rightarrow 0$, we must only have the r^{n_+} solution, leaving

$$S_2(r) = Ar^{n_+} + \frac{1}{3}g^2r^2 \quad (4.45)$$

for some undetermined constant A . For $\gamma = 4/3$, $n_+ = 2.20$, while for $\gamma = 5/3$, $n_+ = 2.24$ —Figure 4.2 shows that n_+ lies between 2 and 2.275 for γ between 0 and 2. The constant A cannot be determined solely from the inertial-range information we have at our disposal—in other words it depends on the form of the spectrum in the low-wavenumber “energy-containing” range.

The equations relating spectra and correlation functions for the axisymmetric case under consideration are

$$S_0(r) = \int_0^\infty \left[\mathcal{S}_0(k) \frac{\sin(kr)}{kr} + \mathcal{S}_2(k) \frac{\cos(kr)}{(kr)^2} - \mathcal{S}_2(k) \frac{\sin(kr)}{(kr)^3} \right] dk \quad (4.46)$$

$$S_2(r) = \int_0^\infty \mathcal{S}_2(k) \left[\frac{\sin(kr)}{kr} + 3 \frac{\cos(kr)}{(kr)^2} - 3 \frac{\sin(kr)}{(kr)^3} \right] dk, \quad (4.47)$$

where the three-dimensional energy spectrum is given by $\mathcal{S}(\mathbf{k}) = \mathcal{S}_0(k) + \mathcal{S}_2(k) \cos(2\psi)$

and the correlation function is $S(\mathbf{r}) = S_0(r) + S_2(r) \cos(2\beta)$, with ψ , β the angles between \mathbf{k} and \mathbf{g} and between \mathbf{r} and \mathbf{g} respectively. In order to get the inertial convective scaling (4.42) for $S_0(r)$, we must have

$$\mathcal{S}_0(k) \sim -\frac{g^2 F(0)}{3D} \frac{1}{(2-\gamma)} \frac{1}{\Gamma(\gamma-3) \sin\left(\frac{(\gamma-3)\pi}{2}\right)} k^{\gamma-3}.$$

We consider power law forms of $\mathcal{S}_2(k)$ which can give (4.45):

$$\begin{aligned} \int_{\frac{1}{L}}^{\infty} k^p \left[\frac{\sin(kr)}{kr} + 3 \frac{\cos(kr)}{(kr)^2} - 3 \frac{\sin(kr)}{(kr)^3} \right] dk = \\ - [3\Gamma(p-2) + 3\Gamma(p-1) + \Gamma(p)] \sin\left(\frac{p\pi}{2}\right) r^{-1-p} - \frac{L^{-1-p}}{p+3} \frac{1}{15} \frac{r^2}{L^2} + O\left(L^{-1-p} \frac{r^4}{L^4}\right), \end{aligned} \quad (4.48)$$

where the lower cutoff is needed for $p \leq -3$, but the first two terms on the right-hand side are the dominant terms in an asymptotic expansion as $r/L \rightarrow 0$. As discussed above, the constant A depends on the large scales of the fluid motion, but is in general nonzero. Then comparison of (4.48) and (4.45) leads us to infer that $\mathcal{S}_2(k)$ scales as $k^{-(1+n_+)}$ in the inertial-convective range, but with a coefficient which depends on the large scale motions. Figure 4.2 shows the exponent $-(1+n_+)$ lies between -3.275 and -3 for the range of physically possible γ values.

To measure the power law scaling of $\mathcal{S}_2(k)$, we recall the total spectrum is $\mathcal{S}(\mathbf{k}) = \mathcal{S}_0(k) + \mathcal{S}_2(k) \cos(2\psi)$ where ψ is the angle between \mathbf{k} and \mathbf{g} . Hence the difference between the longitudinal spectrum (measured parallel to \mathbf{g} , so $\psi = 0$) and the transverse spectrum (perpendicular to \mathbf{g} , so $\psi = \pi/2$) is $2\mathcal{S}_2(k)$ and will scale as $k^{-(1+n_+)}$.

Remark

Our definition of “longitudinal” and “transverse” spectra above are based on our usage of the three-dimensional spectrum $\mathcal{S}(\mathbf{k})$. In experimental work the longitudinal spectrum $\mathcal{S}_{||}(k)$ is defined to be the one-dimensional Fourier transform of the

correlation function measured parallel to \mathbf{g} , i.e.,

$$\mathcal{S}_{\parallel}(k) = \frac{1}{2\pi} \int_{-\infty}^{\infty} S\left(\frac{\mathbf{r} \cdot \mathbf{g}}{g}\right) e^{-ikr} dr$$

and similarly the transverse spectrum is

$$\mathcal{S}_{\perp}(k) = \frac{1}{2\pi} \int_{-\infty}^{\infty} S\left(\mathbf{r} - \frac{\mathbf{r} \cdot \mathbf{g}}{g}\right) e^{-ikr} dr.$$

Using these definitions the spectra \mathcal{S}_{\parallel} and \mathcal{S}_{\perp} can be written in terms of the \mathcal{S}_0 and \mathcal{S}_2 spectra we used above; in particular the difference between them is

$$\mathcal{S}_{\parallel}(k) - \mathcal{S}_{\perp}(k) = \frac{1}{2} \int_k^{\infty} \left(\frac{3k^2}{j^3} - \frac{1}{j} \right) \mathcal{S}_2(j) dj.$$

For the inertial-convective range scaling $\mathcal{S}_2(k) \sim k^{-(1+n_+)}$ derived above this also yields

$$\mathcal{S}_{\parallel}(k) - \mathcal{S}_{\perp}(k) \sim k^{-(1+n_+)}.$$

4.4.5 The Batchelor range

We return to the isotropic case and consider the Batchelor range of wavenumbers, with $r \ll \eta$. In this range the velocity correlation $F(r)$ is approximately parabolic:

$$F(r) - F(0) = \frac{1}{2} F''(0) r^2 + O(r^4) \quad r \ll \eta,$$

and using the integral form (4.28) we find

$$\overline{\langle (\theta - \theta^+)^2 \rangle} \sim \frac{C_0}{6\kappa} r_B^2 \ln \left(1 + \frac{r^2}{r_B^2} \right) \quad (4.49)$$

for

$$r \gg r_B \equiv \sqrt{\frac{2\kappa}{u^2 |F''(0)|}}. \quad (4.50)$$

Thus we have demonstrated a scaling (4.49) which exists for $r_B \ll r \ll \eta$. The existence of such a range clearly requires $r_B \ll \eta$ (which is equivalent to $Pr \gg 1$).

It is also possible to derive this Batchelor-like range from the stationary wavenumber equation (see 4.11 and Section 4.4.6):

$$2\kappa k^2 \mathcal{S}(k) - \int d\mathbf{j} \frac{k^4 j^2}{2\pi} \frac{E_{\text{eff}}(|\mathbf{k} - \mathbf{j}|)}{|\mathbf{k} - \mathbf{j}|^4} (1 - \mu^2) \left[\frac{\mathcal{S}(j)}{j^2} - \frac{\mathcal{S}(k)}{k^2} \right] = \mathcal{C}(k),$$

with E_{eff} representing the time-integrated energy spectrum. Consider wavenumbers k which lie beyond the viscous cutoff for the energy spectrum; for these wavenumbers the integral may be evaluated using the approximation $|\mathbf{k} - \mathbf{j}| \ll k$ and neglecting $\mathcal{C}(k)$. Letting $\mathbf{q} = \mathbf{k} - \mathbf{j}$, expanding in terms of q/k and doing the angular integrals yields

$$2k^2 \mathcal{S}(k) = B \left[2k^2 \frac{d^2}{dk^2} \mathcal{S}(k) - 4\mathcal{S}(k) \right], \quad (4.51)$$

with

$$\begin{aligned} B &= \frac{1}{15\kappa} \int_0^\infty dq \int_0^\infty ds q^2 E(q) R(s, q) \\ &= \frac{1}{15\kappa} \int_0^\infty dq q^2 E_{\text{eff}}(q). \end{aligned}$$

Note that

$$\int_0^\infty q^2 E_{\text{eff}}(q) dq = \frac{15u^2}{2} |F''(0)|$$

and so $B = 1/r_B^2$. The equation (4.51) has the bounded solution

$$\mathcal{S}(k) = \frac{C_0}{6\kappa k_B^2} \left(1 + \frac{k}{k_B} \right) \frac{1}{k} \exp \left[-\frac{k}{k_B} \right], \quad (4.52)$$

defining the Batchelor wavenumber $k_B \equiv 1/r_B$.

This solution is different to Batchelor's form

$$\mathcal{S}(k) = \frac{2C_0}{\kappa k_B^2} \frac{1}{k} \exp \left[-2 \frac{k^2}{k_B^2} \right], \quad (4.53)$$

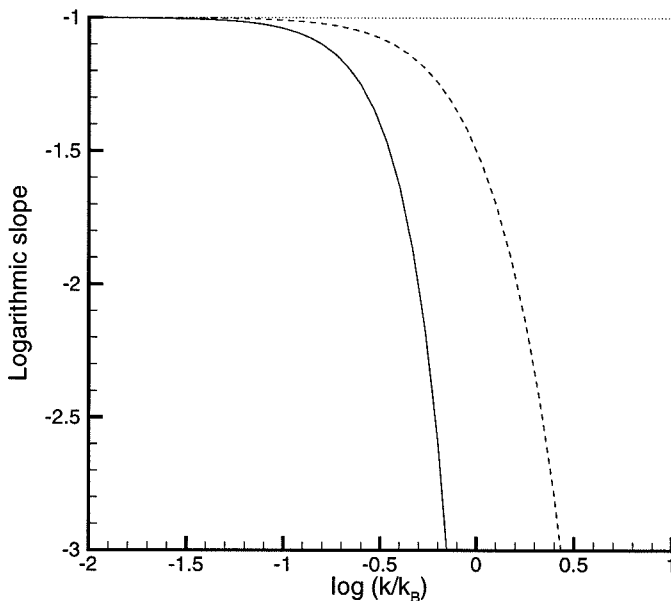


Figure 4.3: Logarithmic slopes of FDC (4.52) (solid), and Batchelor's theory (4.53) (dashed).

although the difference is probably too small to be detected experimentally. We plot the logarithmic slopes of both our solution and Batchelor's in Figure 4.3. The x -axis is $\log_{10}(k/k_B)$ and the y -axis is

$$\frac{d(\log_{10} \mathcal{S})}{d(\log_{10}(\frac{k}{k_b}))}.$$

A power law scaling $\mathcal{S} \propto k^p$ will manifest as a horizontal line $y = p$. Both solutions give a k^{-1} scaling range, but to see it we must be at least 1.5 decades below k_B . As the length of the Batchelor scaling range is $O(Pr^{\frac{1}{2}})$ [27], we conclude that a Prandtl number of order 10^3 is needed before any k^{-1} range will be discernible.

4.4.6 Numerics for stationary spectrum

The equations (4.11), (4.17) and (4.18) are forced integrodifferential equations. In order to investigate possible stationary solutions, we let $t \rightarrow \infty$ and assume $\mathcal{S}(k, t) = \mathcal{S}(k)$. For sufficiently small molecular diffusivity κ , the time integration may be

performed: we set

$$E_{\text{eff}}(k) = \int_0^\infty E(k, \sigma) d\sigma.$$

Thus the stationary version of (4.11) is

$$2\kappa k^2 \mathcal{S}(\mathbf{k}) - \int d\mathbf{j} \frac{k^4 j^2}{2\pi} \frac{E_{\text{eff}}(|\mathbf{k} - \mathbf{j}|)}{|\mathbf{k} - \mathbf{j}|^4} (1 - \mu^2) \left[\frac{\mathcal{S}(\mathbf{j})}{j^2} - \frac{\mathcal{S}(\mathbf{k})}{k^2} \right] = \mathcal{C}(k), \quad (4.54)$$

with analogous equations from (4.17) and (4.18).

To numerically solve a linear integral equation such as (4.54) we begin by discretizing the wavenumber integral and converting the integral to a sum (see, for example, [38]). The integral equation may thus be rewritten as a matrix equation for the unknown vector \mathcal{S} :

$$A\mathcal{S} - \lambda\mathcal{S} = \mathcal{C}. \quad (4.55)$$

We wish to solve (4.55) for different values of the parameter λ . Since the matrix A is symmetric, its eigenvectors form an orthogonal basis and so we may expand the unknown vector \mathcal{S} and the forcing vector \mathcal{C} on this basis:

$$\begin{aligned} \mathcal{S} &= \sum_{i=1}^N a_i \phi_i, \\ \mathcal{C} &= \sum_{i=1}^N b_i \phi_i, \end{aligned} \quad (4.56)$$

where ϕ_i are the eigenvectors of A , a_i are the coefficients to be solved for and b_i are coefficients given by

$$b_i = \frac{\mathcal{C} \cdot \phi_i}{\phi_i \cdot \phi_i}$$

(no summation). Then (4.55) implies

$$\sum_{i=1}^N a_i \lambda_i \phi_i - \sum_{i=1}^N \lambda a_i \phi_i = \sum_{i=1}^N b_i \phi_i$$

where λ_i is the eigenvalue corresponding to ϕ_i , and hence

$$a_i = \frac{b_i}{\lambda_i - \lambda}, \quad \text{for } \lambda \neq \lambda_i, \quad i = 1, \dots, N. \quad (4.57)$$

Having found the coefficients a_i the vector \mathcal{S} is constructed using (4.56). Note that the parameter λ is positive for positive diffusivity and the eigenvalues λ_i are negative, so we never divide by zero in (4.57).

The stationary-state mean gradient equations derived from (4.17) and (4.18) have the matrix form

$$A_1 \mathcal{S}_2 - \lambda \mathcal{S}_2 = \mathcal{C} \quad (4.58)$$

$$A_0 \mathcal{S}_0 - \lambda \mathcal{S}_0 = -\mathcal{C} + B_1 \mathcal{S}_2 \quad (4.59)$$

for symmetric matrices A_1 , A_0 and B_1 , and here \mathcal{C} is the discretized version of $-E_{\text{eff}}(k)g^2/2$. Solving (4.58) for \mathcal{S}_2 by the same method as above allows the construction of the right-hand side of (4.59), which is in turn solved to find \mathcal{S}_0 .

4.4.7 Velocity spectra

We consider two types of velocity spectrum—a “purely inertial” spectrum, which exhibits a $k^{-5/3}$ scaling within a finite range, and is set to zero otherwise. A more physically realistic case is provided by the “full” spectrum, which is piecewise smooth, with power law scaling for the energy and inertial ranges, and an exponential decay in the viscous range.

The time correlation function is taken to have the simple form

$$R(t, k) = \exp(-|t|/\tau_*(k)), \quad (4.60)$$

and $\tau_*(k)$ is chosen to be one of two cases—either the purely inertial time scale

$$\tau_*(k) \propto \epsilon^{-\frac{1}{3}} k^{-\frac{2}{3}},$$

or the “full” time scale which we base on the form used by Comte-Bellot and Corrsin [39].

Purely inertial spectrum

We set the instantaneous energy spectrum to have a purely inertial range form

$$E(k) = \begin{cases} \alpha \epsilon^{\frac{2}{3}} k^{-\frac{5}{3}} & \text{for } k_1 < k < k_2 \\ 0 & \text{otherwise,} \end{cases}$$

where $\alpha = 3/2$ is the Kolmogorov constant. Complementing this spectrum is the correlation time, which we take as

$$\tau_*(k) = \tau_* \epsilon^{-\frac{1}{3}} k^{-\frac{2}{3}} \quad (4.61)$$

for a constant τ_* . This purely inertial time scale is expected to produce a $k^{-\frac{5}{3}}$ scalar spectrum (as seen in Section 4.4.2). The time-integrated energy spectrum is

$$E_{\text{eff}} = \begin{cases} \tau_* \alpha \epsilon^{\frac{1}{3}} k^{-\frac{7}{3}} & \text{for } k_1 < k < k_2 \\ 0 & \text{otherwise} \end{cases}.$$

Full spectrum

A more realistic instantaneous energy spectrum is given by

$$E(k) = \begin{cases} Ak^m & k_0 < k \leq k_1 \\ \alpha \epsilon^{\frac{2}{3}} k^{-\frac{5}{3}} & k_1 < k < k_2 \\ Bk^q \exp(-sk) & k_2 < k \\ 0 & \text{otherwise} \end{cases}$$

where A and B are determined by the continuity of the spectrum, and m , q and s are empirical constants. We follow Comte-Bellot and Corrsin [39] in defining the

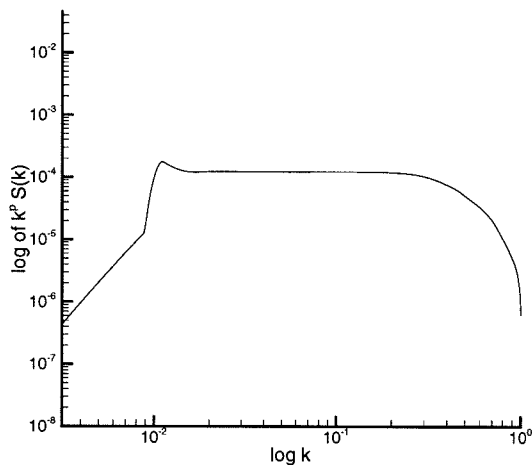


Figure 4.4: Scalar spectrum for purely inertial range velocity spectrum. The spectrum has been multiplied by $k^{1.72}$ to highlight the scaling. Inertial range is $k_1 = 0.01$, $k_2 = 0.316$, with parameter $\tau_* Pr = 0.6$.

correlation time by

$$\tau_*(k) \equiv \tau_* \left\{ \frac{1}{\tau_C} + \frac{1}{\tau_R} + \frac{1}{\tau_S} + \frac{1}{\tau_D} \right\}^{-1}, \quad (4.62)$$

as in Section 4.4.3. Comte-Bellot and Corrsin found that this scaling of the correlation time collapsed experimental data onto a single curve, $R(t/\tau_*(k))$, which we approximate by the exponential form (4.60).

4.4.8 Results

A sample of numerical results is presented in Figures 4.4 through 4.7.

Each figure is a log-log plot of wavenumber against $k^p \mathcal{S}(k)$, where p is a scaling exponent which best matches the power law behavior of $\mathcal{S}(k)$ in the inertial-convective range. The region where the scalar spectrum $\mathcal{S}(k)$ scales as k^{-p} thus appears on the plots as a straight line.

The nondimensional control parameter depends on $\tau_* Pr$, and the form of the spectrum depends on this parameter—we plot results using values of $\tau_* Pr$ which give the most extensive power law ranges.

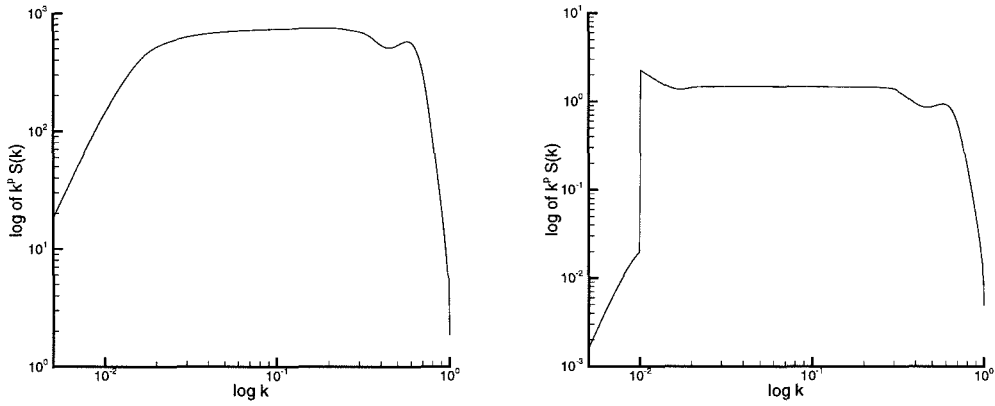


Figure 4.5: (a) Scalar spectrum parallel to \mathbf{g} , multiplied by $k^{1.64}$; (b) difference between longitudinal and transverse spectra, multiplied by $k^{3.12}$: Purely inertial range velocity spectrum. $k_1 = 0.01$, $k_2 = 0.316$, and parameter $\tau_* Pr = 0.8$.

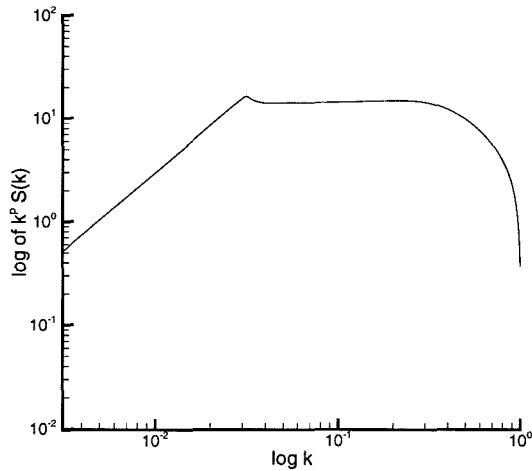


Figure 4.6: Scalar spectrum for full velocity spectrum. $\tau_* Pr = 5$. The spectrum has been multiplied by $k^{1.55}$ to highlight the scaling. $k_1 = 0.0316$, $k_2 = 0.316$.

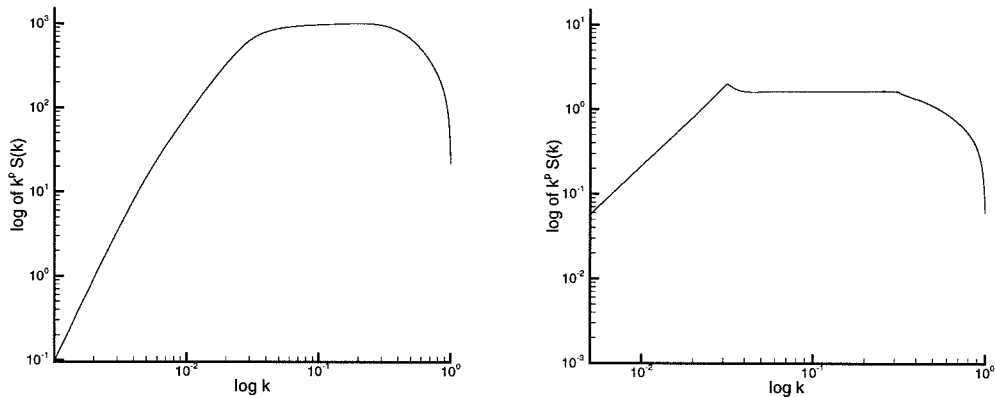


Figure 4.7: (a) Scalar spectrum parallel to \mathbf{g} , multiplied by $k^{1.44}$; (b) difference between longitudinal and transverse spectra, multiplied by $k^{3.14}$. Full velocity spectrum; $k_1 = 0.0316$, $k_2 = 0.316$, and parameter $\tau_* Pr = 0.04$.

The purely inertial velocity spectrum has $\gamma = 4/3$, so from the analysis in Section 4.4.2 we expect the isotropic scalar spectrum to scale as $k^{\gamma-3}$, i.e., with exponent $-5/3$. From Section 4.4.4 the expected longitudinal and transverse scalings for the mean gradient case are $-5/3$ and -3.20 respectively. As shown in Figures 4.4 and 4.5, the numerical isotropic exponent is found to be -1.72 and the mean gradient exponents are -1.64 and -3.12 . The agreement with the analysis is reasonable, especially given that the numerical inertial range is only 1.5 decades in extent, in contrast to the infinite inertial range considered in Sections 4.4.2 and 4.4.4.

The scaling of $\tau_*(k)$ for the full velocity spectrum as given by (4.62) is only approximately a power law. We find for a one-decade inertial range that the time-integrated spectrum $E_{\text{eff}}(k)$ is best fitted by $k^{-2.63}$, hence $\gamma = 1.63$. The theoretical values for the isotropic, longitudinal and transverse scaling exponents are therefore -1.37 , -1.37 and -3.24 respectively (see equations (4.33) and (4.48)). The numerical results (Figures 4.6 and 4.7) are -1.55 , -1.44 and -3.14 . The agreement between theory and numerics is not as good as in the purely inertial case. This is attributable to memory and resolution limitations which constrain the inertial range size to one decade (instead of 1.5 decades for the purely inertial case), and to the fact that $\tau_*(k)$ is not a pure power law throughout the inertial range.

4.5 Decaying spectrum—comparison with DIA

The FDC1 equation for the unforced isotropic scalar spectrum is (4.7):

$$\begin{aligned} \frac{\partial}{\partial t} \mathcal{S}(\mathbf{k}, t) + 2\kappa k^2 \mathcal{S}(\mathbf{k}, t) = \\ \int d\mathbf{j} \int_0^t d\sigma \frac{k^4 j^2}{2\pi} \frac{E(|\mathbf{k} - \mathbf{j}|, t - \sigma)}{|\mathbf{k} - \mathbf{j}|^4} (1 - \mu^2) e^{-\kappa(k^2 + j^2)(t - \sigma)} \left[\frac{\mathcal{S}(\mathbf{j}, \sigma)}{j^2} - \frac{\mathcal{S}(\mathbf{k}, \sigma)}{k^2} \right]. \end{aligned} \quad (4.63)$$

Based upon the analysis of the FDC method in previous chapters, we expect equation (4.63) to provide good approximations to the true scalar spectrum when the correlation time of the velocity is small. To quantify this condition and compare the FDC with more traditional closure methods, we consider also the direct interaction approximation (DIA) for the unforced isotropic scalar spectrum (see [40]):

$$\begin{aligned} \frac{\partial}{\partial t} \mathcal{S}(\mathbf{k}; t, t') + \kappa k^2 \mathcal{S}(\mathbf{k}; t, t') = \\ \int d\mathbf{j} \frac{k^4 j^2}{2\pi |\mathbf{k} - \mathbf{j}|^4} (1 - \mu^2) \left\{ \int_0^{t'} E(|\mathbf{k} - \mathbf{j}|, t - \sigma) g(k, t' - \sigma) \frac{\mathcal{S}(\mathbf{j}; t, \sigma)}{j^2} d\sigma \right. \\ \left. - \int_0^t E(|\mathbf{k} - \mathbf{j}|, t - \sigma) g(j, t - \sigma) \frac{\mathcal{S}(\mathbf{k}; t', \sigma)}{k^2} d\sigma \right\}, \end{aligned} \quad (4.64)$$

where $\mathcal{S}(k; t, t) = \mathcal{S}(k, t)$ and the response function $g(k, \tau)$ is the solution of

$$\begin{aligned} \frac{\partial}{\partial \tau} g(k, \tau) + \kappa k^2 g(k, \tau) = \\ = \int d\mathbf{j} \int_0^t d\sigma \frac{k^2 j^2}{2\pi} (1 - \mu^2) \frac{E(|\mathbf{k} - \mathbf{j}|, t - \sigma)}{|\mathbf{k} - \mathbf{j}|^4} g(k, \tau - \sigma) g(j, \sigma). \end{aligned} \quad (4.65)$$

The stationary velocity field is taken to be

$$E(k, t) = \frac{4u^2 k^4}{\sqrt{\pi} k_0^5} \exp(-k^2/k_0^2) \exp(-\frac{1}{2}u^2 k^2 t^2), \quad (4.66)$$

(compare with (3.47)). This form is especially convenient as it allows the angular

integrals in (4.7), (4.64) and (4.65) to be done exactly—for example, (4.63) becomes

$$\frac{\partial}{\partial t} \mathcal{S}(k, t) + 2\kappa k^2 \mathcal{S}(k, t) = \frac{4u^2}{\sqrt{\pi} k_0^5} H(k, t) \quad (4.67)$$

and

$$\begin{aligned} H(k, t) = & \frac{1}{2} \int_0^\infty dj j^2 k^2 \int_0^t d\sigma \left[e^{2kjw} \left(1 - \frac{1}{2kjw} \right) + e^{-2kjw} \left(1 + \frac{1}{2kjw} \right) \right] \times \\ & \times w^{-2} e^{-w(k^2+j^2)} e^{-\kappa(k^2+j^2)(t-\sigma)} \left[\frac{\mathcal{S}(j, \sigma)}{j^2} - \frac{\mathcal{S}(k, \sigma)}{k^2} \right], \end{aligned} \quad (4.68)$$

with $w = u^2(t - \sigma)^2/2 + 1/k_0^2$. Time and space variables are discretized and we set the initial scalar spectrum to have the form

$$\mathcal{S}(k, 0) \propto k^2 e^{-k^2/k_1^2}.$$

First consider the simpler FDC equation (4.11). At each time step the time and space integrals are approximated by the trapezoidal rule. The scalar spectrum at the next time step is found by using a predictor-corrector scheme to solve (4.67)—two iterations were found to be sufficient (see Lee [40]). A similar procedure was followed for the direct-interaction approximation equations (4.64) and (4.65).

4.5.1 Results

Results of the FDC and DIA calculations are compared in Figures 4.8 to 4.10. Both methods are known to be asymptotically correct as the correlation time goes to zero, and Figure 4.8 shows them to give similar results for the velocity spectrum (4.66) with $\tau_* = 0.1$. For larger values of τ_* however, we see different distributions of scalar variance in wavenumber space—this is despite the fact that both methods predict very similar values for the total scalar variance at time t ,

$$\int_0^\infty \mathcal{S}(k, t) dk.$$

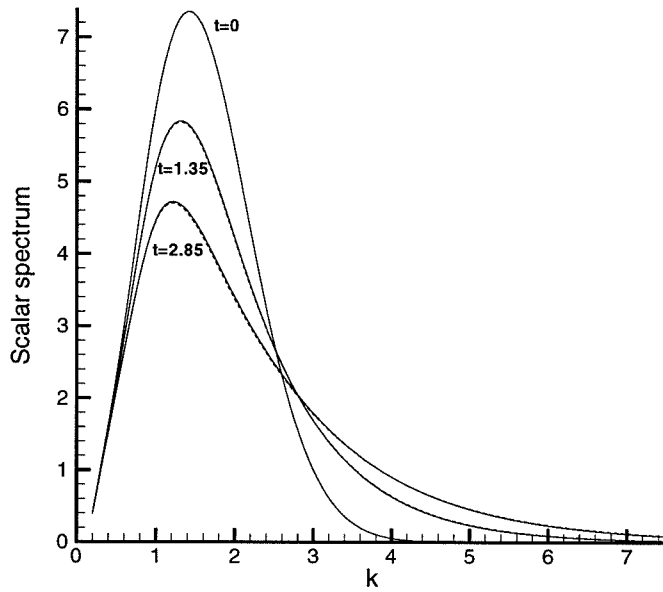


Figure 4.8: Decaying DIA (solid) and FDC1 (dashed) spectra for $\tau_* = 0.1$.

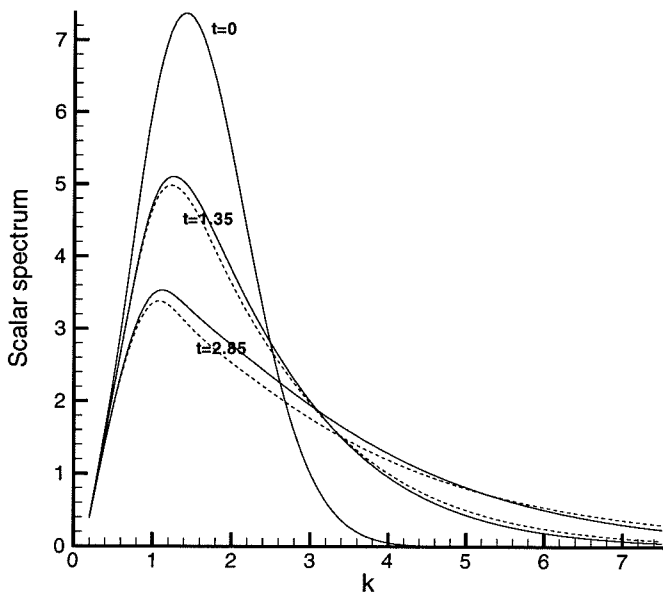


Figure 4.9: Decaying DIA (solid) and FDC1 (dashed) spectra for $\tau_* = 0.3$.

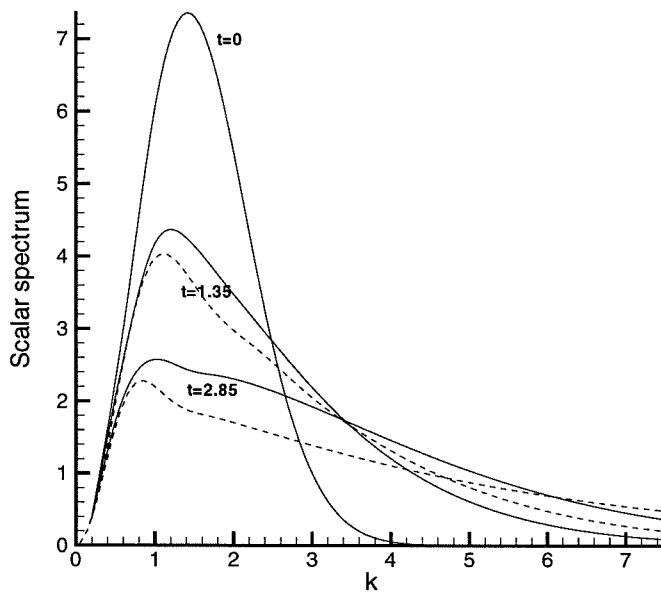


Figure 4.10: Decaying DIA (solid) and FDC1 (dashed) spectra for $\tau_* = 0.5$.

The direct interaction approximation is considered to be reasonably accurate for velocity spectra of the form (4.66) and so the divergence of the FDC and DIA leads us to conclude that the validity of the FDC1 spectral equation is limited to small values of τ_* .

Chapter 5 Conclusion

We briefly summarize our work:

- Outlined the functional derivative closure, a novel closure method for problems which are stochastically nonlinear.
- Used the simple stochastic oscillator example to demonstrate the interpretation of the FDC series as perturbation series in the correlation time τ_* .
- Defined a generalized Padé approximant to derive formulas relating the effective diffusivity and Lagrangian correlation to the Eulerian correlation, and numerically computed random velocity fields to confirm the accuracy of the approximations.
- Applied the first order FDC approximation to derive power laws for the stationary scalar spectrum with isotropic forcing and with a mean gradient. Compared numerical computations of a decaying spectrum with the direct interaction approximation to demonstrate their equivalence for small correlation time.

The effective diffusivity and the Lagrangian correlation approximations are valid for correlation times on the order of the eddy circulation time, whereas the spectral results are likely to be accurate only for smaller correlation times. In Section 4.4.3 we showed that the current experimental and numerical results on turbulence indicate values of τ_* between 1 and 3 times the eddy circulation time.

Further experimental and numerical work on the form of the velocity correlation time would be most welcome, and should permit testing of the predictions made here, for example the Lagrangian-Eulerian formulas and the $k^{-3.2}$ spectral scaling in the mean gradient case. Other ideas for future work include the extension of the FDC to non-Gaussian stochastic fields and to closure modeling for the small scales in large-eddy simulations of engineering flows.

Appendix A Proof of Novikov's Theorem

We present Novikov's [5] proof of the following theorem:

Theorem 1 *For arbitrary Gaussian random functions $f_j(s)$ with zero mean and correlation tensor*

$$\langle f_j(s) f_k(s') \rangle = F_{jk}(s, s')$$

where s represents an aggregate of arguments on which the random function depends, the cross-correlation $\langle f_j(s) R[\mathbf{f}] \rangle$ may be computed as

$$\langle f_j(s) R[\mathbf{f}] \rangle = \int F_{jk}(s, s') \left\langle \frac{\delta R[\mathbf{f}]}{\delta f_k(s')} \right\rangle ds', \quad (\text{A.1})$$

where the integral extends over the region in which the functions are defined. Here R stands for any functional of \mathbf{f} .

To prove the theorem, represent R as a functional Taylor series

$$R[\mathbf{f}] = R[0] + \sum_{n=1}^{\infty} \frac{1}{n!} \int \cdots \int R_{i_1 \dots i_n}^{(n)}(s_1, \dots, s_n) f_{i_1}(s_1) \dots f_{i_n}(s_n) ds_1 \dots ds_n, \\ R_{i_1 \dots i_n}^{(n)}(s_1, \dots, s_n) = \left. \frac{\delta^n R[\mathbf{f}]}{\delta f_{i_1}(s_1) \delta f_{i_2}(s_2) \dots \delta f_{i_n}(s_n)} \right|_{\mathbf{f}=0}. \quad (\text{A.2})$$

Now,

$$\langle f_j(s) R[\mathbf{f}] \rangle = \sum_{n=1}^{\infty} \frac{1}{n!} \int \cdots \int R_{i_1 \dots i_n}^{(n)}(s_1, \dots, s_n) \langle f_j(s) f_{i_1}(s_1) \dots f_{i_n}(s_n) \rangle ds_1 \dots ds_n. \quad (\text{A.3})$$

Using the fact that the mean value of a product of an even number of quantities with a Gaussian distribution is equal to the sum of the products of the mean values of all

possible pairwise combinations, we have

$$\begin{aligned} \langle f_j(s) f_{i_1}(s_1) \dots f_{i_n}(s_n) \rangle = \\ \sum_{\alpha=1}^n \langle f_j(s) f_{i_\alpha}(s_\alpha) \rangle \langle f_{i_1}(s_1) \dots f_{i_{\alpha-1}}(s_{\alpha-1}) f_{i_{\alpha+1}}(s_{\alpha+1}) \dots f_{i_n}(s_n) \rangle, \end{aligned}$$

and thus

$$\begin{aligned} \langle f_i(s) R[\mathbf{f}] \rangle = \sum_{n=1}^{\infty} \frac{1}{(n-1)!} \int F_{ji_1}(s, s_1) \\ \times \left[\int \dots \int R_{i_1 \dots i_n}^{(n)}(s_1, \dots, s_n) \langle f_{i_2}(s_2) \dots f_{i_n}(s_n) \rangle ds_2 \dots ds_n \right] ds_1. \quad (\text{A.4}) \end{aligned}$$

On the other hand, taking the functional derivative

$$\begin{aligned} \frac{\delta R[\mathbf{f}]}{\delta f_k(s')} = \sum_{n=1}^{\infty} \frac{1}{(n-1)!} \\ \times \int \dots \int R_{ki_2 \dots i_n}^{(n)}(s', s_2, \dots, s_n) f_{i_2}(s_2) \dots f_{i_n}(s_n) ds_2 \dots ds_n. \quad (\text{A.5}) \end{aligned}$$

and substituting (A.5) in the right-hand side of (A.1), we see that the resultant expression coincides with (A.4), proving the assertion (A.1).

Appendix B Counting the FDC diagrams

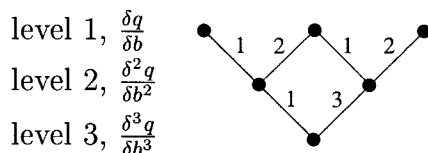
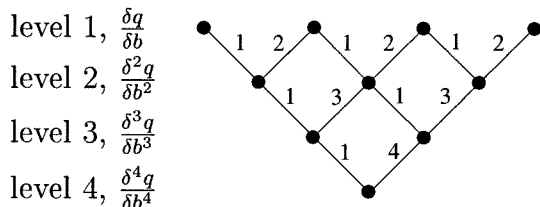
We want to calculate the number of diagrams of order n in the FDC expansion. To begin, we schematically represent the hierarchy of functional derivatives that begins with equations (2.12) and (2.16):

$$\begin{aligned}
 \frac{\delta q}{\delta b} &= q + \int b \frac{\delta q}{\delta b} \\
 \frac{\delta^2 q}{\delta b^2} &= 2 \frac{\delta q}{\delta b} + \int b \frac{\delta^2 q}{\delta b^2} \\
 \frac{\delta^3 q}{\delta b^3} &= 3 \frac{\delta^2 q}{\delta b^2} + \int b \frac{\delta^3 q}{\delta b^3} \\
 &\vdots
 \end{aligned}
 \tag{B.1}$$

The diagram shows three equations stacked vertically. The first equation is $\frac{\delta q}{\delta b} = q + \int b \frac{\delta q}{\delta b}$. The second is $\frac{\delta^2 q}{\delta b^2} = 2 \frac{\delta q}{\delta b} + \int b \frac{\delta^2 q}{\delta b^2}$. The third is $\frac{\delta^3 q}{\delta b^3} = 3 \frac{\delta^2 q}{\delta b^2} + \int b \frac{\delta^3 q}{\delta b^3}$. Below the third equation is a vertical ellipsis. Curved arrows indicate expansion paths: one from the first equation to the second, one from the second to the third, and one from the third back to the second.

Clearly this is a highly schematic representation, for we have not shown the factors of i , the function arguments nor the Heaviside step functions. The arrows indicate the possible paths of expansion, in the following sense: to expand $\langle bq \rangle$ we apply Novikov's Theorem (see (2.11)) and so seek $\langle \frac{\delta q}{\delta b} \rangle$. To find this, we average the first term in the hierarchy (B.1) and find one term containing $\langle q \rangle$ and remainder terms of the form $\int \langle b \frac{\delta q}{\delta b} \rangle$. Applying Novikov to expand these in turn (see (2.15)), we gain a factor of Γ and descend a level in the hierarchy, and now need to expand $\langle \frac{\delta^2 q}{\delta b^2} \rangle$. As in (2.16) this gives 2 terms of the form $\langle \frac{\delta q}{\delta b} \rangle$, plus the $\int \langle b \frac{\delta^2 q}{\delta b^2} \rangle$ remainder. Each $\langle \frac{\delta q}{\delta b} \rangle$ term can in turn be expanded by returning to the highest level in (B.1), while $\int \langle b \frac{\delta^2 q}{\delta b^2} \rangle$ is expanded by Novikov's Theorem, gaining a factor of Γ and descending another level in the hierarchy, etc. Each term which is expanded in this way contains a unique combination of Heaviside terms and so gives a unique FDC diagram.

By definition the FDC_n diagrams contain n Γ factors, and so must result from expansion paths in (B.1) which include $n - 1$ descents (one factor of Γ comes from

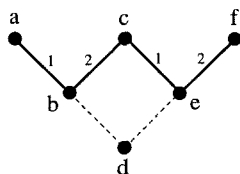
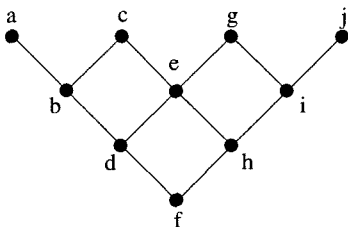
Figure B.1: T_3 , the trellis for $n = 3$.Figure B.2: T_4 , the trellis for $n = 4$.

applying Novikov's Theorem to $\langle bq \rangle$ to get $\int \Gamma \langle \frac{\delta q}{\delta b} \rangle$). Since each diagram finally contains $\langle q \rangle$ (along with the multiple Γ -factors), the expansion path also must include $n - 1$ ascents in the hierarchy (B.1), and so there are $2n - 2$ steps in the expansion path for each integral.

To count the FDC diagrams of order n , we employ some graph theory ideas [41]. We begin with a *trellis* (an ordered graph) of width $2n - 1$ with $n - 1$ levels, such that at each vertex the expansion paths can lead upward or downward in the hierarchy (B.1) as appropriate. The starting and ending vertices are both at the highest level, level 1. The numerical multiplying factors in (B.1) are included as edge weights on the trellis—note each ascending edge has a weight equal to the number of the level from which it ascends, whereas each descending edge has weight 1. For $n = 3$ the trellis T_3 is as shown in Figure B.1, and the $n = 4$ trellis T_4 is in Figure B.2.

Now we have reduced the calculation of the number of FDC diagrams of order n to finding the sum of the weights of each path in the trellis T_n leading from the start to the end vertex—the weight of a path being simply the product of the edge weights along the path. For example, the path shown in Figure B.3 has weight $1 \times 2 \times 1 \times 2 = 4$ and the only other possible path in T_3 has weight $1 \times 1 \times 3 \times 2 = 6$, which tells us that $4 + 6 = 10$ of the 15 diagrams of order 3 are FDC3 diagrams.

In general the sum of the weights of each path in T_n is given by a combinatorial quantity called the *flow* for the trellis and may be calculated by using the matrix

Figure B.3: T_3 labeling for incidence matrices.Figure B.4: T_4 labeling for incidence matrices.

representation of the trellis. Take T_3 as an example and label the vertices as shown in Figure B.3. At each step an *incidence matrix* gives the path weights for moving from each vertex on the current step to each vertex on the next step. For example, the T_3 incidence matrices are:

$$\begin{array}{c}
 b \\
 a \begin{pmatrix} 1 \end{pmatrix}
 \end{array}
 \quad
 \begin{array}{c}
 c \quad d \\
 b \begin{pmatrix} 2 & 1 \end{pmatrix}
 \end{array}
 \quad
 \begin{array}{c}
 e \\
 c \begin{pmatrix} 1 \\ 3 \end{pmatrix}
 \end{array}
 \quad
 \begin{array}{c}
 f \\
 e \begin{pmatrix} 2 \end{pmatrix}
 \end{array}$$

Then by Theorem 4.7.1 of [41], the flow (i.e., the number of FDC3 diagrams) is equal to the matrix multiplication of the incidence matrices:

$$\begin{pmatrix} 1 \end{pmatrix} \begin{pmatrix} 2 & 1 \end{pmatrix} \begin{pmatrix} 1 \\ 3 \end{pmatrix} \begin{pmatrix} 2 \end{pmatrix} = 10.$$

The incidence matrices for T_4 (see Figure B.4) are:

$$\begin{array}{ccc}
 & b & c \ d & e \ f \\
 a & \begin{pmatrix} 1 \\ \end{pmatrix} & b \begin{pmatrix} 2 & 1 \\ \end{pmatrix} & c \begin{pmatrix} 1 & 0 \\ 3 & 1 \\ \end{pmatrix} \\
 & g \ h & i & j \\
 e & \begin{pmatrix} 2 & 1 \\ \end{pmatrix} & g \begin{pmatrix} 1 \\ \end{pmatrix} & i \begin{pmatrix} 2 \\ \end{pmatrix} \\
 f & \begin{pmatrix} 0 & 4 \\ \end{pmatrix} & h \begin{pmatrix} 3 \\ \end{pmatrix} &
 \end{array}$$

and the number of FDC4 diagrams is simply the product

$$(1) \begin{pmatrix} 2 & 1 \\ \end{pmatrix} \begin{pmatrix} 1 & 0 \\ 3 & 1 \\ \end{pmatrix} \begin{pmatrix} 2 & 1 \\ 0 & 4 \\ \end{pmatrix} \begin{pmatrix} 1 \\ 3 \\ \end{pmatrix} (2) = 74.$$

The trellis and incidence matrices for higher orders are readily found—indeed the incidence matrices may easily be inferred without drawing the trellis. We give here the flow for T_5 which is reported in Table 2.2:

$$(1) \begin{pmatrix} 2 & 1 \\ \end{pmatrix} \begin{pmatrix} 1 & 0 \\ 3 & 1 \\ \end{pmatrix} \begin{pmatrix} 2 & 1 & 0 \\ 0 & 4 & 1 \\ \end{pmatrix} \begin{pmatrix} 1 & 0 \\ 3 & 1 \\ 0 & 5 \\ \end{pmatrix} \begin{pmatrix} 2 & 1 \\ 0 & 4 \\ \end{pmatrix} \begin{pmatrix} 1 \\ 3 \\ \end{pmatrix} (2) = 706.$$

Appendix C Proof of Lemma 1

By definition the FDC_n integrals contain $2n - 1$ Γ -factors, each of which occurs as a consequence of the application of Novikov's Theorem. The $\Gamma(t_{2n-2}, t_{2n-1})$ term, for instance, must appear in the combination

$$\int dt_{2n-1} \Gamma(t_{2n-2}, t_{2n-1}) \left\langle \frac{\delta^k q(t_{2n-1})}{\delta b(t_{j_1}) \dots \delta b(t_{j_k})} \right\rangle,$$

with k (the order of the functional derivative) being greater than 1. As a consequence of causality the functional derivative is zero unless t_{2n-1} is later than each of the times t_{j_1}, \dots, t_{j_k} , i.e., the vertex t_{2n-1} must appear in the vertex-ordering with $t_{2n-1} > t_{j_1}, t_{2n-1} > t_{j_2}, \dots, t_{2n-1} > t_{j_k}$. Thus the dotted line representing $\Gamma(t_{2n-2}, t_{2n-1})$ on the diagram has at least one vertex "foot" to the right (i.e., anticlockwise on the diagram) of the vertices $t_{j_1}, t_{j_2}, \dots, t_{j_k}$, and so the diagram cannot be cut so as to separate the $\Gamma(t_{2n-2}, t_{2n-1})$ loop from the rest of the diagram. Since a similar argument applies to each of the other Γ loops, it follows that the FDC diagrams cannot be disconnected diagrams.

That every connected diagram must be an FDC diagram can be shown by a counting argument: the number of FDC_n diagrams equals the number of connected diagrams of order n , and since we have shown that every FDC diagram is connected, it follows that every connected diagram must be an FDC diagram.

Appendix D Proof of Lemma 2

Consider “flattened-out” diagrams as in (2.44). The vertex 0 corresponds to t , and we want to examine the limit $t \rightarrow \infty$. Integration is over all the other vertices, with constraints (e.g., for (2.45) these constraints are $0 > 1 > 2 > 3$). Imagine that the vertices are beads on a wire which cannot pass through each other. The dotted lines between vertices i and j represent a connection of the form $\Gamma(i, j)$. The integrand is composed of the product of n such Γ -factors, and will be non-zero only when each Γ -factor is non-zero. The function Γ is assumed to go to zero at infinity, so we take it to be zero after some cutoff distance τ_* , i.e., $\Gamma(t_i, t_j) = 0$ for $|t_i - t_j| > \tau_*$. It follows that the only non-zero contribution to the integrand comes from such bead configurations as have each pair $|t_i - t_j| < \tau_*$ for each factor $\Gamma(i, j)$. In connected diagrams, the leftmost bead cannot be further than $n\tau_*$ from the rightmost bead (which is bead 0), and so the integrand over the vertices is finite, even as $t \rightarrow \infty$ (i.e., as bead 0 moves arbitrarily far to the right). That this does not happen for unconnected diagrams is clear from the (2.45) diagram. The beads-on-a-wire model of the diagram tells us that we get non-zero contribution to the integral when bead 1 stays within a distance τ_* of bead 0, and bead 3 within τ_* of bead 2. As bead 0 moves to the right, however, the 2–3 pair can roam freely over a larger and larger region, and so the integral may become arbitrarily large.

Bibliography

- [1] G. K. Batchelor, “*The theory of homogeneous turbulence*,” Cambridge University Press (1953).
- [2] D. S. Dean, I. T. Drummond and R. R. Horgan, “Perturbation schemes for flow in random media,” *J. Phys. A* **27** 5135 (1994).
- [3] R. H. Kraichnan, “Dynamics of nonlinear stochastic systems,” *J. Math. Phys.* **2** 124 (1961).
- [4] S. A. Orszag, “Lectures on the statistical theory of turbulence” in “*Fluid Dynamics, Les Houches 1973*,” eds. R. Balian and J. L. Peule, Gordon and Breach (1973).
- [5] E.A. Novikov, “Functionals and the random-force method in turbulence,” *Sov. Phys. JETP* **20** 1290 (1965).
- [6] J. Zinn-Justin, “*Quantum field theory and critical phenomena*,” 2nd ed. Oxford University Press (1993).
- [7] P. G. Saffman, “On the effect of the molecular diffusivity in turbulent diffusion,” *J. Fluid Mech.* **8** 273 (1960).
- [8] P. H. Roberts, “Analytical theory of turbulent diffusion,” *J. Fluid Mech.* **11** 257 (1961).
- [9] R. H. Kraichnan, “The structure of isotropic turbulence at very high Reynolds numbers,” *J. Fluid Mech.* **5** 497 (1959).
- [10] R. Phythian and W. D. Curtis, “The effective long-term diffusivity for a passive scalar in a Gaussian model fluid flow,” *J. Fluid Mech.* **89** 241 (1978).

- [11] N. A. Silant'ev, "Comparison of methods for calculating turbulent diffusion coefficients," *Sov. Phys. JETP* **84** 479 (1997).
- [12] P. G. Saffman, "An approximate calculation of the Lagrangian auto-correlation coefficient for stationary homogeneous turbulence," *Appl. Sci. Res.* **A 11** 245 (1961).
- [13] R. E. Davis, "On relating Eulerian and Lagrangian velocity statistics: single particles in homogeneous flows," *J. Fluid Mech.* **114** 1 (1982).
- [14] G. T. Csanady, "*Turbulent diffusion in the environment*," D. Reidel Publishing Company (1973).
- [15] C. M. Bender and S. A. Orszag, "*Advanced mathematical methods for scientists and engineers*," McGraw-Hill (1978).
- [16] G. A. Baker, "*Essentials of Padé approximants*," Academic Press, (1975).
- [17] R. H. Kraichnan, "Diffusion by a random velocity field," *Phys. Fluids* **13** 22 (1970).
- [18] R. W. Hamming, "Stable predictor corrector methods for ordinary differential equations," *J. Assoc. Comp. Mach.* **6** 37 (1959).
- [19] A. Ralston, "Numerical integration methods for the solution of ordinary differential equations" in "*Mathematical methods for digital computers*," eds. A. Ralston and H. S. Wilf, John Wiley & Sons (1960).
- [20] P. G. Saffman, "Application of the Wiener-Hermite expansion to the diffusion of a passive scalar in a homogeneous turbulent flow," *Phys. Fluids* **12** 1786 (1969).
- [21] G. B. Whitham, "Linear and nonlinear waves," Wiley-Interscience (1974).
- [22] M. Zlámal, "The mixed problem for hyperbolic equations with a small parameter," *Czech. Math. J.* **10** 80 (1960) (in Russian).

- [23] G. B. Nagy, O. E. Ortiz and O. A. Reula, "The behavior of hyperbolic heat equations' solutions near their parabolic limits," *J. Math. Phys.* **35** 4334 (1994).
- [24] A. M. Obukhov, "Structure of the temperature field in turbulent flows," *Izv. Akad. Nauk SSSR, Geogr. Geophys. Ser.* **13** 58 (1949).
- [25] S. Corrsin, "On the spectrum of isotropic temperature fluctuations in isotropic turbulence," *J. Appl. Phys.* **22** 469 (1951).
- [26] A. N. Kolmogorov, "The local structure of turbulence in incompressible fluid at very high Reynolds number," *Dokl. Acad. Sci. USSR* **30** 299 (1941).
- [27] G. K. Batchelor, "Small-scale variation of convected quantities like temperature in turbulent fluid" *J. Fluid Mech.* **5** 113 (1959).
- [28] R. H. Kraichnan, "Isotropic turbulence and inertial range structure in the abridged LHDI approximation," *Phys. Fluids* **9** 1728 (1966).
- [29] R. H. Kraichnan, "Small scale structure of a scalar field convected by turbulence," *Phys. Fluids* **11** 945 (1968).
- [30] K. Gawedzki and A. Kupiainen, "Anomalous scaling of the passive scalar," *Phys. Rev. Lett.* **75** 3834 (1995).
- [31] A. Pumir, "A numerical study of the mixing of a passive scalar in three dimensions in the presence of a mean gradient," *Phys. Fluids* **6** 2118 (1994).
- [32] M. R. Overholt and S. B. Pope, "Direct numerical simulation of a passive scalar with imposed mean gradient in isotropic turbulence," *Phys. Fluids* **8** 3128 (1996).
- [33] Jayesh et al., "On temperature spectra in grid turbulence," *Phys. Fluids* **6** 306 (1994).
- [34] S. Herr et al., "EDQNM model of a passive scalar with a uniform mean gradient," *Phys. Fluids* **8** 1588 (1996).

- [35] T. Elperin et al., “Isotropic and anisotropic spectra of passive scalar fluctuations in turbulent fluid flow,” *Phys. Rev. E* **53** 3431 (1996).
- [36] T. Sanada and V. Shanmugasundaram, “Random sweeping effect in isotropic numerical turbulence,” *Phys. Fluids A* **4** 1245 (1992).
- [37] W. D. McComb, V. Shanmugasundaram and P. Hutchinson, “Velocity-derivative skewness and two-time velocity correlations of isotropic turbulence as predicted by the LET theory,” *J. Fluid Mech.* **208** 91 (1989).
- [38] C. T. H. Baker, “*The numerical treatment of integral equations*,” Oxford University Press (1978).
- [39] G. Comte-Bellot and S. Corrsin, “Space-time correlation measurements in isotropic turbulence,” *J. Fluid Mech.* **48** 273 (1971).
- [40] J. Lee, “Decay of scalar quantity fluctuations in a stationary isotropic turbulent velocity field,” *Phys. Fluids* **8** 1647 (1965).
- [41] R. P. Stanley, “*Enumerative Combinatorics*,” vol. 1, Cambridge University Press (1997).